nature immunology



Article

https://doi.org/10.1038/s41590-025-02153-3

Inhibition of ENT1 relieves intracellular adenosine-mediated T cell suppression in cancer

Received: 19 November 2023

Accepted: 8 April 2025

Published online: 12 May 2025

Check for updates

Theodore J. Sanders $\mathbb{O}^{1,2}$, Christopher S. Nabel 3,4 , Margreet Brouwer 1,2 , Annelise L. Hermant 1,2 , Lucas Chaible 1,2 , Jean-Philippe Deglasse $\mathbb{O}^{1,2}$, Nicolas Rosewick 1,2 , Angélique Pabois $\mathbb{O}^{1,2}$, Wilfried Cathou 1,2 , Aurore Smets 1,2 , Michael Deligny 1,2 , João Marchante 1,2 , Quentin Dubray $\mathbb{O}^{1,2}$, Marie-Claire Letellier 1,2 , Chiara Martinoli 1,2 , Reece Marillier 1,2 , Olivier De Henau 1,2 , Yvonne McGrath 1,2 , Matthew G. Vander Heiden $\mathbb{O}^{3,5}$ & Erica Houthuys $\mathbb{O}^{1,2}$

The benefit of immune checkpoint blockade for cancer therapy is limited to subsets of patients because of factors including the accumulation of immunosuppressive metabolites, such as adenosine, within tumors. Pharmacological inhibition of adenosine generation and signaling is an active area of clinical investigation, but only limited clinical benefit has been reported. Here, we show that adenosine suppresses anti-cancer T cell responses following uptake into activated T cells by equilibrative nucleoside transporter 1 (ENT1) and inhibition of de novo pyrimidine nucleotide synthesis. We identify EOS301984 as a potent ENT1 antagonist that restores pyrimidine levels in activated T cells in adenosine-rich environments, resulting in enhanced tumor cell killing by memory T cells and increased ex vivo expansion of functional human tumor-infiltrating lymphocytes. A combination of EOS301984 with anti-PD-1 led to synergistic control of tumor growth in a humanized mouse model of triple-negative breast cancer. ENT1 inhibition, therefore, augments anti-cancer immune responses through the restoration of pyrimidine nucleotide synthesis in T cells suppressed by adenosine.

Immune checkpoint blockade therapy, such as targeting programmed cell death protein (PD-1) and its ligand (PD-L1), has achieved remarkable results for patients across several cancer indications 1,2 . However, most patients do not receive durable clinical benefit because of primary and acquired resistance 3 . Novel targets and combination therapies are needed to improve outcomes.

Many tumor microenvironment (TME) factors limit the efficacy of immunotherapies. In particular, increases in the levels of extracellular adenosine contribute to immunosuppression in tumors. Adenosine activates adenosine receptor $2A\left(A_{2A}R\right)$ signaling, which directly impairs

cytotoxic T cell activity⁴ and exerts a range of additional immunosuppressive effects⁵. Extracellular adenosine levels are kept low in healthy tissues through adenosine deaminase (ADA)-mediated conversion to inosine and cellular uptake through concentrative or equilibrative nucleoside transporters (CNTs and ENTs, respectively)⁵. ATP released from apoptotic and necrotic cells within tumors contributes to a local accumulation of adenosine from nanomolar to micromolar levels through the activities of enzymes, including the ectonucleotidases CD39 and CD73 (refs. 6,7).

Therapeutic strategies to limit adenosine-mediated immunosuppression in cancer include reduction of adenosine generation within

¹iTeos Therapeutics, Gosselies, Belgium. ²iTeos Therapeutics, Watertown, MA, USA. ³Koch Institute for Integrative Cancer Research at MIT, Cambridge, MA, USA. ⁴Massachusetts General Hospital, Boston, MA, USA. ⁵Dana-Farber Cancer Institute, Boston, MA, USA. —e-mail: erica.houthuys@iteostherapeutics.com

the TME by inhibition of the extracellular nucleotidases CD39 or CD73 (ref. 5), although redundancy in enzymes producing extracellular adenosine remains a major hurdle 6 . $A_{2A}R$ antagonists, including inupadenant, ciforadenant and imaradenant, seek to restore immune cell function by antagonism of adenosine-mediated immunosuppressive signaling $^{8.9}$. How high adenosine levels in tumors may affect immune cells apart from adenosine receptor signaling is poorly understood. Inferences can be made from human genetics: mutations in the ADA gene result in autosomal recessive severe combined immunodeficiency, in which intracellular adenosine transport by ENT1 leads to accumulation of toxic metabolites, resulting in severe lymphopenia 10,11 . These data suggest a role for ENT1-mediated control of intracellular adenosine levels in normal T cell biology, raising the possibility that uptake of adenosine may promote immune suppression.

Here, we show that high adenosine concentrations in the TME can be taken up by T cells, impairing their expansion and effector function. Activation of human T cells induces ENT1 expression, facilitating adenosine uptake and suppressing de novo pyrimidine synthesis, contributing to immunosuppression. We report that a potent ENT1 antagonist, EOS301984, can restore T cell and tumor-infiltrating lymphocyte (TIL) expansion and effector function in high-adenosine environments. ENT1 inhibition, when combined with anti-PD-1, can control tumor growth in a humanized mouse model of triple-negative breast cancer that is normally resistant to anti-PD-1 blockade. Together, these data identify ENT1 as a target to enhance anti-cancer immune responses and introduce EOS301984 as a potent ENT1 antagonist.

Results

Adenosine uptake via ENT1 suppresses T cells

Quantitative mass spectrometry imaging (QMSI) enables metabolite measurements with spatial resolution within snap-frozen tumor tissue. We assessed adenosine levels by QMSI in 19 resected tumor samples from six different cancer types. Average tumor concentrations of adenosine ranged from near the lower limit of quantification, approximately 49 μ M, to over 350 μ M (Fig. 1a,b and Extended Data Fig. 1a,b), higher than levels reported previously in tumor interstitial fluid obtained by microdialysis 7 . QMSI-derived adenosine levels in syngeneic or xenograft tumors were broadly consistent with the levels measured in interstitial fluid from matched samples (Extended Data Fig. 1c,d). These data indicate that extracellular adenosine may be present at even higher concentrations within the TME in some tumors than previously appreciated, prompting us to consider the impact on immune responses.

Elevated extracellular adenosine concentrations can influence T cell activity through $A_{2A}R$ signaling, but whether uptake of adenosine into human T cells can also exert an immunomodulatory effect is unknown. Expression of all four ENT family members was observed at the mRNA level in human T cells, and anti-CD3/CD28 stimulation led to increased expression of SLC29A1, encoding ENT1, while other ENT expression remained unchanged (Fig. 1c). No CNT family members could be detected at the mRNA level in resting or activated T cells. To assess whether ENT1 protein expression at the T cell surface is

also increased, we first validated a fluorescent ENT1-binding probe (SAHENTA-DY647)¹² using wild-type (WT) and ENT1-knockout (KO) IAR cells (Extended Data Fig. 2a-c). Importantly, the ENT1-specificity of the probe was confirmed by pre-incubating cells with the ENT1 inhibitor NBMPR before staining. T cell ENT1 surface protein increased within 24 h of activation, reaching a peak after 48 h and remaining high for several days (Fig. 1d and Extended Data Fig. 2d,e). ENT1 expression was associated with proliferation (Fig. 1e,f) and expression of the activation marker CD25 (Extended Data Fig. 2f). Activated human T cells took up [3H]adenosine, which was reduced in the presence of the ENT1 inhibitor dilazep (Fig. 1g). Notably, rare populations of ENT1⁺Ki-67⁺ T cells were observed in peripheral blood, and this fraction was enhanced in central memory and effector memory cells compared to naive T cell populations (Extended Data Fig. 2g-i). Finally, analysis of publicly available chromatin immunoprecipitation followed by sequencing (ChIP-seq) data¹³ identified an increased association of NFAT1 with the SLC29A1 promoter of human naive CD4⁺T cells within 5 h of activation, supporting an association between T cell activation and ENT1 expression (Extended Data Fig. 2j). Together, these data indicate that ENT1 is expressed on human T cells, is further upregulated upon activation and is the principal nucleoside transporter involved in adenosine uptake in T cells.

As expected14, adenosine treatment inhibited tumor necrosis factor (TNF) and interferon-y (IFNy) production as well as proliferation by activated human T cells in a dose-dependent manner (Extended Data Fig. 3a-c). This was associated with a loss of viability that was not observed in the absence of stimulation with anti-CD3/ CD28 (Extended Data Fig. 3d), indicating that adenosine is not inherently toxic to T cells. The A_{2A}R antagonist inupadenant partially restored production of TNF and increased IFNy production in the presence of 100 µM adenosine, but had no effect on the restoration of T cell proliferation and viability after 72 h of activation (Fig. 1h-l). By contrast, the ENT1 inhibitor dilazep restored production of IFNy, both at a global cytokine level and also on a per-cell basis (Fig. 11 and Extended Data Fig. 3e), and it also restored T cell proliferation and viability (Fig. 1h-j). Of note, the combination of ENT1 inhibition with an A_{2A}R antagonist was required to fully rescue T cell cytokine production, proliferation and viability (Fig. 1h-l), suggesting an additive effect of ENT1 and A₂₄R inhibition.

The short half-life of adenosine 15 represents a technical challenge for modeling chronic adenosine exposure in vitro. Metabolism of extracellular ATP by the sequential activities of CD39 and CD73 generates adenosine in the TME 16 . As CD39 and CD73 expression are observed on CD4 $^+$ and CD8 $^+$ T cells (Extended Data Fig. 3f), we reasoned that ATP could be a source of dynamic adenosine regeneration through T cell-mediated conversion of ATP into adenosine. Indeed, ATP suppressed T cell proliferation and viability in an ENT1-dependent manner (Extended Data Fig. 3g,h). Although ATP also suppressed TNF production, this was primarily through $A_{2A}R$ signaling, as the effect was reversed with inupadenant (Extended Data Fig. 3i). Together, these data suggest that the suppressive effect of ATP and adenosine on T cell proliferation, viability and cytokine production is in part mediated by

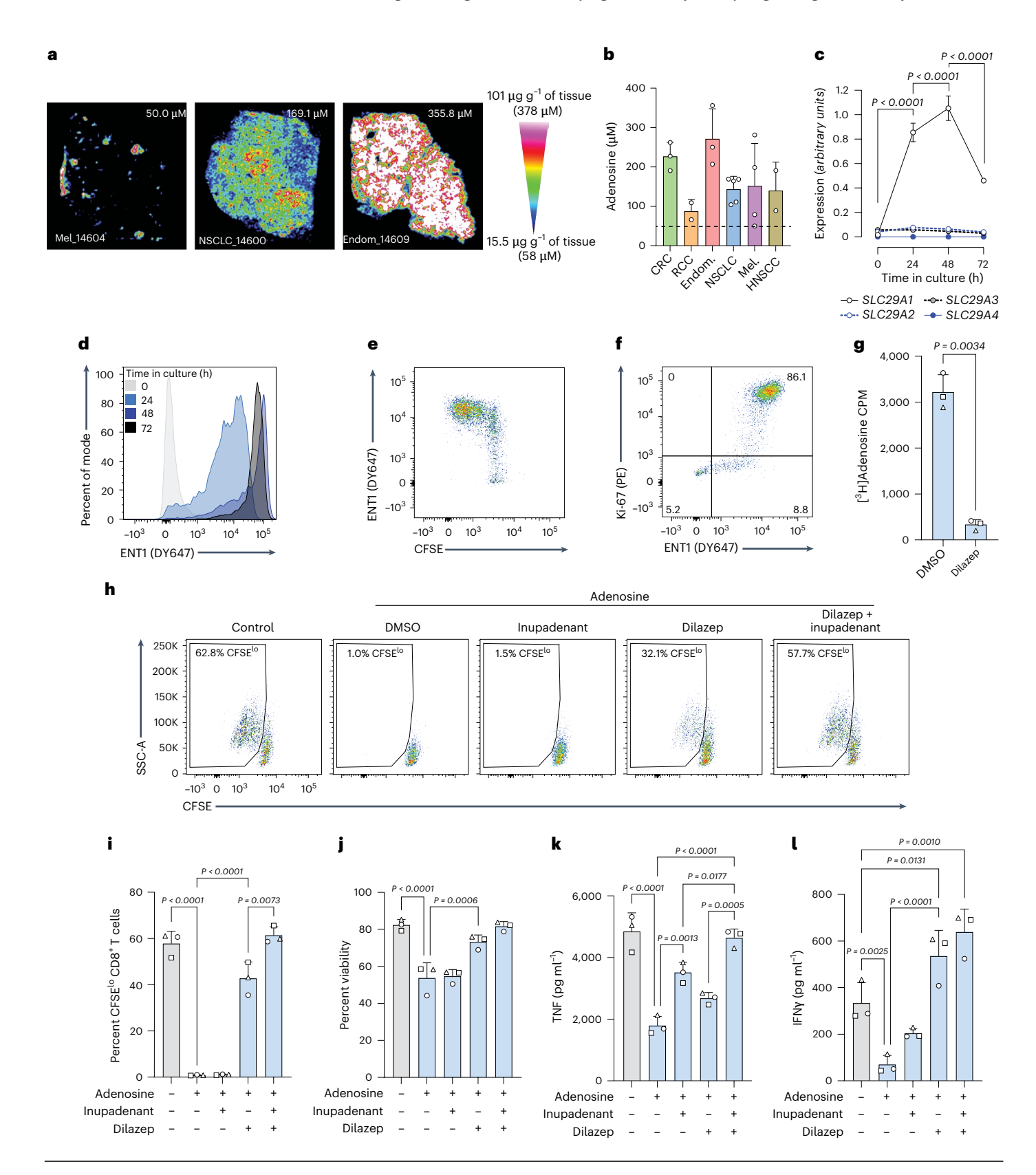
Fig. 1| **Adenosine uptake via ENT1 suppresses T cells. a**, Resected tumor samples were frozen and adenosine levels determined by QMSI. Representative QMSI images of samples with low, medium and high adenosine levels (left to right). **b**, Mean concentrations of adenosine across all (n=19) samples tested. Each symbol represents one sample (biological replicate); dotted bar indicates lower limit of quantification. Mean value shown; error bars, s.d. CRC, colorectal cancer; RCC, renal cell carcinoma; Endom., endometrial cancer; Mel., melanoma; HNSCC, head and neck squamous cell carcinoma. **c**, Expression of *SLC29A* (ENT) genes in activated human T cells during culture. Symbols represent mean values from three donors; error bars, s.d. *P* values from two-way ANOVA with Tukey's multiple comparisons test. **d**, Flow cytometry analysis of surface ENT1 protein expression by CD8* T cells at different time points of activation. Representative of

three donors. **e,f**, Flow cytometry analysis of ENT1 expression on activated CD8 $^{+}$ T cells in relation to proliferation (**e**) and Ki-67 expression (**f**) after 72 h of culture. Representative of three donors. **g**, [3 H]adenosine uptake assay using activated human T cells from three donors (biological replicates) in the presence of dilazep or DMSO; CPM, counts per minute. Mean value shown; error bars, s.d. *P* value from two-tailed paired *t*-test. **h**, Suppressive effect of 100 μ M adenosine on CD8 $^{+}$ T cell proliferation and reversal with dilazep, an ENT1 inhibitor, combined with an $A_{2A}R$ antagonist. Representative of three donors. **i–1**, Suppressive effect of adenosine and restoration with dilazep and/or inupadenant on CD8 $^{+}$ T cell proliferation (**i**), T cell viability (**j**), TNF production (**k**) and IFN γ production (**l**). *P* values from two-way ANOVA with Tukey's multiple comparisons test. Mean values from three donors: error bars. s.d.

ENT1-dependent uptake, with additional contributions from the known $A_{2A}R$ -mediated immunosuppressive signaling pathway.

To understand whether ENT1 has a role in regulating physiological immune responses in high-adenosine TMEs in a non-cancer cell autonomous manner, syngeneic cancer cell lines were engrafted into WT mice and mice in which ENT1 was genetically deleted (ENT1-KO). ENT1-KO mice are viable and exhibit mild hematological changes¹⁷ as

well as increased plasma adenosine levels ¹⁸. A delay in tumor growth was observed when MCA205 (fibrosarcoma), MC38 (colon adenocarcinoma) and Pan02 (pancreatic ductal adenocarcinoma) cells were implanted subcutaneously in ENT1-KO compared to WT mice (Fig. 2a–c). Average adenosine concentrations measured in tumor interstitial fluid were above 200 μ M, highlighting the relevance of these models in studying adenosine pathway targets (Fig. 2d). The improved control



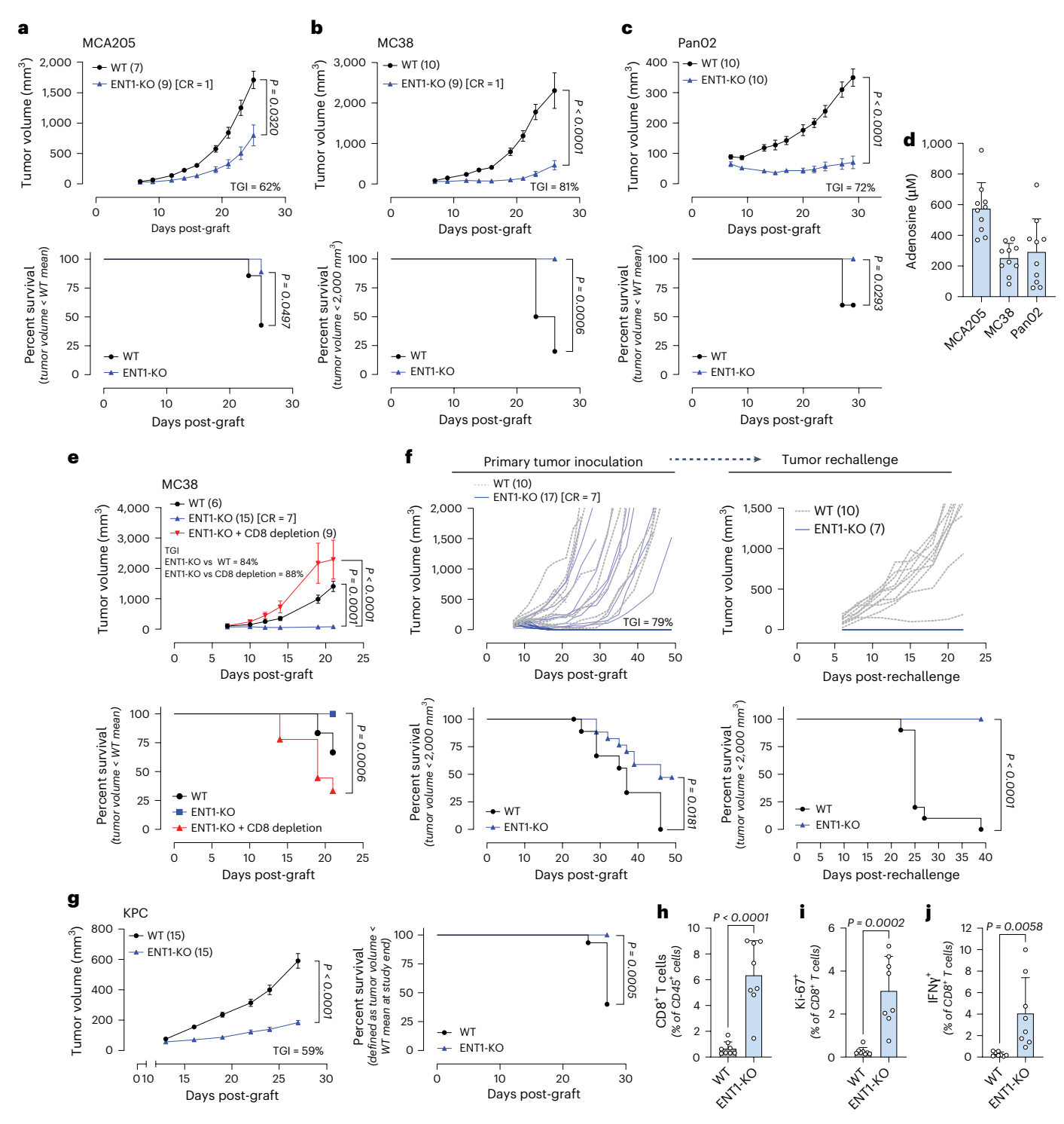


Fig. 2 | ENT1 deficiency leads to strong anti-tumor immunity in various mouse cancer models. a-c, Tumor growth curves and survival (defined as tumor volume less than the lower of WT mean at study end or 2,000 mm³) analysis of MCA205 (a), MC38 (b) and Pan02 (c) subcutaneous tumors in WT and ENT1-KO mice from one experiment for each model. Number of mice with complete tumor regression (CR) noted where relevant. TGI, tumor growth inhibition. d, Adenosine concentrations in tumor interstitial fluid derived from MCA205, MC38 and Pan02 subcutaneous tumors implanted in WT mice (n=10 in all cases), as indicated. Symbols represent individual mice; bars represent group mean value; error bars, s.d. e, MC38 tumor growth curves and survival (defined as tumor volume less than WT mean at study end) analysis in WT, ENT1-KO mice and ENT1-KO mice following CD8+T cell depletion. f, Tumor growth curves and survival (defined as tumor volume of <2,000 mm³) analysis of rechallenge experiments following MC38 tumor growth in WT and ENT1-KO mice with

primary inoculation and secondary inoculation in n=7 complete regressors from the ENT1-KO group. Representative of two experiments. ${\bf g}$, Tumor growth curves and survival (defined as tumor volume less than WT mean at study end) analysis of KPC subcutaneous tumors in WT and ENT1-KO mice from one experiment. ${\bf h}$ - ${\bf j}$, Profiling of CD8* T cell infiltration (${\bf h}$), Ki-67 expression (${\bf i}$) and IFN ${\bf y}$ production (${\bf j}$) following ex vivo restimulation of CD8* TILs of WT and ENT1-KO mice bearing KPC tumors (see also Supplementary Fig. 2). Mean values displayed; error bars, s.d. P values from two-tailed unpaired t-test, n=8 per group from one experiment. In ${\bf a}$ - ${\bf c}$, ${\bf e}$ and ${\bf g}$, mean values are displayed; error bars, s.e.m.; P values are from two-way ANOVA of log-transformed tumor volumes with Šídák's multiple comparisons test on days 25, 26, 29, 21 and 27, respectively. Kaplan-Meier survival analysis with log-rank (Mantel-Cox) test (${\bf a}$ - ${\bf c}$, ${\bf e}$ - ${\bf g}$) corrected for multiple comparisons with the Bonferroni method (${\bf e}$). All mice were C57BL/6 females, 8 weeks of age at tumor inoculation.

of MC38 tumor growth observed in ENT1-KO mice was lost upon depletion of CD8 $^{\scriptscriptstyle +}$ T cells (Fig. 2e), and ENT1-KO mice with complete tumor regression were resistant to secondary rechallenge, consistent with the induction of immunological memory (Fig. 2f). Growth of tumors derived from pancreatic ductal adenocarcinoma isolated from the autochthonous KPC mouse model (*LSL-Kras* $^{G12D/+}$; *LSL-Trp53* $^{R172H/+}$; Pdx-1-Cre) was significantly reduced in ENT1-KO versus WT mice (Fig. 2g); this was associated with an increased proportion of CD8 $^+$ T cells within the TME (Fig. 2h). Furthermore, the frequency of CD8 $^+$ T cells that were Ki-67 $^+$ and capable of producing IFN γ was also increased in tumors that formed in ENT1-KO mice compared to those that formed in WT mice (Fig. 2i,j). Taken together, these data show that adenosine levels are high in the TME and suggest that ENT1 allows uptake of adenosine by T cells, leading to suppression of anti-tumor immune responses independent of $A_{2A}R$ signaling.

Adenosine inhibits de novo pyrimidine synthesis in T cells

To understand how increased intracellular adenosine suppresses T cell responses, we considered the principal metabolic fates of adenosine following uptake into cells: deamination to inosine by ADA or phosphorylation to AMP by adenosine kinase (AdK)⁵. Patients with loss-of-function mutations in ADA have severe lymphopenia¹⁹, and CD4⁺ T cells from these individuals display diminished proliferation¹⁰. Therefore, we reasoned that the suppressive effect of adenosine may lie downstream of its conversion to AMP. Consistent with this hypothesis, the AdK inhibitor ABT-702 (ref. 20) completely restored the proliferation of CD8⁺ T cells activated with anti-CD3/CD28 in the presence of 50 μ M adenosine (Fig. 3a,b). The EC₅₀ for the rescue of activated CD8⁺ T cell proliferation by ABT-702 was 23.8 nM (Fig. 3c).

The pyrimidine nucleosides uridine and cytidine (also substrates for ENT1 (ref. 21)) did not suppress T cell proliferation. However, uridine restored adenosine-mediated inhibition of T cell proliferation (EC₅₀ = $1.1 \,\mu\text{M}$), an effect that was not observed with cytidine (Fig. 3d-f). Human T cells lack cytidine deaminase²², which limits uridine regeneration from cytidine. The inability of cytidine to rescue adenosine-mediated suppressive effects argues against uridine acting through competitive inhibition of adenosine transport. Developing effector T cells are vulnerable to pyrimidine starvation shortly after activation²³, suggesting that high adenine nucleotide levels might impair the ability of T cells to acquire sufficient pyrimidines. To test this hypothesis, we profiled the effect of adenosine on metabolites in human T cells 24 h after activation. At this time point, there was an increase in the levels of carbamoyl aspartate, dihydroorotate (DHO) and orotate in adenosine-treated T cells relative to vehicle controls (Fig. 3g). These metabolites are upstream of reactions catalyzed by uridine monophosphate synthase (UMPS) to generate pyrimidines (Fig. 3h), whereas all metabolites downstream of this enzyme were dose-dependently depleted in adenosine-treated cells (Fig. 3g). These data suggest that adenosine inhibits de novo pyrimidine synthesis in human T cells at the level of UMPS. Indeed, the adenosine metabolites AMP^{24,25} and uric acid²⁶ are known inhibitors of UMPS, acting through inhibition of the OMP decarboxylase domain. Dose-dependent increases in all adenosine metabolites were observed in adenosine-treated versus dimethylsulfoxide (DMSO)-treated T cells (Fig. 3i). The relative increase in ATP levels exceeded that of ADP or AMP, arguing against depletion of the ATP/AMP ratio as an indicator of 'energy stress' with resulting inhibition of the mammalian target of rapamycin (mTOR) pathway²⁷.

ENT1 inhibition with dilazep in adenosine-exposed cells increased the levels of uridine monophosphate (UMP), uridine diphosphate (UDP), uridine triphosphate (UTP) and cytidine triphosphate (CTP) relative to the untreated cells and reduced adenosine-driven increases in carbamoyl aspartate, DHO and orotate (Fig. 3j). This effect was not observed with inupadenant (Fig. 3k), consistent with an $A_{2A}R$ -independent effect of adenosine on pyrimidine biosynthesis. Inhibition of AdK with ABT-702 also restored pyrimidine metabolism in

the presence of adenosine (Fig. 3k). These data suggest that AMP itself, or AMP-derived metabolites, mediate the intracellular suppressive effects of adenosine. Consistent with its effect on T cell proliferation, uridine supplementation normalized pyrimidine levels in activated T cells exposed to high levels of adenosine (Fig. 3k), as uridine can be salvaged to UTP in cells. UTP feedback inhibits the carbamoyl phosphate synthetase activity of CAD²⁸, the first step in de novo pyrimidine synthesis, and probably explains why uridine supplementation also suppresses adenosine-driven accumulation of pyrimidine synthesis pathway metabolites.

ENT1 antagonist EOS301984 protects T cells from adenosine

We set out to develop an ENT1 antagonist with properties optimized to limit human T cell uptake of adenosine despite high levels found within the TME. EOS301984 (ref. 29) was found to be a more potent ENT1 antagonist than dilazep, with over 150-fold selectivity for ENT1 versus ENT2 (Fig. 4a and Extended Data Fig. 4a) and little to no inhibitory activity against ENT4 or CNT1, CNT2 or CNT3 (Extended Data Fig. 4b-e). EOS301984 inhibited adenosine uptake into activated human T cells with sub-nanomolar potency and restored T cell proliferation both in the presence of adenosine and also dose-dependently in the presence of ATP acting as a source of adenosine (Fig. 4b-d), with increased potency compared to dilazep. The K_d values for EOS301984 binding to human and mouse ENT1 were 0.5 nM (Extended Data Fig. 4f-j) and 14.4 nM (Extended Data Fig. 4k-o), respectively, indicating that EOS301984 is optimized for binding to human ENT1. EOS301984 dose-dependently increased the levels of UMP, UDP, UTP and CTP in adenosine-treated T cells while also reducing adenosine-driven increases in carbamoyl aspartate, DHO and orotate (Fig. 4e). Finally, we observed that adenosine exposure reduced mitochondrial respiration in activated human T cells (Fig. 4f,g). This impaired respiration could be rescued by treatment with EOS301984, while EOS301984 treatment alone had no effect on mitochondrial respiration. By contrast, the A_{2A}R antagonist inupadenant did not reverse the suppressive effect of adenosine on mitochondrial respiration in activated T cells (Fig. 4h), consistent with intracellular adenosine causing the effect on mitochondrial respiration.

We next evaluated whether EOS301984 could reverse the ENT1-dependent intracellular suppressive effects of adenosine in a physiologically relevant system. Peripheral blood mononuclear cells (PBMCs), obtained from healthy volunteer blood donors with a history of cytomegalovirus (CMV) infection, were stimulated in vitro with the peptide NLVPMVATV derived from the immunodominant CMV antigen pp65, and the proportion of antigen-specific CD8⁺ T cells in the population was determined using tetramer staining. In the absence of peptide stimulation, the frequency of such cells was below 1%. Culture with the peptide together with a dosing regimen of IL-7 and IL-2 led to an increase in the percentage of peptide-specific CD8⁺T cells (Extended Data Fig. 5a). Although the majority of tetramer CD8 T cells were ENT1^{-/lo} and Ki-67⁻, tetramer⁺ CD8⁺ T cells were universally ENT1⁺ and Ki-67⁺ (Extended Data Fig. 5b). Inclusion of ATP in the cultures to mimic high levels of TME-derived adenosine led to profound suppression of tetramer + CD8 + T cell expansion (Fig. 4i-j). EOS301984 partially reversed adenosine-mediated suppression of tetramer⁺ CD8⁺T cell expansion, which was further improved by combination with anti-PD-1 (Fig. 4i, j). Although anti-PD-1 alone boosted the expansion of the tetramer CD8 T cell population in the absence of ATP in two out of three donors, its stimulatory activity was blunted in the presence of ATP. Analysis of the frequency of IFNy-producing T cells within the PBMC cultures upon stimulation with the NLVPMVATV peptide revealed that ATP reduced the frequency of such cells, and the effects were reversed by EOS301984 (Fig. 4k and Extended Data Fig. 5c). There was also a trend toward a further increase in the frequency of IFNy⁺ cells in the EOS301984-anti-PD-1 combination group. By contrast, no restoration was observed in the absence of EOS301984, with broadly similar findings also observed for granzyme B (Extended Data Fig. 5d,e), indicating

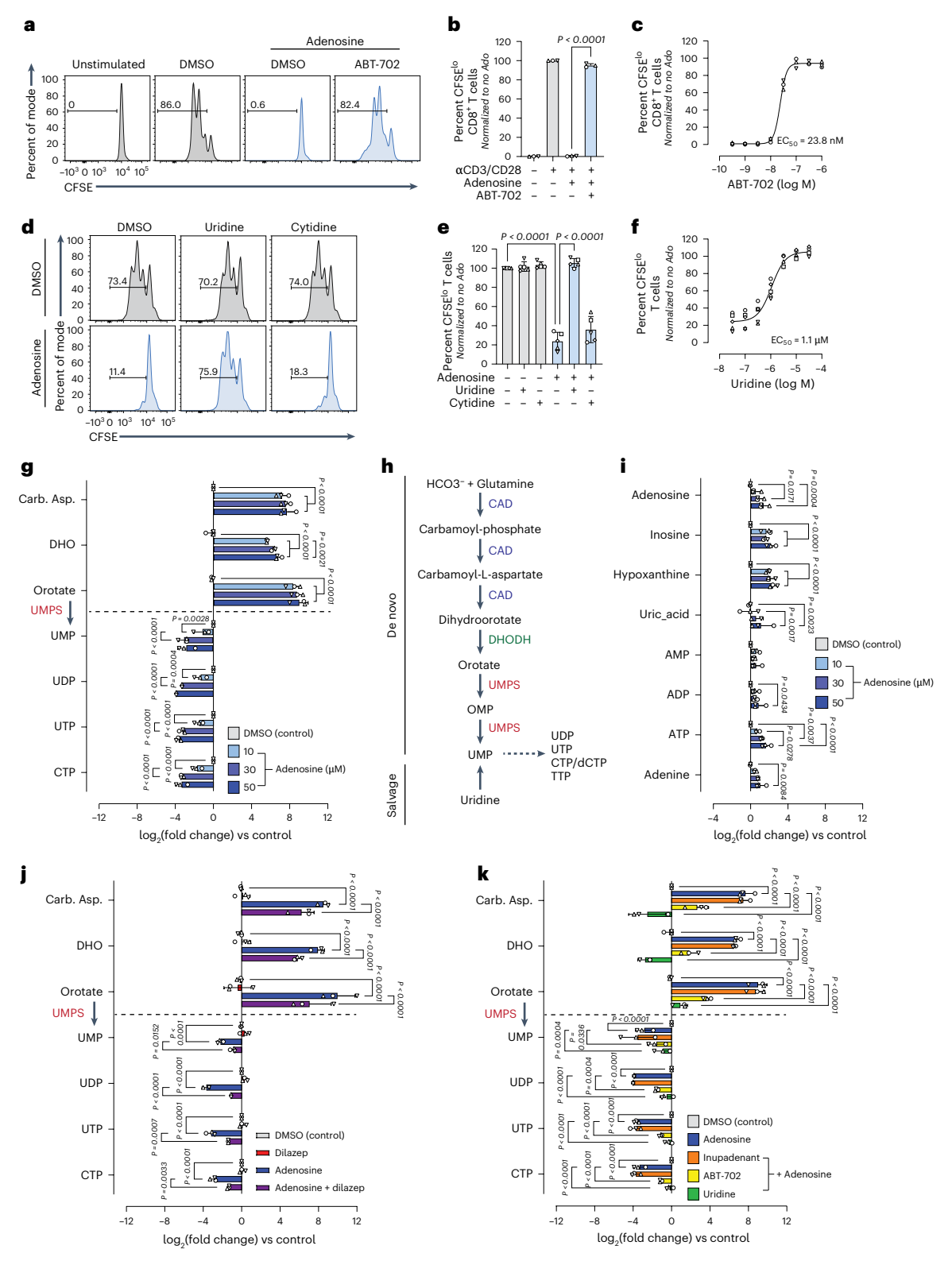


Fig. 3 | Adenosine inhibits pyrimidine synthesis in T cells following uptake by ENT1. a, CD8 $^{+}$ T cell proliferation in the presence of adenosine (50 μ M) \pm AdK inhibitor ABT-702 (300 nM). Representative example from three donors shown. b, Summary data from a. c, Dose–response curve of CD8 $^{+}$ T cell proliferation rescue effect of ABT-702 with a fixed dose of adenosine (50 μ M). d, T cell proliferation in the presence of adenosine \pm uridine or cytidine (all 30 μ M). Representative example from five donors shown. e, Summary data from d. f, Dose–response curve of T cell proliferation rescue effect of uridine with a fixed dose of adenosine (30 μ M). g, Pyrimidine metabolite levels in adenosine-

treated relative to DMSO-treated activated human T cells. **h**, Summary of de novo pyrimidine synthesis pathway. **i**, Analysis of purine metabolites in T cells activated for 24 h in the presence of increasing concentrations of adenosine. **j**,**k**, Pyrimidine metabolite levels in activated human T cells treated with adenosine and/or dilazep (**j**) or additional reagents as indicated (**k**). Symbols represent each of the n = 3 (**b**,**c**,**g**,**i**-**k**) or n = 5 (**e**,**f**) donors; bars are group means; error bars, s.d. (**b**,**e**,**g**,**i**-**k**) with two-way ANOVA with Tukey's multiple comparisons test (**b**,**e**) or mixed-effects model with Tukey's multiple comparisons test (**g**,**i**-**k**).

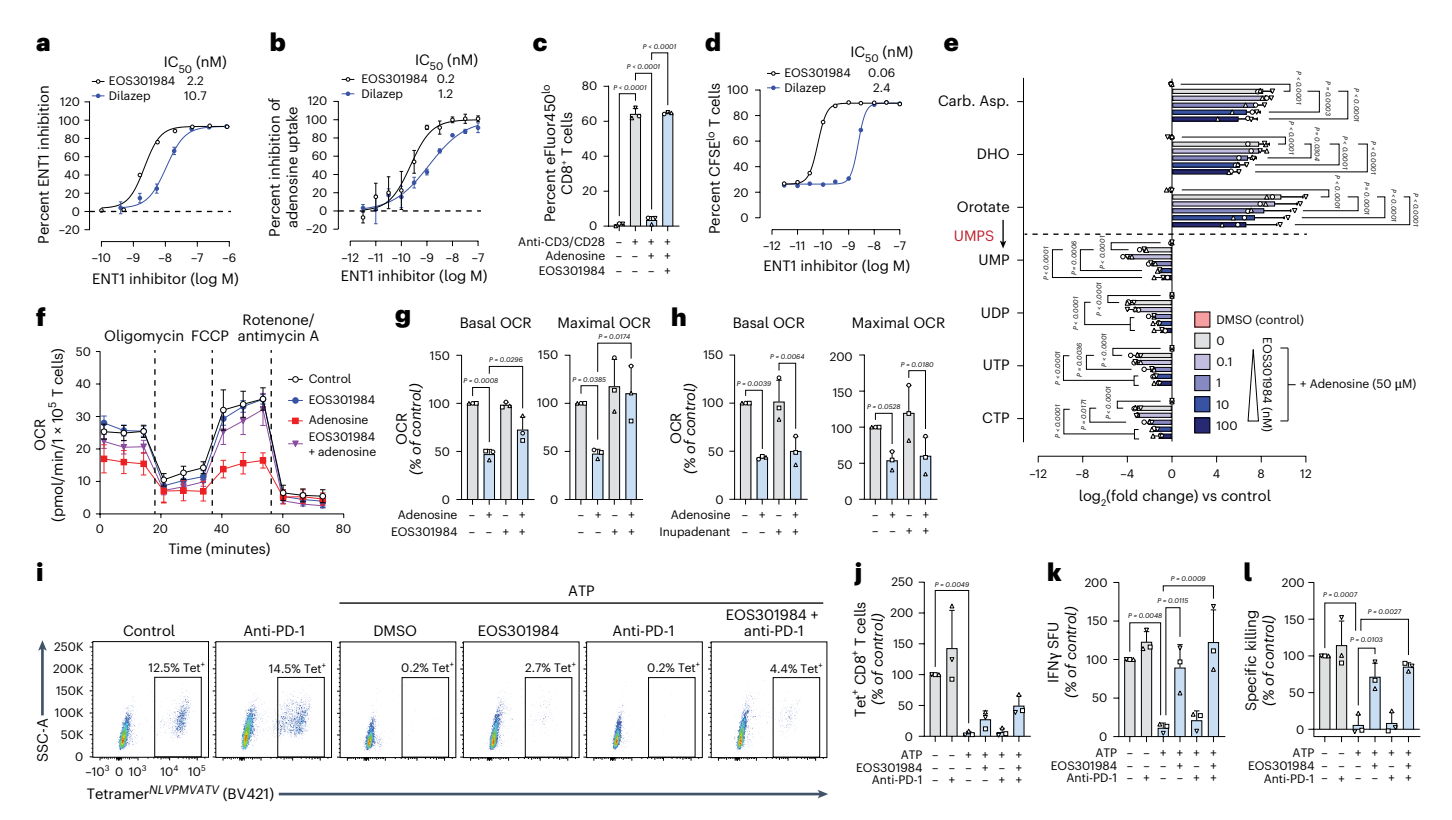


Fig. 4 | **EOS301984 inhibits ENT1 to restore T cell expansion in high-adenosine environments. a**, Percent inhibition of ENT1 in a transporter assay by dose ranges of EOS301984 or dilazep. Mean values from technical replicates (n = 2 and 4, respectively) are displayed; error bars, s.d. **b**, Percent inhibition of adenosine uptake by T cells preactivated in the presence of EOS301984 or dilazep. Mean values from n = 3 donors are displayed; error bars, s.d. **c**, Rescue of T cell proliferation by EOS301984 (300 nM) in the presence of adenosine (100 μM). **d**, Rescue of T cell proliferation by EOS301984 and dilazep in the presence of ATP (100 μM). Mean values from technical duplicates, representative of nine donors. **e**, Pyrimidine metabolite levels in activated human T cells treated with adenosine (50 μM) and EOS301984 relative to DMSO-treated cells. **f**, Seahorse Mito Stress Test analysis of T cell oxygen consumption rate (OCR) following 24 h CD3/CD28 activation in the presence or absence of adenosine (50 μM) and EOS301984

(100 nM). Mean values from n=4 technical replicates are displayed; error bars, s.d. Representative example of n=3 donors. ${\bf g}$, Summary of basal and maximal OCR from experiments performed as in ${\bf f}$. ${\bf h}$, Seahorse Mito Stress Test analysis of T cell OCR following 24 h CD3/CD28 activation in the presence of adenosine (50 μ M) and inupadenant (300 nM), as indicated. ${\bf i}$, CMV pp65 antigen recall assay performed in the presence of exogenous ATP as a source of adenosine and the indicated reagents. Representative of three donors. ${\bf j}$, Summary data from ${\bf i}$. ${\bf k}$, FluoroSpot analysis of IFN γ production from PBMC cultures as performed in ${\bf i}$. ${\bf i}$, Antigen-specific killing activity of PBMC cultures as performed in ${\bf i}$ and normalized to the levels observed in the absence of ATP as a reference control. Symbols represent each of the n=3 donors (biological replicates); bars are group means; error bars, s.d.; P values are from two-way ANOVA with Tukey's multiple comparisons test (${\bf c}$, ${\bf e}$, ${\bf p}$, ${\bf j}$.

that ENT1 inhibition enhances antigen-specific functional T cell expansion in high-adenosine environments.

PBMC preparations enriched for NLVPMVATV-specific CD8⁺T cells were co-cultured with T2 cells that had been pulsed (eFluor450^{lo}) or not (eFluor450^{hi}) with the NLVPMVATV peptide (Extended Data Fig. 6a). Co-culture with enriched PBMC preparations led to specific killing of the antigen-pulsed subset (Extended Data Fig. 6b), with the caveat that non-specific cell death was also observed in both antigen-pulsed and non-pulsed T2 cells. Given donor-to-donor variation in PBMCs, we normalized specific killing to the reference condition in the absence of ATP to establish the relative, normalized changes with experimental conditions. In conditions for which 'specific killing' is increased relative to this reference control, such as PD-1 blockade, normalized values can exceed 100% (raw data available for review in Supplementary Fig. 3). Inclusion of ATP during the expansion phase of the cultures reduced overall antigen-specific killing by the PBMC population compared to the control sample (Fig. 4l and Extended Data Fig. 6c,d). In the absence of ATP, anti-PD-1 did not have a clear effect on the killing capacity of these cells. EOS301984 restored killing across all samples tested in the presence of ATP, with a trend towards the combination of EOS301984 and anti-PD-1 as having the greatest restorative effect overall (Fig. 41 and Extended Data Fig. 6c,d). The frequency of tetramer + CD8 + cells was positively correlated with antigen-specific killing activity (Extended Data Fig. 6e). However, the correlation was stronger between production of the cytokines IFNy or granzyme B and killing activity (Extended Data Fig. 6f,g and see also Supplementary Fig. 3), with IFNy providing the strongest overall correlation ($R^2 = 0.82, P < 0.0001$), illustrating the association between IFNy production and the tumor-cell-killing capacity of T cells. The near complete restoration of T cell function by EOS301984 despite the more partial effect on expansion of antigen-specific T cells suggests that although other factors, such as chronic extracellular adenosine exposure, may influence T cell proliferation, intracellular adenosine exerts a substantial ENT1-dependent effect on T cell activity. Owing to cell number limitations in the CMV antigen recall assay, direct comparison of EOS301984 alongside the ENT1 antagonist dilazep (as performed in Fig. 4a,b,d) was not feasible. These data demonstrate that EOS301984 can protect T cells from the ENT1-dependent suppressive effects of adenosine and can promote antigen-specific and functional T cell expansion in high-adenosine environments.

EOS301984 counteracts adenosine suppression of TIL function

We reasoned that the effect of high adenosine concentrations within the TME on T cells would depend on T cell-specific expression of ENT1. Therefore, we used flow cytometry to profile ENT1 expression

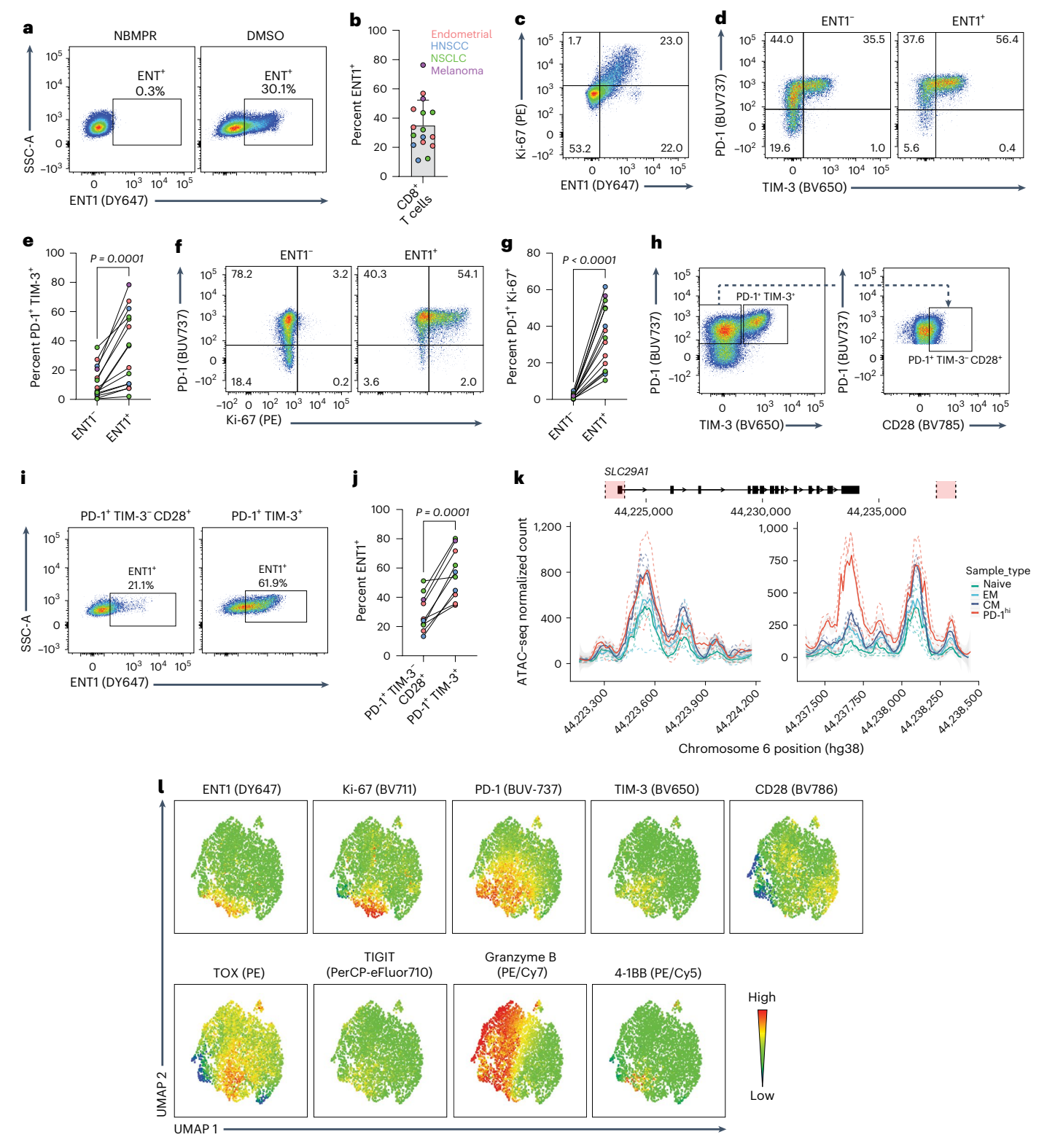


Fig. 5 | CD8 $^+$ TILs express ENT1, which is associated with an activated and proliferative phenotype. a, ENT1 staining on CD8 $^+$ TILs from dissociated human tumors, representative of 16 donors. An example gating strategy is provided in Supplementary Fig. 4. b, Summary data of percent ENT1 $^+$ CD8 $^+$ TILs as in a. Symbols represent each of the n=16 donors, bar is group mean; error bars, s.d. c, Example of co-expression of ENT1 and Ki-67 in CD8 $^+$ TILs. d, Expression of PD-1 and TIM-3 on pre-gated ENT1 $^+$ and ENT1 $^-$ CD8 $^+$ T cells. e, Analysis of percent PD-1 $^+$ TIM-3 $^+$ cells on pre-gated ENT1 $^+$ and ENT1 $^-$ CD8 $^+$ T cells. f, Expression of PD-1 and Ki-67 on pre-gated ENT1 $^+$ and ENT1 $^-$ CD8 $^+$ T cells. g, Analysis of percent

PD-1* Ki-67* cells on pre-gated ENT1* and ENT1* CD8* T cells. **h**–**j**, Identification of PD-1* TIM-3* (**h**) and PD-1* TIM-3* (**i**) CD28* CD8* T cell subsets, ENT1 expression within each subset and summary data (**j**). **k**, ATAC–seq normalized counts for regions in the SLC29AI promoter in PD-1* CD8* TILs and naive, central (CM) and effector memory (EM) CD8* T cells from healthy donors. **l**, Uniform manifold approximation and projection (UMAP) analysis of CD8* TILs. Pooled data from n = 9 donors. Data from n = 16 (**b**), n = 15 (**e**,**g**) and n = 10 (**j**) tumor samples (biological replicates) with analysis by two-tailed paired t-test (**e**,**g**,**j**).

in T cells from surgically resected endometrial carcinoma, head and neck squamous cell carcinoma, non-small cell lung cancer (NSCLC) and melanoma samples. ENT1 expression was identified on a subset of CD8 $^{+}$ T cells across all samples studied (Fig. 5a,b), with an overall mean value of 34.9 \pm 17.5% of CD8 $^{+}$ TILs defined as ENT1 $^{+}$ and with consistent co-staining with Ki-67 (Fig. 5c). ENT1 expression was also observed on CD4 $^{+}$ T cells and was enriched in FOXP3 $^{+}$ regulatory T (T $_{\rm reg}$) cells (Extended Data Fig. 7a,b).

Antigen-specific activation of CD8⁺ TILs is associated with a transition from a 'stem-like' memory cell state with a PD-1⁺TIM-3⁻CD28⁺ phenotype to a state of 'terminal differentiation', indicated by co-expression of PD-1 and TIM-3 (refs. 30,31). Although this transition renders T cells less sensitive to subsequent stimulation³², expansion of pre-existing CD8⁺ TIL populations is associated with clinical response to anti-PD-1 (ref. 33). A greater frequency of ENT1+CD8+T cells were PD-1⁺TIM-3⁺ compared to their ENT1⁻ counterparts (Fig. 5d,e). The ENT1⁺ subset also contained a greater frequency of PD-1⁺ Ki-67⁺ cells (Fig. 5f,g), while an enhanced fraction of PD-1*TIM-3* CD8* TILs cells were ENT1⁺ compared to their PD-1⁺TIM-3⁻ CD28⁺ counterparts (Fig. 5h-j). Analysis of published assay for transposase-accessible chromatin followed by sequencing (ATAC-seq) data³⁴ identified a region of selectively increased chromatin accessibility downstream of the SLC29A1 gene locus in CD8⁺PD-1^{hi} TILs from melanoma and NSCLC patients compared with naive, central or effector memory CD8⁺T cells from healthy donors (Fig. 5k). Therefore, ENT1 is mostly expressed on the specific subpopulation of TILs that expands upon and is associated with clinical response to anti-PD-1 therapy.

Single-cell analysis of CD8⁺T cells from nine pooled samples confirmed consistent overlap between ENT1, Ki-67, PD-1 and TIM-3 expression, as well as TIGIT, an inhibitory immunoreceptor associated with 'exhausted' TILs³⁵ (Fig. 51). Furthermore, this cluster also expressed TOX, a transcription factor associated with 'late dysfunctional' or 'terminally differentiated' TILs36 and was low for CD28 expression, indicative of chronic activation³⁷. A subset of the ENT1⁺ cluster was positive for 4-1BB, a member of the TNF receptor superfamily that has been used to identify tumor neoantigen-specific CD8⁺T cells^{38,39}. These data indicate that ENT1 expression is associated with a proliferating and terminally differentiated state among CD8⁺T cells within tumors. Similar analysis of CD4⁺ T cells revealed a clear distinction between FOXP3⁺ T_{reg} cells and non-T_{reg} CD4⁺ cells (Extended Data Fig. 7c), where ENT1⁺ subsets expressed CD28, PD-1, TIGIT and TOX. Overall, these data indicate that ENT1 is expressed on CD8⁺ as well as CD4⁺ TILs, where it is closely linked with activation and proliferation of these cells in situ.

We next evaluated whether chronic adenosine exposure would suppress the expansion and function of tumor-infiltrating T cells upon activation and whether this could be prevented with EOS301984. CD3/ CD28 microbeads induced robust proliferation of CD8⁺ and CD4⁺T cells from dissociated tumors, which was strongly suppressed when ATP was supplemented into the cultures (Fig. 6a-c). Despite the lack of proliferation, the adenosine-suppressed T cells still upregulated ENT1. Inclusion of EOS301984 restored T cell proliferation in the presence of ATP, which was not further enhanced by the presence of anti-PD-1 (Fig. 6a-c). Production of cytokines associated with cytotoxic T cell function was also suppressed by ATP, and all were restored, to varying extents, by EOS301984 (Fig. 6d-i). Production of TNF was further enhanced when EOS301984 was combined with anti-PD-1 (Fig. 6d). Percent rescue was determined using vehicle treatment as a reference for normal T cell function (100%) and ATP treatment as a reference for suppressed T cell function (0%). This normalization approach was used to account for donor variation in T cell activity and to highlight the effects of EOS301984 in the context of ATP-derived adenosine suppression (raw data available in Supplementary Fig. 6). Ex vivo stimulation of 'terminally differentiated' PD-1⁺TIM-3⁺CD39⁺CD8⁺T cells⁴⁰ isolated from a NSCLC sample led to an increased fraction of cells producing IFNy and granzyme B, which was suppressed by adenosine and restored

with EOS301984 (Extended Data Fig. 8). These data are consistent parallel stimulations of peripheral blood CD8⁺T cells (Extended Data Fig. 8). indicating that EOS301984 restores cytokine production by T cells within tumors, including those characterized as 'terminally differentiated' or 'exhausted', in the presence of high adenosine concentrations. To better understand the influence of adenosine on the transition of TILs to terminal differentiation and exhaustion, we stimulated PD-1⁻ CD8⁺ TILs isolated from resected NSCLC samples ex vivo. The induction of a PD-1⁺TIM-3⁺ and TOX⁺ phenotype amongst these cells was reduced by adenosine, with a restorative effect in the presence of EOS301984 (Fig. 6j). This suggests that although adenosine limits the response of TILs to activation, including the transition to terminal differentiation, ENT1 inhibition with EOS301984 restores this process. Thus, T cells within tumors increase ENT1 expression upon activation, rendering them vulnerable to suppressive effects of adenosine uptake, including limiting expansion and cytokine production following activation. Notably, the effects of high adenosine are mitigated by pharmacological inhibition of ENT1.

We assessed the ability of EOS301984 to reduce the growth of the anti-PD-1-resistant tumor model MD-MBA-231 in humanized mice, favoring the humanized setting because of the lower affinity of EOS301984 for mouse ENT1. Although both EOS301984 and anti-PD-1 had limited independent efficacy in this model, the combination of both agents synergistically limited tumor growth compared to either compound alone (Fig. 6k). Overall, these data indicate that inhibiting ENT1 with EOS301984 can improve the efficacy of immune checkpoint blockade therapies in cancer.

Discussion

Expanding the benefits of immunotherapy to more patients will require a deep understanding of the factors suppressing natural anti-tumor immune responses. Modulating the immunosuppressive effects of adenosine in the TME through inhibition of $A_{\rm 2A}R$ or $A_{\rm 2B}R$ signaling or by limiting adenosine generation by blocking CD39 or CD73 (ref. 5) are both approaches under clinical investigation. Notably, the anti-CD73 antibody oleclumab in combination with the anti-PD-L1 antibody durvalumab demonstrated a higher response rate and prolonged progression-free survival compared to durvalumab alone in patients with unresectable stage III NSCLC⁴¹. Modulating the adenosine pathway, therefore, has the potential to improve clinical responses to anti-PD(L)-1; however, redundancy of enzymes generating extracellular adenosine remains a hurdle for agents inhibiting specific ectoenzymes, and these may not reveal the full potential of blocking the immunosuppressive effects of adenosine.

Here, we report a mechanism whereby intracellular adenosine mediates immunosuppression by inhibiting pyrimidine synthesis in T cells. This involves adenosine uptake through ENT1, given that blocking the transporter rescued pyrimidine nucleotide levels and T cell expansion and effector function in vitro. Activation of effector T cells is associated with increased de novo pyrimidine synthesis, which is required for proliferation^{42–44}. Moreover, inhibition of DHODH, a critical enzyme for de novo pyrimidine synthesis, limits the expansion of functional effector T cells²³. Exposure to intracellular adenosine within the TME may therefore phenocopy DHODH inhibition in T cells, resulting in compromised anti-cancer effector T cell responses. Indeed, the growth of multiple syngeneic tumors was significantly reduced in ENT1-KO mice, which was associated with increased T cell infiltration, proliferation and effector function in the TME, even in the immune desert KPC tumor model⁴⁵.

We developed and characterized the potent ENT1 antagonist EOS301984, which restores expansion of functional TILs in high-adenosine environments. A limitation of the current study is that EOS301984 is optimized for human versus mouse ENT1 inhibition, restricting the ability to characterize the effects of pharmacological inhibition of ENT1 in murine syngeneic tumor models. Therefore, we

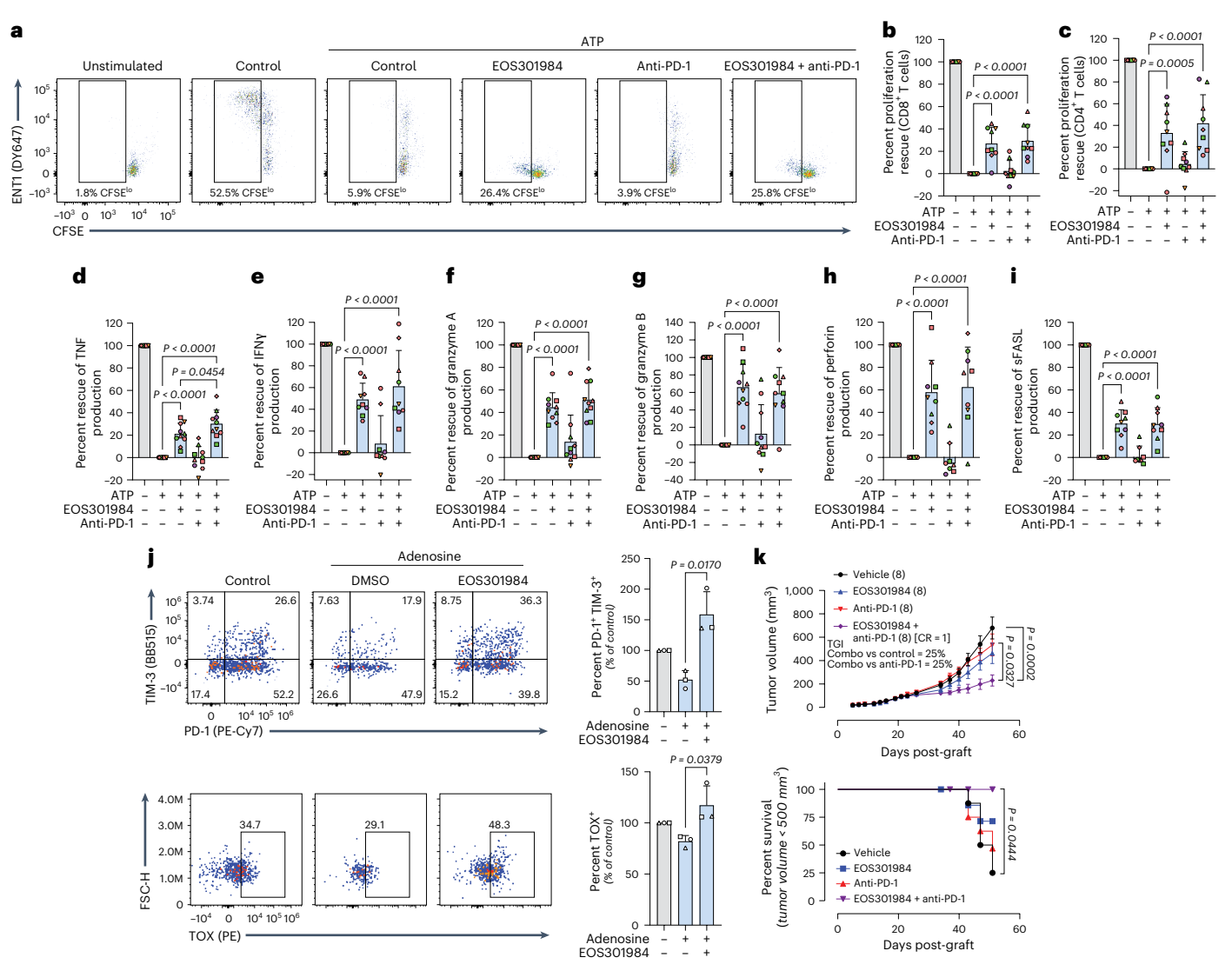


Fig. 6 | **Adenosine suppresses TIL function, which is restored by EOS301984. a**, Proliferation of CD8 $^+$ T cells in dissociated tumor cell suspensions in the presence of ATP as a source of high adenosine concentrations and EOS301984 and anti-PD-1 as indicated. Representative example from n = 9 donors. An example gating strategy is provided in Supplementary Fig. 5. \mathbf{b} - \mathbf{i} , Summary data of EOS301984-mediated rescue of CD8 $^+$ (\mathbf{b}) and CD4 $^+$ (\mathbf{c}) T cell proliferation, TNF (\mathbf{d}), IFN γ (\mathbf{e}), granzyme A (\mathbf{f}), granzyme B (\mathbf{g}), perforin (\mathbf{h}) and sFASL (\mathbf{i}) production from dissociated tumor cell suspension cultures. Rescue refers to the degree to which adenosine-mediated suppression has been reversed. \mathbf{j} , FACS analysis of TIM-3, PD-1 and TOX expression by PD-1 $^-$ CD8 $^+$ TILs isolated from NSCLC tumor samples, stimulated with anti-CD3/CD28 microbeads for 72 h in the

presence of reagents as indicated. **k**, Tumor growth curves and survival (defined as tumor volume of <500 mm³) analysis of female NCG mice bearing MDA-MB-231 subcutaneous tumors (aged 18 weeks at inoculation) treated with anti-PD-1, EOS301984 or a combination of both. Mean values from one experiment are displayed; error bars, s.e.m.; n=8 mice per group. Two-way ANOVA of log-transformed tumor volumes with Šídák's multiple comparisons test, P values are displayed for day 51. Kaplan–Meier survival analysis with log-rank (Mantel–Cox) test, P values corrected for multiple comparisons with the Bonferroni method. Symbols represent each donor (biological replicates), from n=9 (**b,c,e,h,i**), n=10 (**d,f,g**) and n=3 (**j**) tumor samples. Bars are group means; error bars, s.d.; analysis by two-way ANOVA with Tukey's multiple comparisons test (**b-i,j**).

assessed its activity in a humanized mouse model of triple-negative breast cancer resistant to anti-PD-1 blockade, where it synergized with anti-PD-1 therapy to delay tumor growth.

ENT1 expression was enriched in human CD8⁺ TILs expressing Ki-67, PD-1 and TIM-3, consistent with a proliferating and chronically activated phenotype associated with tumor antigen-specific T cells⁴⁶. Clinical response to anti-PD-1 therapy is associated with increased proliferation of CD8⁺ T cells within the TME³³ and a stem-like memory to a terminally differentiated trajectory^{31,47,48}. ENT1 co-expression on PD-1⁺ TILs would expose these cells to the immunosuppressive effects of intracellular adenosine when levels of adenosine are high, restricting the ability of anti-PD-1 therapy to perform to its full potential. Together, the data suggest that in response to activation, adenosine impedes proliferation as well as the normal differentiation and

function of T cells, including TILs, and also prevents the acquisition of markers associated with terminal differentiation and exhaustion. Inhibition of ENT1 with EOS301984 reverses these effects. These phenotypes could be explained by alterations in intracellular nucleotide balance, although changes in mitochondrial respiration may also contribute. Future studies using EOS301984 will enable further characterization of parameters of TIL exhaustion and effector function, an area that was constrained in this study owing to the inherently low recovery of TILs from human patient tumors. How intracellular adenosine limits the function of CD4⁺ T cells within the TME also remains a question for future work^{49–51}. Lastly, single-cell sequencing analysis of tumor-infiltrating immune cells confirms ENT1 expression at the mRNA level in a subset of T cell populations but also highlights the presence of ENT1 on other immune cell subsets, notably macrophages

(Extended Data Fig. 7d). ENT1 expression across other immune cells, as well as some cancer cells, suggest alternative contexts in which pharmacologic ENT1 inhibition could be beneficial to restrict tumor growth and should be explored in future humanized mouse studies, given the species-selectivity of EOS301984.

Overall, our data confirm that adenosine levels are high in many tumors, and we report a previously undescribed role for intracellular uptake of adenosine to block de novo pyrimidine nucleotide synthesis in T cells, leading to suppression of T cell expansion and effector functions. In the context of such increased extracellular adenosine, the confluence of environmental factors and metabolic wiring for nucleoside transport is maladaptive for both T cell proliferation and function. We identified ENT1 as an immunotherapy target and developed the potent ENT1 antagonist EOS301984. Inhibition of adenosine uptake with EOS301984 in combination with A24R antagonists could protect T cells from both intracellular and extracellular effects of adenosine and thus maximize TIL expansion and effector function in adenosine-rich TMEs. This may allow agents such as anti-PD-1 antibodies that support expansion of tumor antigen-specific CD8⁺T cells to be more effective at controlling adenosine-rich cancers (Extended Data Fig. 9). Based on these findings, EOS301984 is being evaluated in phase I clinical studies in patients with solid tumors.

Online content

Any methods, additional references, Nature Portfolio reporting summaries, source data, extended data, supplementary information, acknowledgements, peer review information; details of author contributions and competing interests; and statements of data and code availability are available at https://doi.org/10.1038/s41590-025-02153-3.

References

- Huang, A. C. & Zappasodi, R. A decade of checkpoint blockade immunotherapy in melanoma: understanding the molecular basis for immune sensitivity and resistance. *Nat. Immunol.* 23, 660–670 (2022).
- Yu, J. X. et al. Trends in clinical development for PD-1/PD-L1 inhibitors. Nat. Rev. Drug Discov. 19, 163–164 (2020).
- Sharma, P., Hu-Lieskovan, S., Wargo, J. A. & Ribas, A. Primary, adaptive, and acquired resistance to cancer immunotherapy. *Cell* 168, 707–723 (2017).
- Ohta, A. et al. A2A adenosine receptor protects tumors from antitumor Tcells. Proc. Natl Acad. Sci. USA 103, 13132–13137 (2006).
- Allard, B., Allard, D., Buisseret, L. & Stagg, J. The adenosine pathway in immuno-oncology. *Nat. Rev. Clin. Oncol.* 17, 611–629 (2020).
- Boison, D. & Yegutkin, G. G. Adenosine metabolism: emerging concepts for cancer therapy. Cancer Cell 36, 582–596 (2019).
- Blay, J., White, T. D. & Hoskin, D. W. The extracellular fluid of solid carcinomas contains immunosuppressive concentrations of adenosine. Cancer Res. 57, 2602–2605 (1997).
- 8. Buisseret, L. et al. Phase 1 trial of the adenosine A_{2A} receptor antagonist inupadenant (EOS-850): update on tolerability, and antitumor activity potentially associated with the expression of the A_{2A} receptor within the tumor. *J. Clin. Oncol.* **39**, 2562 (2021).
- Willingham, S. B., Hotson, A. N. & Miller, R. A. Targeting the A2AR in cancer; early lessons from the clinic. Curr. Opin. Pharmacol. 53, 126–133 (2020).
- Cassani, B. et al. Altered intracellular and extracellular signaling leads to impaired T-cell functions in ADA-SCID patients. *Blood* 111, 4209–4219 (2008).
- Flinn, A. M. & Gennery, A. R. Adenosine deaminase deficiency: a review. Orphanet J. Rare Dis. 13, 65 (2018).

- Robins, M. J. et al. Improved syntheses of 5'-S-(2-aminoethyl)-6-N-(4-nitrobenzyl)-5'-thioadenosine (SAENTA), analogues, and fluorescent probe conjugates: analysis of cell-surface human equilibrative nucleoside transporter 1 (hENT1) levels for prediction of the antitumor efficacy of gemcitabine. *J. Med. Chem.* 53, 6040–6053 (2010).
- 13. Yukawa, M. et al. AP-1 activity induced by co-stimulation is required for chromatin opening during T cell activation. *J. Exp. Med.* **217**, e20182009 (2019).
- Linnemann, C. et al. Adenosine regulates CD8 T-cell priming by inhibition of membrane-proximal T-cell receptor signalling. *Immunology* 128, e728–e737 (2009).
- Moser, G. H., Schrader, J. & Deussen, A. Turnover of adenosine in plasma of human and dog blood. *Am. J. Physiol.* 256, C799–C806 (1989).
- Chiarella, A. M., Tyu, Y. K., Manji, G. A. & Rustgi, A. K. Extracellular ATP and adenosine in cancer pathogenesis and treatment. *Trends Cancer* 7, 731–750 (2021).
- 17. Mikdar, M. et al. The equilibrative nucleoside transporter 1 (ENT1) is critical for nucleotide homeostasis and optimal erythropoiesis. *Blood* **137**, 3548–3562 (2021).
- Rose, J. B. et al. Absence of equilibrative nucleoside transporter 1 in ENT1 knockout mice leads to altered nucleoside levels following hypoxic challenge. *Life Sci.* 89, 621–630 (2011).
- Bradford, K. L., Moretti, F. A., Carbonaro-Sarracino, D. A., Gaspar, H. B. & Kohn, D. B. Adenosine deaminase (ADA)-deficient severe combined immune deficiency (SCID): molecular pathogenesis and clinical manifestations. *J. Clin. Immunol.* 37, 626–637 (2017).
- Lee, C.-H. et al. Discovery of 4-amino-5-(3-bromophenyl)-7-(6-morpholino-pyridin-3-yl)pyrido[2,3-d]pyrimidine, an orally active, non-nucleoside adenosine kinase inhibitor. J. Med. Chem. 44, 2133–2138 (2001).
- Ward, J. L., Sherali, A., Mo, Z.-P. & Tse, C.-M. Kinetic and pharmacological properties of cloned human equilibrative nucleoside transporters, ENT1 and ENT2, stably expressed in nucleoside transporter-deficient PK15 cells. ENT2 exhibits a low affinity for guanosine and cytidine but a high affinity for inosine. *J. Biol. Chem.* 275, 8375–8381 (2000).
- Scholar, E. M. & Calabresi, P. Identification of the enzymatic pathways of nucleotide metabolism in human lymphocytes and leukemia cells. *Cancer Res.* 33, 94–103 (1973).
- 23. Scherer, S. et al. Pyrimidine de novo synthesis inhibition selectively blocks effector but not memory Tcell development. *Nat. Immunol.* **24**, 501–515 (2023).
- Traut, T. W. & Jones, M. E. Inhibitors of orotate phosphoribosyl-transferase and orotidine-5'-phosphate decarboxylase from mouse Ehrlich ascites cells: a procedure for analyzing the inhibition of a multi-enzyme complex. *Biochem. Pharmacol.* 26, 2291–2296 (1977).
- Tax, W. J. M. & Veerkamp, J. H. Inhibition of orotate phosphoribosyltransferase and orotidine-5'-phosphate decarboxylase of human erythrocytes by purine and pyrimidine nucleotides. *Biochem. Pharmacol.* 28, 829–831 (1979).
- Cantor, J. R. et al. Physiologic medium rewires cellular metabolism and reveals uric acid as an endogenous inhibitor of UMP synthase. Cell 169, 258–272.e17 (2017).
- 27. Chi, H. Regulation and function of mTOR signalling in T cell fate decisions. *Nat. Rev. Immunol.* **12**, 325–338 (2012).
- 28. Jones, M. E. Pyrimidine nucleotide biosynthesis in animals: genes, enzymes, and regulation of UMP biosynthesis. *Annu. Rev. Biochem.* **49**, 253–279 (1980).
- 29. Deligny, M., Crosignani, S. & Houthuys, E. Macrocyclic diamine derivatives as ENT1 inhibitors for the treatment of cancers, and combination thereof with adenosine receptor antagonists. Patent WO/2021/204896 (2021).

- Fourcade, J. et al. Upregulation of Tim-3 and PD-1 expression is associated with tumor antigen–specific CD8⁺T cell dysfunction in melanoma patients. J. Exp. Med. 207, 2175–2186 (2010).
- Jansen, C. S. et al. An intra-tumoral niche maintains and differentiates stem-like CD8 Tcells. Nature 576, 465–470 (2019).
- 32. Blank, C. U. et al. Defining 'T cell exhaustion'. *Nat. Rev. Immunol.* **19**, 665–674 (2019).
- 33. Tumeh, P. C. et al. PD-1 blockade induces responses by inhibiting adaptive immune resistance. *Nature* **515**, 568–571 (2014).
- Philip, M. et al. Chromatin states define tumour-specific Tcell dysfunction and reprogramming. Nature 545, 452–456 (2017).
- Manieri, N. A., Chiang, E. Y. & Grogan, J. L. TIGIT: a key inhibitor of the cancer immunity cycle. *Trends Immunol.* 38, 20–28 (2017).
- Scott, A. C. et al. TOX is a critical regulator of tumour-specific Tcell differentiation. *Nature* 571, 270–274 (2019).
- Weng, N., Akbar, A. N. & Goronzy, J. CD28⁻ Tcells: their role in the age-associated decline of immune function. *Trends Immunol.* 30, 306–312 (2009).
- Parkhurst, M. et al. Isolation of T-cell receptors specifically reactive with mutated tumor-associated antigens from tumor-infiltrating lymphocytes based on CD137 expression. Clin. Cancer Res. 23, 2491–2505 (2017).
- Wolfl, M. et al. Activation-induced expression of CD137 permits detection, isolation, and expansion of the full repertoire of CD8⁺ T cells responding to antigen without requiring knowledge of epitope specificities. *Blood* 110, 201–210 (2007).
- 40. Eberhardt, C. S. et al. Functional HPV-specific PD-1* stem-like CD8 Tcells in head and neck cancer. *Nature* **597**, 279–284 (2021).
- 41. Herbst, R. S. et al. COAST: an open-label, phase II, multidrug platform study of durvalumab alone or in combination with oleclumab or monalizumab in patients with unresectable, stage III non-small-cell lung cancer. *J. Clin. Oncol.* **40**, 3383–3393 (2022).
- Fairbanks, L. D., Bofill, M., Ruckemann, K. & Simmonds, H. A. Importance of ribonucleotide availability to proliferating T-lymphocytes from healthy humans. Disproportionate expansion of pyrimidine pools and contrasting effects of de novo synthesis inhibitors. J. Biol. Chem. 270, 29682–29689 (1995).
- Quéméneur, L. et al. Differential control of cell cycle, proliferation, and survival of primary T lymphocytes by purine and pyrimidine nucleotides. J. Immunol. 170, 4986–4995 (2003).
- 44. Martin, E. et al. CTP synthase 1 deficiency in humans reveals its central role in lymphocyte proliferation. *Nature* **510**, 288–292 (2014).

- Li, J. et al. Tumor cell-intrinsic factors underlie heterogeneity of immune cell infiltration and response to immunotherapy. *Immunity* 49, 178–193.e7 (2018).
- 46. Oliveira, G. et al. Phenotype, specificity and avidity of antitumour CD8⁺T cells in melanoma. *Nature* **596**, 119–125 (2021).
- 47. Miller, B. C. et al. Subsets of exhausted CD8⁺ Tcells differentially mediate tumor control and respond to checkpoint blockade. *Nat. Immunol.* **20**, 326–336 (2019).
- Prokhnevska, N. et al. CD8⁺ T cell activation in cancer comprises an initial activation phase in lymph nodes followed by effector differentiation within the tumor. *Immunity* 56, 107–124.e5 (2023).
- 49. Alspach, E. et al. MHC-II neoantigens shape tumour immunity and response to immunotherapy. *Nature* **574**, 696–701 (2019).
- Seung, E. et al. A trispecific antibody targeting HER2 and Tcells inhibits breast cancer growth via CD4 cells. *Nature* 603, 328–334 (2022).
- Oh, D. Y. et al. Intratumoral CD4⁺ T cells mediate anti-tumor cytotoxicity in human bladder cancer. Cell 181, 1612–1625.e13 (2020).

Publisher's note Springer Nature remains neutral with regard to jurisdictional claims in published maps and institutional affiliations.

Open Access This article is licensed under a Creative Commons Attribution-NonCommercial-NoDerivatives 4.0 International License, which permits any non-commercial use, sharing, distribution and reproduction in any medium or format, as long as you give appropriate credit to the original author(s) and the source, provide a link to the Creative Commons licence, and indicate if you modified the licensed material. You do not have permission under this licence to share adapted material derived from this article or parts of it. The images or other third party material in this article are included in the article's Creative Commons licence, unless indicated otherwise in a credit line to the material. If material is not included in the article's Creative Commons licence and your intended use is not permitted by statutory regulation or exceeds the permitted use, you will need to obtain permission directly from the copyright holder. To view a copy of this licence, visit http://creativecommons.org/licenses/by-nc-nd/4.0/.

© The Author(s) 2025

Methods

Mice

ENT1-KO mice were generated upon request from Cyagen, using a C57BL/6J background. Specifically, a genomic region corresponding to exons 1–12 was deleted from the mouse genome through the application of CRISPR–Cas9 technology. To validate the KO, germ lines underwent downstream analysis, including DNA sequencing and protein detection using western blotting. The colony of ENT1-KO mice was established and maintained at Taconic Facilities in Denmark. Once established, the mice were transported to the animal facility at Université Libre de Bruxelles (ULB) for experimentation. For comparative purposes, 7–8-week-old WT C57BL/6J female mice were obtained from Taconic (Denmark).

Mice were housed under pathogen-free conditions at ULB facilities, following all animal guidelines set by FELASA (Federation of European Laboratory Animal Science Associations). Mice were maintained on 12 h light/dark cycles, and the housing facility was kept at 20–25 °C and 30–70% humidity. Mice were fed CRM (P) (DS801727G10R) from SDS Diets. Animal protocols underwent thorough review and received approval from the Institute of Animal Care and Use Committee at ULB (agreement LA-150055-18, project code BUC 2020-03).

Cell lines

CT26, HT29, A375, JAR, MDA-MB-231 and T2 cells were obtained from ATCC (American Type Culture Collection). MCA205 and MC38 cells were acquired from Sigma-Aldrich. KPC cells (clone 6419c5) were obtained from Kerafast. Pan02 cells were obtained from the National Cancer Institute Division of Cancer Treatment and Diagnosis Tumor Repository.

ENT1-KO JAR cells were generated using CRISPR-Cas9 technology, with delivery of the ribonucleoprotein complex to the JAR cells through Lipofectamine CRISPRMAX Cas9 Transfection Reagent. The specific single guide RNA (sgRNA) was designed to target exon 5, and its sequence was GCTCAGTTCAGCAGTGACCA. After 1 week of ribonucleoprotein delivery, the cells were stained with SAHENTA-DY647 dye to identify ENT1 expression, and the negative population was isolated through single-cell sorting by FACS. The resulting clones were subsequently expanded and subjected to validation through Sanger sequencing and western blotting.

MCA205-ENT2-KO cells were generated as described above using the sgRNA GCAAGCCAGCCTTTTTGGTC and GAGCTGTCAGAAAGCGCCTT to target exons 7 and 8, respectively.

All tumor cell lines were tested regularly for mycoplasma contamination by PCR and were verified to be negative before using them for different assays and studies.

Cell culture

Cell lines were cultured following the provider's recommendations. In brief, MCA205 was cultured in DMEM high glucose (Lonza) supplemented with 10% FBS (Gibco) and 1.5% of HEPES (Lonza); MC38, KPC and A375 were cultured in DMEM (Lonza) with 10% FBS; CT26, PanO2 and JAR were cultured in RPMI (Lonza) supplemented with 10% FBS and 1% HEPES; MDA-MB-231 was cultured in L-15 medium supplemented with 10% FBS and 1% glutamine (Gibco); and HT29 was cultured with McCoy's 5a supplemented with 10% FBS. All cell lines were cultured in culture flasks (Greiner) and incubated at $37\,^{\circ}\mathrm{C}$ with 5% CO $_2$. For in vivo studies, the cells were expanded and passaged three times before inoculation.

Mouse syngeneic tumor experiments

Cultured tumor cells were dissociated into single cells with 0.25% trypsin (Gibco), washed with serum-free medium and counted in preparation for subcutaneous implantation. The cells were then resuspended in 100 μ l of PBS. The total number of inoculated cells was specific to each model: MCA205 and KPC, 2×10^5 ; MC38 and CT26, 5×10^5 ; Pan02, 2×10^6 . Tumor-bearing mice were randomized into groups with

equivalent average tumor volumes when the tumors reached 60 mm^3 . The animals were monitored daily, checking for clinical signs of distress and recording body weight, and tumors were measured three times per week using an electronic caliper. Tumor volume was determined as volume = length \times width² \times 0.5.

In some experiments, CD8 $^+$ T cell depletion was performed by injecting 250 μ g of anti-CD8 monoclonal antibody (clone 53-6.7, BioX-cell) intraperitoneally on days –7, –4, 0, 7, 14 and 21, with day 0 marking tumor implantation.

Tumor growth inhibition was calculated after logarithmic transformation of tumor volumes. Times were transformed to orthogonal polynomials, making the intercept of the analysis equivalent to overall tumor burden (area under the curve) during the entire experiment⁵³. Maximal tumor size was 2,000 mm³ and was not exceeded in the study.

Human xenografts in humanized mice

Human cell line xenograft experiments were performed at TransCure BioServices (France), and all associated animal procedures were reviewed and approved by the local ethics committee (CELEAG-TCS agreement number A7418324.09DEC2021: APAFIS##30873-202112011817784 V2; 17MAR2021: APAFIS#38383-20220824134 16895 V7). The experiment was carried out using the NOD-Prkdc $^{\it em26Cd52} \emph{Il2rg} e^{\it m26Cd22}/ NjuCrl\ immunode ficient\ mouse\ strain\ (NCG,\ from\ mouse\ mouse\$ Charles River Laboratories). Mice were housed on a 12 h light/dark cycle in a housing facility maintained at 20-25 °C and 30-70% humidity and were fed a diet of Teklad Global 18% Protein Rodent Diet (2018) (Envigo, formerly Harlan). In brief, 4-week-old immunodeficient NCG mice were engrafted with cord-blood-derived human CD34⁺ hematopoietic stem and progenitor cells (French Blood Institute) 2 days after chemical myeloablative treatment. Then, 14 weeks after cell injection, the engraftment level was monitored with the analysis of human CD45⁺ cells among total blood leukocytes using flow cytometry (Attune, Life Technologies/Thermo Fisher Scientific). After engraftment confirmation (hCD45/total CD45 > 25%), mice were assigned to each treatment group by manual randomization based on their humanization rate, tumor volume and the cord-blood donor ID. The mice were then inoculated subcutaneously with 5×10^6 MDA-MB-231 cells resuspended in 50% Matrigel (Corning). When the tumors reached approximately 60 mm³ (day 19 after tumor cell inoculation), the animals were randomized into groups before initiating treatment. Mice received 30 mg kg⁻¹EOS301984 formulated in 2.5% DMSO, 10% solutol Hs-15 (Sigma-Aldrich) and 87.5% PBS twice a day intraperitoneally in a final volume of 200 μl, 10 mg kg⁻¹ nivolumab in a final volume of 200 μl PBS intraperitoneally once every 5 days or a combination of both. All animals were monitored daily, checking for clinical signs of distress and recording body weight; tumors were measured three times a week using an electronic caliper. The tumor volume was calculated as volume = length \times width² \times 0.5. Maximal tumor size was 2,000 mm³ and was not exceeded in the study.

Human specimens

Tumor samples were collected from individuals with colorectal cancer, renal cell carcinoma, NSCLC, endometrial cancer, melanoma or head and neck squamous cell carcinoma, all of whom voluntarily gave their informed consent according to the protocol approved by the local ethics commission at CNE KRD 'Kyiv Regional Oncology Dispensary' (Ukraine). Sample procurement and shipment were managed by BioPartners (USA; https://biopartners.science). In addition, NSCLC samples for the isolated TIL experiments were sourced by Fidelis Research (https://fidelis-research.com) according to the protocol approved by the National Commission for Bioethics of Medicines and Medical Supplies (Academia De Ştiințe Medical, Romania). Cancer specimens were shipped at 4 °C in T-STORE medium (Life Science Production) and arrived within 48 h post surgery. Alternatively, samples

were snap-frozen in liquid nitrogen for subsequent QMSI analysis. Patient characteristics are provided in Supplementary Table 1.

Venous blood from healthy volunteers, all of whom signed an informed consent approved by the Ethics Committee (FOR-UIC-BV-050-01-01 ICF_HBS_HD v.5.0), was obtained by Centre Hospitalier Universitaire Tivoli, La Louviere, Belgium. PBMCs were collected by density gradient centrifugation, using SepMate-50 tubes and Lymphoprep (STEMCELL Technologies) according to the manufacturer's instructions. CD3⁺ T cells were isolated by immunomagnetic negative selection, using the EasySep Human T Cell Isolation Kit (STEM-CELL Technologies) as per the manufacturer's instructions. PBMCs and CD3⁺ T cells were stored in heat-inactivated FBS and 10% DMSO (Sigma-Aldrich) in liquid nitrogen. Alternatively, cryopreserved PBMCs derived from donors with a history of previous CMV infection and known HLA-A*02:01 expression were purchased from ImmunXperts (Gosselies, Belgium).

QMSI of adenosine in tumor tissue

Tumor tissues, stored at $-80\,^{\circ}\text{C}$, were placed inside the cryostat with the temperature maintained at $-20\,^{\circ}\text{C}$, and $10\,\mu\text{m}$ tissue sections were obtained for each sample. Tissue cross-sections were placed on indium tin oxide (ITO) glass slides for MALDI imaging, and adjacent sections were collected on SuperFrost glass slides for H&E staining. The region of interest included tumor cells and possibly stroma and necrosis areas. Additional sections from a control sample were added for calibration curve purposes. Tissue sections on ITO slides were placed in a desiccator for 15 min. A solution of inhibitors was prepared to prevent the degradation of ADO in the tissue sections 54 and was applied with a TM Sprayer (HTX imaging) on the sections immediately after the drying step in the desiccator and before any further treatment (calibrant deposit or spray of the MALDI matrix).

Two stable isotopic-labeled ADO (SIL-ADO) compounds were then considered in the next step for the QMSI for endogenous ADO, including a SIL-ADO calibrant as ADO-D2 and a SIL-ADO normalizer as ADO-13C5 (Toronto Research Chemical, cat. nos. A280409 and A280402, respectively), assuming a similar response of ionization between ADO and ADO-D2.

For quantification purposes, including the limit of detection, lower limit of quantification and upper limit of quantification, the different concentrations of ADO-D2 were deposited as follows: $1\,\mu l$ of each ADO-D2 calibrant (including a zero calibrant) was spotted on the additional tissue sections and placed in a desiccator for 15 min before spraying the MALDI matrix on the entire slide. DAN (1,5-diaminonaphthalene; Merck, cat. no. 56451) was selected as the MALDI matrix for the detection of adenosine and was spiked with ADO-13C5 normalizer for spraying with the TM sprayer. The concentration of ADO-13C5 was adjusted to the expected signal of endogenous species in the tissue sections.

The MALDI-FTICR acquisition parameters were as follows: CASI mode; negative ionization; mass range, 272 ± 15 Da; laser frequency, 2,000 Hz; calibration mode, 2; spatial resolution, 130 μm for the regions of interest in the tumor sections with one region of interest selected per sample; 200 μm spatial resolution for the calibration range and 300 μm for the quality controls. Staining of adjacent or imaged sections (depending on their integrity after imaging) by H&E was prepared to overlay or compare the molecular images side by side with the histological structures.

MSI data were acquired and analyzed with FlexImaging, Data Analysis and the proprietary software MultImaging (v1.2.6.2). Pannoramic viewer (3D Histech) and ImageScope (Aperio) were used for histology.

Intensity scales representing the molecular signal were adjusted for each image to discriminate the noise from the molecular signal and to give the best visualization of the signal across the sections. A convolution step was performed on the original images using a normalized uniform kernel, which simply averages the values around a position.

The kernel size was manually optimized for the analysis, minimizing the background noise.

Normalization of the data was performed with the stable ADO-13C5 based on an intensity ratio of the endogenous ADO (or ADO-D2 calibrant) and ADO-13C5 per pixel. A correlation between the calibration curve and the signal obtained on the tissues was then performed to determine the concentration of ADO per histological structure in $\mu g \, g^{-1}$ of tissue or μM in the tissue sections.

Measurement of adenosine concentration in tumor interstitial fluid

Cell lines were subcutaneously inoculated into mice; when tumors reached ~300-400 mm³, they were removed and placed in nylon mesh with a pore size of 10 um. The meshes containing the tumors were transferred to 1.5 ml tubes containing 10 µM pentostatin (Tocris) + 1 µM 5-iodotubericidin (Tocris). The samples were centrifuged at 450g for 10 min at 4 °C. The volume of fluid collected was measured and snap-frozen in dry ice and then stored at -80 °C. Total adenosine was quantified by liquid chromatography-mass spectrometry at Eurofins ADME Bioanalysis (France). In brief, calibration curves using a sample surrogate spiked with adenosine (Sigma-Aldrich) were used to set up a quantification method, with the limit of detection between 50 and 10,000 ng ml⁻¹. Testing samples were prepared by using a QMA anion exchange cartridge to separate fractions with a potassium chloride salt gradient. After introducing QMA fractions into the cartridge, a centrifugation step at 100g was performed. Subsequent washes involved using 2×1 ml of 250 mM ammonium acetate followed by 2×1 ml of methanol. To elute the analytes, a solution of 20% formic acid in methanol was used, and the eluted material was then dried down and reconstituted in UP-water before injection into the liquid chromatography-tandem mass spectrometry system.

RNA extraction and real-time PCR

Cells were washed in cold PBS, resuspended in 350 µl of RLT+ buffer, mixed by pipetting up and down and vortexing for 30 s, and then the cell lysates were stored at -80 °C. RNA extraction was performed on all cell lysates at the same time, following the manufacturer's protocol of the RNeasy plus micro kit from Qiagen (or mini kit for cell lysates with more than 1.5×10^6 cells). The concentration of RNA was measured using a NanoDrop One. Between 300 ng and 1 µg of RNA per sample was used for the reverse transcription step using the RevertAid kit from ThermoFisher Scientific according to the manufacturer's instructions. A total of 10 ng of cDNA was loaded per well for the qPCR. TagMan Fast Advanced Master Mix (10 µl per well) and the following Applied Biosystems TagMan Gene Expression assays with FAM-MGB dye (1 µl per well; ThermoFisher Scientific) were used: SLC29A1 (assay ID, Hs01085706_ m1), SLC29A2 (Hs01546959 g1), SLC29A3 (Hs00983219 m1), SLC29A4 (Hs00928283 m1), *SLC28A1* (Hs00984391 m1), *SLC28A2* (Hs01035846 m1), SLC28A3 (Hs00223220 m1), POLR2A (Hs00172187 m1) and SDHA (Hs00417200 m1). Nuclease-free water was added to reach a total volume of 20 µl per well. The plates were placed in a LightCycler 96 thermal cycler (Roche) for qPCR with the following steps: 95 °C for 20 s, 95 °C for 1 s and 60 °C for 20 s; steps two and three were performed 40× with a temperature ramp of 3.5 °C s⁻¹. The assay was performed with a minimum of technical duplicates, and two housekeeping genes (POLR2A and SDHA) were included. These were selected based on stability of expression across samples as assessed with the geNorm application of qbase+ software (v.3.3). Normalization of expression values against the reference genes was performed on LightCycler 96 software (v.1.1.0.1320; Roche).

Western blot

Snap-frozen cells were lysed in a modified RIPA buffer (Sigma-Aldrich) with 1× protease inhibitor cocktail (Thermo Scientific) by pipetting up and down, followed by 30 min incubation on ice. Samples were

centrifuged for 10 min at 18,000g at 4 °C. The supernatant was transferred to a new microtube and stored at 4 °C. Protein concentration was quantified using a BCA protein assay kit (Pierce Thermo Scientific). Proteins were denatured at 95 °C for 5 min, separated electrophoretically using an Any kD Mini-Protean TGX gel (Bio-Rad) and then transferred onto 0.2 μ M Nitrocellulose Filter Paper sandwiches (Bio-Rad). The membranes were blocked in 5% dry milk for 1 h and incubated with a specific primary antibody at 4 °C overnight. Blots were probed with rabbit anti-ENT1 (Abcam) and β -actin (Cell Signaling Technology) antibodies. After hybridization with horseradish-peroxidase-conjugated secondary antibody (Cell Signaling Technology), protein bands were visualized.

T cell activation cultures

Cryopreserved human CD3⁺ T cells were thawed and washed twice with RPMI1640 medium, UltraGlutamine (Lonza) containing 10% FBS. CD3⁺T cells were resuspended in PBS with 10% FBS at a concentration of 2×10^7 cells per ml. One volume of cells was combined with one volume of CFSE solution in PBS to give a final CFSE concentration of $1\,\mu\text{M}$. Alternatively, cells were incubated with eBioscience Cell Proliferation Dye eFluor 450 (final concentration, 4 μM). The cell suspension was mixed and incubated at 37 °C for 5 or 10 min, respectively, before cells were topped up with PBS with FBS (10%) to quench remaining excess labeling agent, then centrifuged at 450g for 5 min. T cells were resuspended in X-VIVO15 medium, and $5-8 \times 10^4$ cells were added to the wells of sterile round-bottom 96-well plates. Cells were activated by adding 50 µl of anti-CD3/CD28-coated microbeads (Dynabeads human T-activator CD3/CD28; Life Technologies), suspended in X-VIVO15 medium at a ratio of one microbead per two cells. Cells were cultured in the presence or absence of adenosine or ATP (Sigma-Aldrich) and additional reagents as indicated in the relevant figures. The final well volume was 200 µl in all cases, with DMSO concentration adjusted to 0.1% in all wells. Experiments were performed in technical duplicates. Cells were mixed by pipetting up and down and incubated for 3 days in a 37 °C humidified tissue culture incubator with 5% CO₂.

In some experiments, GolgiPlug Protein Transport inhibitor (BD Biosciences) was added to T cell cultures (final dilution, 1:1,000) after 24 h of activation, and cells were cultured for a further 16 h before analysis of cytokine production by intracellular flow cytometry (see 'Flow cytometry' section).

CMV antigen recall assay

Cryopreserved human PBMCs were thawed and washed with RPMI 1640 medium containing 10% heat-inactivated FBS. The cells were suspended at 2×10^7 cells per ml in X-VIVO15 medium containing 5% (v/v) human serum and 1 mM sodium pyruvate. Then, 50 μ l of cell suspension was added to the wells of sterile round-bottom 96-well plates. Cells were activated by adding CMV pp65 NLVPMVATV peptide (10 μ g ml $^{-1}$; day 0 of culture), IL-7 (days 0,1 and 3 or 4 of culture) and IL-2 (day 3 or 4). A total of 300 μ M of ATP was added to the cells in combination with 300 nM EOS301984 and/or 10 μ g ml $^{-1}$ anti-PD-1 or 10 μ g ml $^{-1}$ isotype anti-B-gal IgG4 in a 200 μ l final volume. At day 1 and day 3 or 4, 100 μ l of medium was removed and replaced with fresh medium including all compounds and cytokines at the original concentrations noted above. On day 6 or 7 of culture, cells were collected for flow cytometry analysis or rested before subsequent stimulation steps.

FluoroSpot analysis

After 6 or 7 days of incubation, the cells from CMV cultures were washed twice with X-VIVO15 medium and left overnight at 37 °C in X-VIVO15 medium with 5% human serum and 1 mM sodium pyruvate. The following day, cells were processed for FluoroSpot analysis using the Human TNFa/IFN γ /Perforin/GranzymeB FluoroSpotFLEX kit (MABTECH) according to the manufacturer's instructions. In brief, cells were counted and plated at either 5 or 10 × 10⁴ cells per well in pre-coated

FluoroSpot plates. NLVPMVATV peptide ($10 \, \mu g \, ml^{-1}$) was added to the wells, with non-peptide-supplemented wells serving as controls, and plates were incubated overnight at 37 °C. The wells of the plate were then washed five times with PBS and incubated for 2 h at room temperature (20–25 °C) with the relevant detection antibodies. Plates were again washed five times with PBS and incubated for 1 h at room temperature with the relevant fluorophore conjugates. Following a further five washes with PBS, the fluorescence enhancer was added and the plate was left for 5–15 min at room temperature. The underdrain of the plate was removed and the plate left to dry in low light for a minimum of 24 h before being read on a FluoroSpot MABTECH IRIS reader (software v.1.1.45).

Cell killing assay

The lymphoblast cell line T2 was selected as a target for the killing assay based on HLA-A*02:01 expression, allowing presentation of the NLVPM-VATV peptide. T2 cells were cultured in IMDM with 20% FBS, and on the day of the assay, the cells were washed in PBS and stained with cell proliferation dye eFluor 450 at final concentrations of 10 μ M and 300 nM to create eFluor 450 and eFluor 450 populations, respectively. After a 10-min incubation at 37 °C in low light, 10 ml of cold IMDM with 20% FBS was added, and the cells were incubated for 5 min on ice. Cells were centrifuged and resuspended in 1 ml IMDM with 20% FBS. eFluor 450 T2 cells were pulsed with NLVPMVATV peptide at a final concentration of 5 μ g ml $^{-1}$ and incubated for 2 h at 37 °C. Cells were washed twice and resuspended in X-VIVO15 containing 5% human serum and 1 mM sodium pyruvate at a final concentration of 1 or 2 \times 10 5 cells per ml.

CMV-PBMC preparations were generated as outlined above and collected on day 6 or 7 of culture, washed and resuspended in X-VIVO15 with 5% human serum and 1 mM sodium pyruvate and left to rest overnight at 37 °C. On day 7 or 8, the pulsed and non-pulsed T2 cells and PBMC preparations were combined in different ratios. Based on the cell numbers available for the experiment, either 5 or 10×10^3 pulsed T2 cells were used and combined with an equal number of non-pulsed T2 cells and tenfold more PBMCs to give a ratio of 10:1 PBMCs to pulsed T2 cells. The mixture of cells was centrifuged for 20 s and incubated at 37 °C for 3 h. Cells were washed with PBS and stained with 400 nM ApoTracker for 15 min at room temperature in low light. Fixable viability eFluor 780 was then added before a final incubation of 15 min at 4 °C. Cells were washed and resuspended in FACS buffer before acquisition on a BD LSRFortessa FACS machine.

Frequency of viable (viability dye⁻ and ApoTracker⁻) T2 cells was determined, and the percent of viable pulsed T2 cells was divided by the percent of viable non-pulsed T2 cells, multiplied by 100 and then subtracted from 100 to generate the percent specific killing activity for each condition.

K_d derivation for EOS301984 binding to human and mouse ENT1

The K_d for EOS301984 binding to human and mouse ENT1 was determined in competitive binding experiments with [3 H]HBMPR (Moravek, cat. no. MT-682) using membranes derived from JAR and MCA205-ENT2-KO cells, respectively.

Cells were amplified to mid-log phase in complete culture medium and then scraped from the culture vessels in ice-cold Ca $^{2^+}$ -free and Mg $^{2^+}$ -free PBS. Cells were centrifuged for 10 min at 5,000 g at 4 °C, and the pellets were suspended in buffer A (15 mM Tris-HCl pH 7.5; 2 mM MgCl $_2$; 0.3 mM EDTA; 1 mM EGTA) and homogenized in a glass–glass homogenizer. The crude membrane fraction was collected by two consecutive centrifugation steps at 35,000 g and 4 °C for 30 min, separated by a washing step in buffer A. The final membrane pellet was suspended in buffer B (75 mM Tris-HCl pH 7.5, 12.5 mM MgCl $_2$, 0.3 mM EDTA, 1 mM EGTA, 250 mM sucrose) and flash-frozen in liquid nitrogen. Protein content was determined by the BCA method (Interchim, UP40840A).

The specific binding of [3 H]NBMPR to ENT1 was confirmed in saturation binding experiments by incubating increasing concentrations of [3 H]NBMPR with 10 µg of membrane preparation per well with the addition of unlabeled NBMPR (10 µM final assay concentration) or concentration-matched DMSO for 1 h at 4 $^\circ$ C in a 96-well plate. All components were diluted in assay buffer (Tris 50 mM, KCl 100 mM, MgCl₂ 0.1 mM, CaCl₂ 0.1 mM). The samples were then filtered over a GF/B filter plate (pre-incubated in 0.5% PEI (Sigma-Aldrich, cat. no. P3143) with a Filtermate Harvester (Perkin Elmer). After washing the filters five times with 0.5 ml of ice-cold assay buffer, 50 µl of Microscint 20 (Packard) was added to the filters, and the samples were incubated for 15 min on an orbital shaker and then counted with a TopCount for 1 min per well to derive CPM values. B_{max} and K_d values for [3 H]NBMPR specific binding (total binding – non-specific binding) were determined using the 'One site – total and non-specific binding' function in Graphpad Prism (v.10.0.2).

The $k_{\rm on}$ for [3 H]NBMPR was determined by incubating membrane extracts with a dose range of [3 H]NBMPR for different times at 4 $^{\circ}$ C and then determining the CPM values as described above. The 'One-phase association' function in GraphPad Prism was used to derive the $K_{\rm obs}$ value for each concentration of [3 H]NBMPR, which was then plotted against the matching concentration to derive the $k_{\rm on}$ value (slope of the linear regression).

The $k_{\rm off}$ for [3 H]NBMPR was determined by pre-incubating 45 μ l of membrane extracts with 45 μ l [3 H]NBMPR (10 nM final concentration) for 10 min until binding equilibrium was reached. A 200-fold excess of unlabeled NBMPR (10 μ l) was then added to each well, and the CPM values were derived after various amounts of time as described above. The 'Dissociation – one phase exponential decay' function in GraphPad Prism was used to derive the $k_{\rm off}$ value.

Competitive binding experiments were performed in which 50 μ l of EOS301984 at various doses was combined with 25 μ l of [³H] NBMPR (10 nM final concentration) and 25 μ l of membrane extracts. Samples were incubated for 60 min at 4 °C, and CPM values were derived as described above. IC₅₀ values for the effect of EOS301984 on the binding of [³H]NBMPR to ENT1 were determined with the 'Log(inhibitor) vs response – variable slope (four parameters)' function in GraphPad Prism.

Finally, 50 μ l of EOS301984 at various concentrations above and below the IC $_{50}$ value determined as above was incubated with 25 μ l [3 H]NBMPR (10 nM final concentration) and 25 μ l membrane preparation at 4 $^{\circ}$ C for various periods of time. CPM values were generated as described above and used to generate $k_{\rm on}$ and $k_{\rm off}$ values for EOS301984 by using the 'Kinetics of competitive binding' function in GraphPad Prism 55 , in which the $k_{\rm on}$ and $k_{\rm off}$ values for [3 H]NBMPR were constrained to those as derived above and B $_{\rm max}$ as a shared value. $K_{\rm d}$ for EOS301984 was derived by dividing the $k_{\rm off}$ by the $k_{\rm on}$ values.

Polar metabolite measurement by liquid chromatographytandem mass spectrometry

T cell activation cultures were set up as outlined above (without CFSE staining). Following 24 h of culture, T cells were collected by combining three separate wells per condition into a single 1.5 ml microcentrifuge tube. Cells were pelleted by centrifugation at 4 °C for 5 min at 400g. Media was aspirated and cell pellets washed with chilled blood bank saline, followed by an additional centrifugation step at 4 °C for 5 min at 400g. Following aspiration of blood bank saline, cells were extracted in 80% MeOH/20% acetonitrile v/v with 250 nM 13 C-labeled amino acids provided by the Whitehead Institute Metabolomics Core facility. Cells were extracted by vortex shaking in a 4 °C cold room, followed by centrifugation at 4 °C for 10 min at 16,000g to pellet insoluble material. The supernatant was transferred to a fresh microcentrifuge tube and dried down over gaseous nitrogen and stored at -80 °C before mass spectrometry analysis.

On the day of analysis, dried metabolites were resuspended in high-performance liquid chromatography-grade H₂O. Metabolites

were measured by liquid chromatography-mass spectrometry on a O Exactive bench-top Orbitrap mass spectrometer equipped with an Ion Max source and a HESI II probe, which was coupled to a Dionex UltiMate 3000 HPLC system (Thermo Fisher Scientific). External mass calibration was performed using the standard calibration mixture every 7 days. From each sample, 4 µl was injected onto a SeQuant ZIC-pHILIC 150×2.1 mm analytical column equipped with a 2.1×20 mm guard column (both 5 µm particle size; EMD Millipore). Buffer A was 20 mM ammonium carbonate, 0.1% ammonium hydroxide; buffer B was acetonitrile. The column oven and autosampler tray were held at 25 °C and 4 °C, respectively. The chromatographic gradient was run at a flow rate of 0.150 ml min⁻¹ as follows: 0-20 min: linear gradient from 80-20% B; 20-20.5 min: linear gradient from 20-80% B; 20.5-28 min: hold at 80% B. The mass spectrometer was operated in full-scan, polarity-switching mode, with the spray voltage set to 3.0 kV, the heated capillary held at 275 °C and the HESI probe held at 350 °C. The sheath gas flow was set to 40 units, the auxiliary gas flow was set to 15 units and the sweep gas flow was set to 1 unit. MS data acquisition was performed in a range of m/z = 70-1,000, with the resolution set at 70,000, the AGC target at 1×10^6 and the maximum injection time at 20 ms. Relative metabolite quantification was performed in XCaliber QuanBrowser (v.2.2) (ThermoFisher Scientific) with 5 ppm mass tolerance, referencing an in-house library of chemical standards. Total ion counts for respective metabolites were exported into Microsoft Excel. To control for extraction efficiency, all samples within the same run were normalized to ion counts for ¹³C-labeled valine. To normalize metabolite levels to biomass, additional normalization was performed relative to unlabeled isoleucine. For each metabolite, the average of all three vehicle-controlled conditions was determined and used to determine log₂(fold change) for the respective experimental conditions.

Tumor dissociation and cell culture

Human tumor pieces were rinsed with cold PBS and cut into 1-2 mm fragments with a scalpel blade and transferred into GentleMACS C tubes. Dissociation of the tissue was completed with a Tumor Dissociation kit (Miltenyi Biotec) according to the manufacturer's instructions. In brief, 5 ml of dissociation solution (200 µl of enzyme H, 20 µl of enzyme R and 25 µl of enzyme A, with the addition of RPMI to 5 ml) was added per gram of tumor. The tube was placed in the gentleMACS dissociator, and the 1st program was run. An incubation step of 30 min at 37 °C was applied with rotation (MACSmix tube rotator). After this incubation, a brief centrifugation (30g, 1 min) was performed, and the supernatant containing the dissociated cells was collected in a new tube containing FBS (30% of the total volume with supernatant) and placed at 4 °C. A second round of dissociation was performed on the remaining tissue fragments; after the addition of dissociation solution (same volume and content as the first round), the second gentleMACS program was run, and the tube was incubated for 30 min at 37 °C with rotation. Another brief centrifugation was performed, and the cells in the supernatant were pooled with the first collection and filtered through a 100 µm cell strainer, which was washed with 10 ml RPMI, 10% FBS and 2% penicillin-streptomycin. After centrifugation at 350g for 10 min, cells were resuspended in 20 ml RPMI, 10% FBS and 2% penicillin-streptomycin and counted with a haemocytometer. If cell agglomerates were visible, the cell suspension was filtered through a 100 µm cell strainer before counting. Dissociated tumor cells (DTCs) were either used directly for FACS analysis or washed into FBS with 10% DMSO and cryopreserved in liquid nitrogen until required.

Mouse tumors were digested as above with the following modifications: 100 μ l of enzyme D, 50 μ l of enzyme R and 12.5 μ l of enzyme A were used in a final volume of 2.4 ml of RPMI per tumor. Processing was performed in the GentleMACS dissociator, followed by a 40 min digestion at 37 °C with shaking every 5 min. Samples were resuspended and passed through a 70 μ m cell strainer over a 50 ml Falcon tube. The

strainer was rinsed with 5 ml of RPMI, and the cells were centrifuged at 700g for 5 min and then resuspended in RPMI.

Cryopreserved human DTCs were thawed and washed twice with RPMI 1640 medium (Lonza) containing 10% heat-inactivated FBS. Cells were resuspended in PBS with 10% FBS at a concentration of 10^7 cells per ml. One volume of cells was combined with one volume of CFSE solution in PBS to give a final CFSE concentration of 1 μM. The cell suspension was mixed and incubated at 37 °C for 5 min before cells were topped up with PBS with FBS (10%) to quench remaining excess CFSE and then centrifuged at 450g for 5 min. The cells were resuspended at 4×10^6 cells per ml in X-VIVO15 medium containing 5% (v/v) human serum (Biowest), 1 mM Na-Pyr and 2% penicillin-streptomycin (Westburg/Lonza). Cell suspension (50 μ l, 2×10^5 cells) was added to wells of sterile round-bottom 96-well plates. Cells were left unstimulated or were activated by adding IL-2 (50 U ml⁻¹ final concentration, Proleukin-Novartis) with anti-CD3/CD28-coated microbeads (Dynabeads human T-activator CD3/CD28: Life Technologies) at a ratio of one microbead to five cells. ENT1 inhibitor EOS301984 (300 nM, iTeos Therapeutics; stock solution of 10 mM in DMSO) and anti-PD-1 (10 μg ml⁻¹; OPDIVO (nivolumab), Bristol-Myers Squibb) were prepared and distributed to the relevant wells of the culture plate. A concentration-matched isotype control antibody was added to all wells not containing nivolumab, and DMSO concentrations were matched across all samples to 0.1%. Cells were cultured in the presence or absence of ATP (Sigma-Aldrich) at a final concentration of 500 μM. The final well volume was 200 µl in all cases. At a minimum, experiments were performed in technical duplicates. Cells were mixed by pipetting up and down and incubated for 3 days in a 37 °C humidified tissue culture incubator with 5% CO₂. An additional dose of ATP at a final concentration of 500 µM was added 18 hafter the start of culture.

For the summary analysis of T cell proliferation and cytokine production, the mean value of the readout recorded in the presence of ATP but with no other treatments was subtracted from all values. These were then expressed as a percentage of the mean value of control samples stimulated in the absence of ATP. This generated a scale of rescue from 0 to 100, in which 0 represents no difference from the ATP level and 100 represents a full rescue.

T cell populations isolated from cryopreserved DTCs (as outlined in the following section) were stimulated by culturing with anti-CD3/CD28 microbeads (one bead per two cells) at 2.5×10^4 cells per well in X-VIVO15 medium in the presence or absence of adenosine (100 μ M) and EOS301984 (300 nM), as indicated in the relevant figure. Cells were processed for flow cytometry directly after 3 days of culture or resuspended in Cell Stimulation Cocktail (ThermoFisher Scientific) and incubated for 1 h at 37 °C. GolgiPlug Protein Transport inhibitor was added, followed by a further 4 h incubation before proceeding to flow cytometry.

For analysis of cytokine production by intracellular flow cytometry, mouse DTCs were stimulated at 1×10^6 cells per well in a 96 flat well plate in the presence of $0.4\times$ Cell Stimulation Cocktail and $1\times$ Protein Transport Inhibitor Cocktail (Fisher Scientific) in RPMI with 10% FBS and $50~\mu\text{M}~\beta$ -mercaptoethanol for 3~h at 37~C in a humidified incubator. Cells were centrifuged at 700g for 5~min at 4~C before further processing for analysis by flow cytometry.

Flow cytometry

Cells were centrifuged at 450g for 5 min (used for all subsequent centrifugation steps), and the supernatant was discarded. For proliferation experiments (without ENT1 staining), cells were resuspended in PBS containing fixable viability dye and human Fc block (BD) and incubated for 15 min at 4 °C. For ENT1 staining, cells were resuspended in 50 μ l NBMPR solution (20 μ M, 0.02% DMSO; used as negative control for ENT1 expression) or DMSO (0.02% DMSO for ENT1 staining) as well as Fc block and then incubated 15 min at 4 °C; then, 50 μ l of PBS containing SAHENTA-DY647 (0.2 μ M for a final concentration of 0.1 μ M)

and fixable viability dye was added, followed by an incubation step of 30 min at 4 °C. Cells were washed in FACS buffer (PBS with 2 mM EDTA and 0.1% BSA) and resuspended in a solution of FACS buffer and relevant antibodies. After an additional 15 min of incubation at 4 °C, cells were centrifuged and resuspended in FACS buffer. In some experiments, cells were subsequently prepared for intracellular staining using the eBioscience Foxp3/Transcription Factor Staining Buffer Set (human cells); alternatively, IC fixation buffer and permeabilization buffers (mouse cells, eBioscience) were used according to the manufacturer's instructions. Samples were analyzed on a BD LSRFortessa Cell Analyzer using BD FACSDiva software (v.9.0.1; Becton, Dickinson and Company) or a Cytek Aurora (SpectroFlo software, v.3.0.1). Analysis of FACS data, including uniform manifold approximation and projection, was performed using Flowlo (BD, v.10.8.1). Identification of discrete populations was performed manually; less well-defined populations were determined using fluorescence-minus-one controls or isotype control staining on matching DTC cell suspensions.

In some experiments, cryopreserved DTCs were thawed and washed with RPMI 1640 medium with 10% heat-inactivated FBS, washed in FACS buffer and resuspended at 8×10^7 cells per ml in PBS containing Fc receptor blocking solution. After 5 min at room temperature, cells were stained with fixable viability dye as outlined above, then washed in FACS buffer and resuspended in a solution of Brilliant Stain Buffer and relevant FACS antibodies. After a 20 min incubation at $4\,^{\circ}$ C, cells were washed twice in FACS buffer, resuspended at 1×10^7 cells per ml in FACS buffer and filtered through a 70 μ m strainer. Sorting of PD-1 CD8+T cells and PD-1+TIM-3+CD39+CD8+T cells was performed using a FACSAria II (BD FACSDiva v.9.0.1), and cell populations were collected in polystyrene tubes previously coated with FBS and containing X-VIVO15 medium with 1% penicillin–streptomycin. The purity of the sorted populations was assessed post-sort (Supplementary Fig. 7). Sorted cells were stored on ice until seeding.

A list of FACS antibodies and dilutions used in this study is provided in Supplementary Table 2.

Cytokine analysis

Cell culture supernatants were collected, and $5\,\mu$ l of each was analyzed for TNF and IFN γ concentration using the TNF α (human) AlphaLISA Biotin-Free Detection Kit and IFN- γ (human) AlphaLISA Biotin-Free Detection Kit (Perkin Elmer), respectively, according to the manufacturer's instructions, in 384-well OptiPlates (Perkin Elmer). Analysis was performed on a SpectraMax i3x (Molecular Devices) using SoftMax Pro 7 software (v.7.0.3; Molecular Devices). Alternatively, cytokines were analyzed with the Biolegend LegendPlex hCD8/NK kit according to the manufacturer's instructions. The samples were run on a BD LSRFortessa and analyzed using Biolegend software (legendplex.qognit.com).

[3H]adenosine uptake assay

Human T cells were activated for 48 h with anti-CD3/CD28 microbeads in X-VIVO15 medium and then washed into 'transport buffer' (50 mM Tris-HCl pH 7.4, 120 mM NaCl, 3 mM K₂HPO₄, 10 mM glucose, 1 mM $MgCl_2$, 1 mM $CaCl_2$) before being dispensed in triplicate (2 × 10⁵ per 25 µl) into the wells of a 96-well plate (Master Block, Greiner) containing 50 µl transport buffer or 50 µl dilazep diluted in transport buffer (1 µM final assay concentration). Cells were incubated for 15 min at room temperature before the reaction was initiated by the addition of 25 µl of a [3H]adenosine (Moravek Biochemicals)/adenosine mix (1:3) (1 µM final assay concentration). The reaction was incubated for 10 min at room temperature before rapid filtration through a GF/C SAN Unifilter plate pre-soaked in 0.5% PEI for 2 hat room temperature and washed five times with 500 µl of ice-cold transport buffer. Next, 50 µl of Microscint 20 (Packard) was added per filter, the plates were sealed, incubated for 15 min on an orbital shaker and then counted with a TopCount for 1 min per well. Alternatively, T cells were activated as described above for 48 h in the presence of a dose range of dilazep or

EOS301984 and then centrifuged for $5 \, \text{min}$ at 450 g before resuspension in transport buffer and used in adenosine uptake experiments as described above.

Nucleoside transporter inhibition assays

Nucleoside transporter inhibition assays were performed using Madin-Darby canine kidney strain II (MDCKII) cells (German Cancer Research Center) stably expressing either human ENT1, ENT2, CNT1, CNT2 or CNT3; or HEK293 cells (Invitrogen) stably expressing human ENT4. Transfected cell lines were developed and characterized by SOLVO Biotechnology, a Charles River Company. Mock-transfected control and transfected cells were cultured in DMEM high glucose (4.5 g l $^{-1}$) (Lonza) at 37 °C in an atmosphere with 5% CO $_2$. Cells were plated onto standard 96-well tissue culture plates at a density of 1 × 10 5 cells per well. Uptake studies were performed 24 h after cell seeding.

Culture medium was removed and cells were washed twice with 100 µl of the respective assay buffer at pH 7.4 (Supplementary Table 3). Uptake experiments were conducted in duplicate at 25 ± 1 °C (CNT1, CNT2, CNT3 and ENT1 inhibition) or 37 ± 1 °C (ENT2 and ENT4 inhibition) in 50 µl of the respective assay buffer (pH 7.4). Cells were pre-incubated for 30 min with a concentration range of EOS301984 before addition of the appropriate probe substrate ([3H] uridine, [3H]adenosine (Moravek Biochemicals) or [3H]1-methyl-4-p henylpyridinium (MPP+; Perkin Elmer), and additional culture period as indicated in Supplementary Table 2. DMSO concentrations were equal in all wells and did not exceed 1.5% (v/v). After the experiment, cells were washed twice with 100 µl of appropriate cold assay buffer and lysed with 150 µl scintillation cocktail. Radio-labeled probe substrate transport was determined by measuring an aliquot (35 µl) from each well for liquid scintillation counting using a MicroBeta2 liquid scintillation counter (Perkin Elmer).

CPM values were corrected for non-specific transport by subtracting values obtained from control cells not expressing the relevant transporter and then transformed to a relative scale in which 100% is defined as transport in the absence of EOS301984. This value was subtracted from 100 to generate the percent inhibition of the relevant transporter.

Processing of published ChIP-seq, ATAC-seq and scRNA-seq data

NFAT ChIP-seq data were downloaded from NCBI Geo Set Omnibus (accession no. GSE116695 (ref. 13)) and visualized in the IGV browser⁵⁶.

Human CD8-T ATAC–seq normalized count and raw fastq files were downloaded from NCBI Geo Set Omnibus (accession no. GSE89309 (ref. 34)). Raw fastq were aligned on human genome hg38 using bwa mem⁵⁷ (v.0.7.18), and bigwig files were generated using bamCoverage from deepTools⁵⁸ (v.3.5.4).

The Tumor Immune Cell Atlas was used to examine *SLC29A1* and *SLC29A2* expression across immune cells in multiple cancers⁵². The R package Seurat (v.5.1.0) was used for gene expression visualization⁵⁹.

Oxygen consumption measurements

Following 24 h of culture, T cells were collected by combining three separate wells per condition into a single 50 ml conical tube. Cells were pelleted by centrifugation at 4 °C for 8 min at 400g. Media was aspirated and cell pellets were resuspended in unbuffered RPMI 1640 medium supplemented with 1 mM sodium pyruvate (Sigma-Aldrich). Then, 1.5–2.5 × 10 5 cells were plated into Seahorse XFe96/XF tissue culture plates (Agilent), previously coated with CellTak (Corning) according to the manufacturer's instructions. Cells were allowed to recover in a 37 °C incubator without buffered CO $_{2}$ before the Seahorse analysis.

For the Seahorse analysis, oxygen consumption measurements were determined (1) at baseline; (2) following oligomycin A injection (final concentration, 1.5 μ M); (3) following FCCP (carbonyl cyanide 4-(trifluoromethoxy)phenylhydrazone) injection (final concentration, 2 μ M); and (4) following antimycin A (all Sigma-Aldrich) and

rotenone (Selleck Chemicals) injection (final concentration, $2\,\mu M$ for both drugs). All values were normalized to total cell counts. Basal oxygen consumption rate was determined as the average of measurements at baseline minus the average of measurements following rotenone and antimycin A injection. Maximal oxygen consumption rate was determined as the average of measurements following FCCP injection minus the average of measurements following rotenone and antimycin A injection.

Statistics

Statistical analysis was performed with GraphPad Prism (v.10.0.2) using a combination of two-tailed paired t-tests, one-way or two-way ANOVA with correction for multiple comparisons and matching for samples as appropriate and indicated in the relevant figure legends. Doseresponse curves were generated through the non-linear regression function 'Log(inhibitor) vs response – variable slope (four parameters) and used to generate IC50 values (the concentration required for 50% maximal observed effect). Some additional statistics and data visualization were performed in RStudio (2023.03.1 Build 446).

Survival data were analyzed using the 'Simple survival analysis (Kaplan–Meier)' package in GraphPad Prism, with survival in mouse syngeneic tumor experiments defined as the time to reach the average tumor volume of the control group on the final day of measurement or 2,000 mm³, whichever was lower. For the xenograft experiments in humanized mice, survival was defined as the time to reach 500 mm³. Curves were compared using the log-rank (Mantel–Cox) test, and *P* values were corrected for multiple comparisons with the Bonferroni method.

No statistical methods were used to predetermine sample sizes. Sample size was chosen based on preliminary experiments or previously published results 60. Data distribution was assumed to be normal, but this was not formally tested. Data collection and analysis were not performed blind to the conditions of the experiments. Randomization was performed for the xenograft experiment as described based on humanization rate and tumor volume, but not for syngeneic tumors in WT and ENT1-KO mice, as no treatment was applied. For in vitro experiments, all relevant treatments were applied to cells from each donor, so no randomization was required. No data were excluded from the analysis.

Reporting summary

Further information on research design is available in the Nature Portfolio Reporting Summary linked to this article.

Data availability

ChIP-seq data for *SLC29A1* expression in activated T cells and ATAC-seq data for *SLC29A1* expression in TILs were accessed from the NCBI Geo Set Omnibus (accession numbers GSE116695 and GSE89309, respectively). Source data are provided with this paper.

References

- 52. Nieto, P. et al. A single-cell tumor immune atlas for precision oncology. *Genome Res.* **31**, 1913–1926 (2021).
- Mirman, D., Dixon, J. A. & Magnuson, J. S. Statistical and computational models of the visual world paradigm: growth curves and individual differences. J. Mem. Lang. 59, 475–494 (2008).
- Löfgren, L., Pehrsson, S., Hägglund, G., Tjellström, H. & Nylander,
 S. Accurate measurement of endogenous adenosine in human blood. PLoS ONE 13, e0205707 (2018).
- Motulsky, H. J. & Mahan, L. C. The kinetics of competitive radioligand binding predicted by the law of mass action. *Mol. Pharmacol.* 25, 1–9 (1984).
- Robinson, J. T. et al. Integrative Genomics Viewer. Nat. Biotechnol. 29, 24–26 (2011).

- Li, H. & Durbin, R. Fast and accurate long-read alignment with Burrows-Wheeler transform. Bioinformatics 26, 589-595 (2010).
- Ramírez, F. et al. deepTools2: a next generation web server for deep-sequencing data analysis. *Nucleic Acids Res.* 44, W160– W165 (2016).
- 59. Hao, Y. et al. Dictionary learning for integrative, multimodal and scalable single-cell analysis. *Nat. Biotechnol.* **42**, 293–304 (2024).
- Preillon, J. et al. Restoration of T-cell effector function, depletion of T_{regs}, and direct killing of tumor cells: the multiple mechanisms of action of a-TIGIT antagonist antibodies. *Mol. Cancer Ther.* 20, 121–131 (2021).

Acknowledgements

C.S.N. acknowledges support from a Young Investigator Award from the ASCO Conquer Cancer Foundation, the Koch Institute Clinical Investigators Program, an American Association for Cancer Research-Bristol-Myers Squibb Immuno-oncology Research Fellowship and the Dana-Farber Harvard Cancer Center SPORE in Lung Cancer (P50CA265826). M.G.V.H. acknowledges grant support from the United States NCI (P30CA1405141, R35CA242379), the MIT Center for Precision Cancer Medicine, the Ludwig Center at MIT and the Lustgarten Foundation. Radioligand binding and adenosine uptake experiments were performed at EuroscreenFast (https:// euroscreenfast.com). We thank L. Meeus for the critical review of the relevant sections. Nucleoside transporter inhibition assays were performed at SOLVO Biotechnology, a Charles River Company (https://www.solvobiotech.com). We thank A. Klukovits and E. Kis for their critical review of the relevant sections and B. M. Tóth and V. Juhász (all employees of SOLVO Biotechnology) for the development of the nucleoside transporter expressing cell lines. Adenosine QMSI was performed at Aliri Bioanalysis. We acknowledge support from T. Kunchok at the Whitehead Institute Metabolomics Core Facility for liquid chromatography-mass spectrometry measurements. Quantification of adenosine in interstitial fluid by liquid chromatography-tandem mass spectrometry was performed at Eurofins ADME BIOANALYSES (https://www.eurofins.com/ biopharma-services/adme). The schema in Extended Data Fig. 9 was generated in BioRender.com.

Author contributions

E.H., T.J.S, M.G.V.H., C.S.N., Y.M. and O.D.H. conceived and designed the project. T.J.S., C.S.N., M.B., A.L.H., N.R., L.C., J.-P.D., A.P., W.C., A.S., M.D., J.M., Q.D., M.-C.L. and R.M. acquired the data. T.J.S., C.S.N., E.H., M.G.V.H. and C.M. wrote the manuscript and/or were involved with review and critical revision. E.H. and M.G.V.H. supervised the study.

Competing interests

T.J.S., M.B., A.L.H., N.R., L.C., J.-P. D., A.P., W.C., A.S., M.D., J.M., Q.D., M.-C.L., C.M., R.M., O.D.H., Y.M. and E.H. are employees of and own stock options and/or shares in iTeos Therapeutics, a company with ownership of EOS301984 described in the paper. M.D. and E.H. are listed as inventors on patent WO/2021/204896 related to EOS301984. C.S.N. acknowledges receiving royalty income from Cambridge Epigenetix and stock ownership in Opko Health. M.G.V.H. is a member of the scientific advisory board for iTeos Therapeutics. M.G.V.H. is also a scientific advisor for Agios Pharmaceuticals, Sage Therapeutics, Auron Therapeutics, Pretzel Therapeutics, Lime Therapeutics, MPM Capital and DROIA Ventures.

Additional information

Extended data is available for this paper at https://doi.org/10.1038/s41590-025-02153-3.

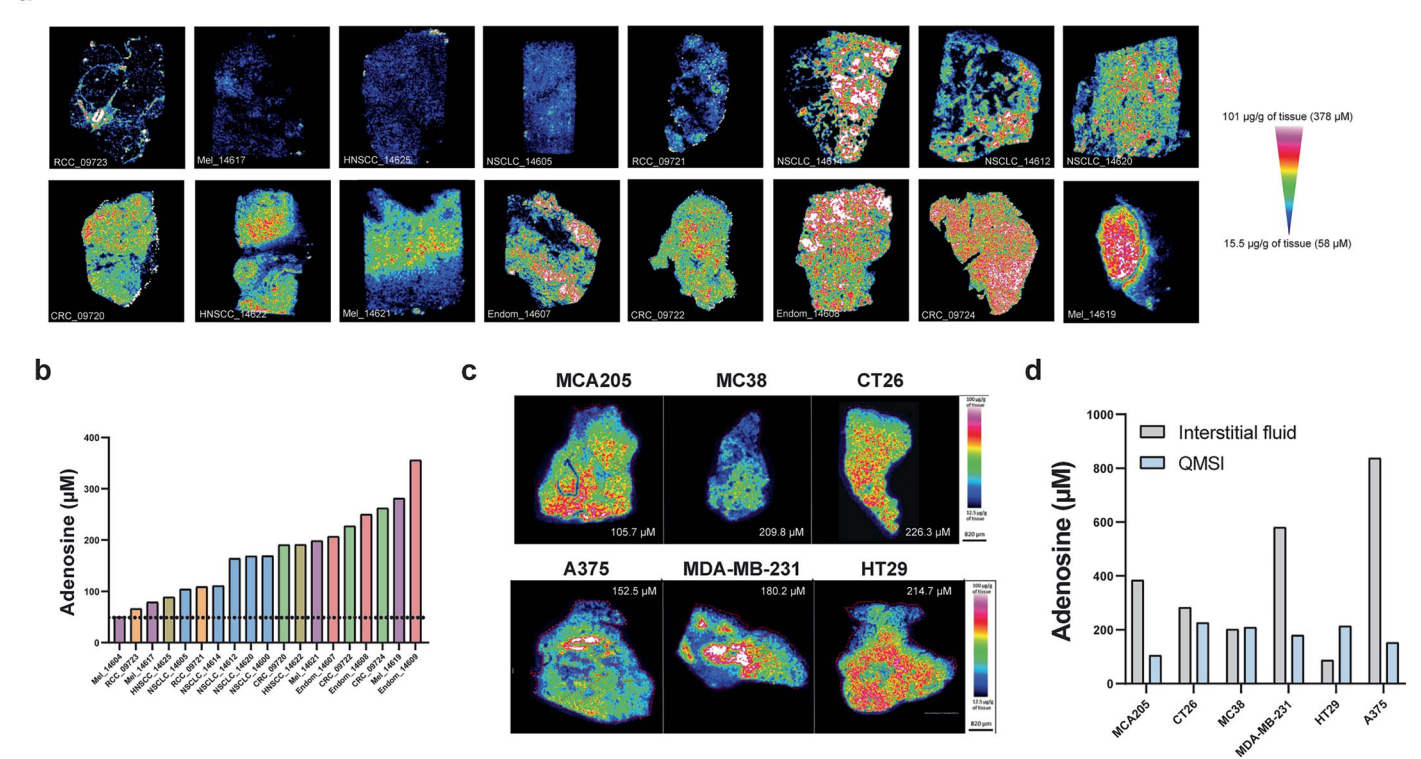
Supplementary information The online version contains supplementary material available at https://doi.org/10.1038/s41590-025-02153-3.

Correspondence and requests for materials should be addressed to Erica Houthuys.

Peer review information *Nature Immunology* thanks Greg Delgoffe and the other, anonymous, reviewer(s) for their contribution to the peer review of this work. Primary Handling Editor: Nick Bernard, in collaboration with the *Nature Immunology* team. Peer reviewer reports are available.

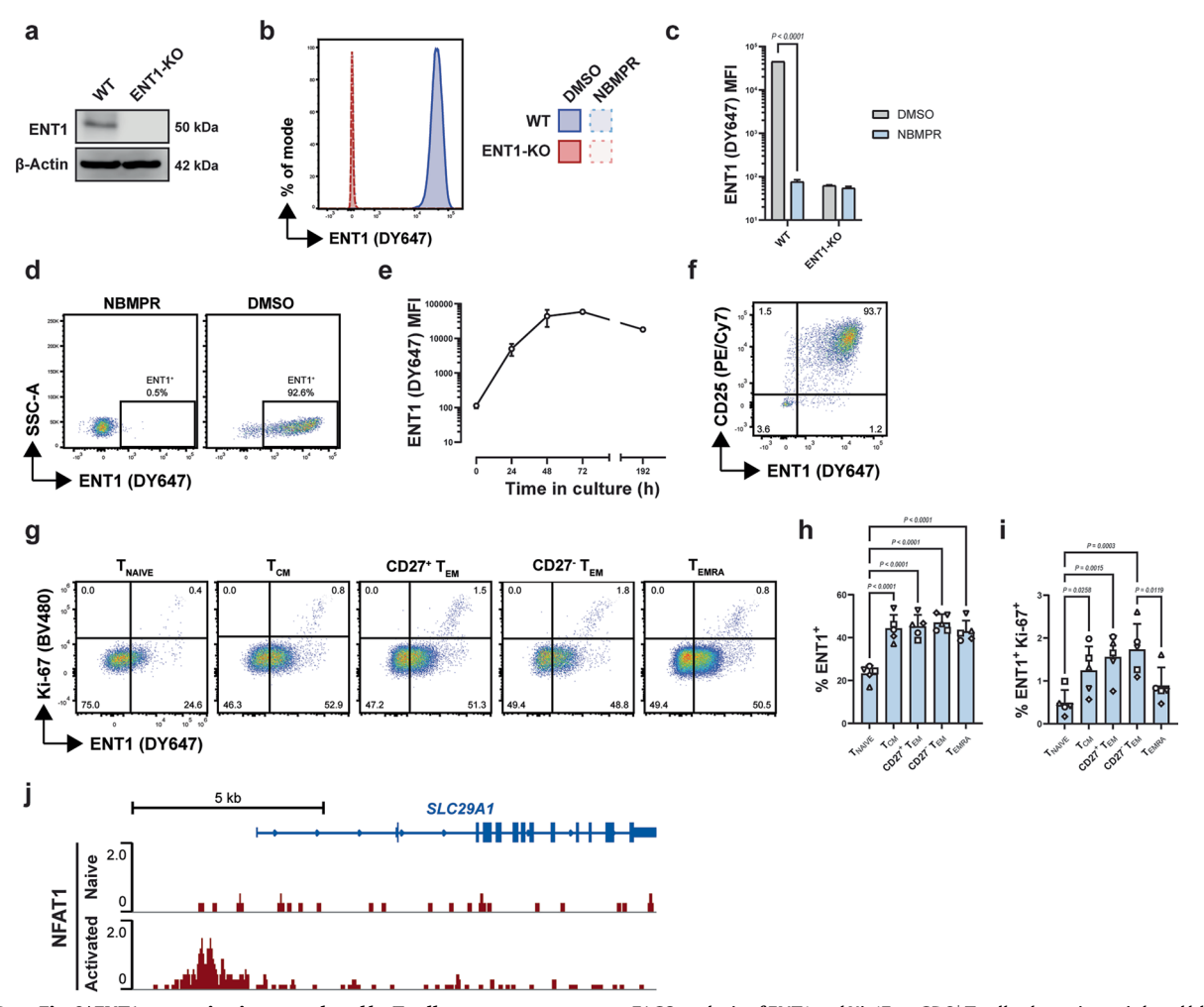
Reprints and permissions information is available at www.nature.com/reprints.

a



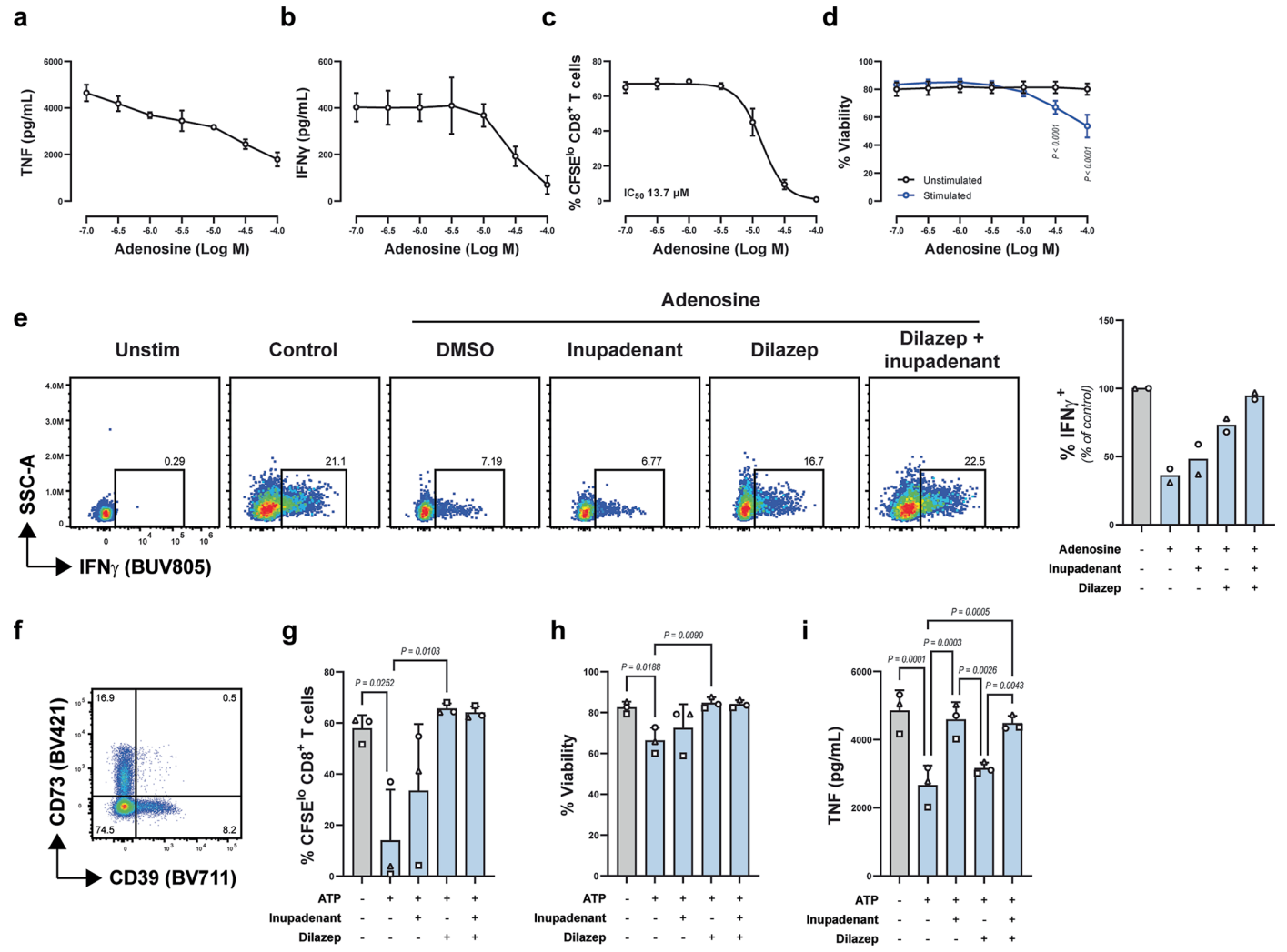
Extended Data Fig. 1 | **Quantification of adenosine in human tumors by QMSI. a**, Resected tumor samples were frozen and adenosine levels determined by QMSI. Samples representative of 19 analyzed in total. **b**, Concentration of adenosine across all samples tested. Dotted line indicates lower limit of

quantification. \mathbf{c} , Analysis of adenosine concentrations in syngeneic and human cell line-derived tumors grown in mice. One sample analyzed per cell line-derived tumor. \mathbf{d} , Comparison of adenosine concentration in tumor interstitial fluid and QMSI from matched tumors as depicted in (\mathbf{c}) .



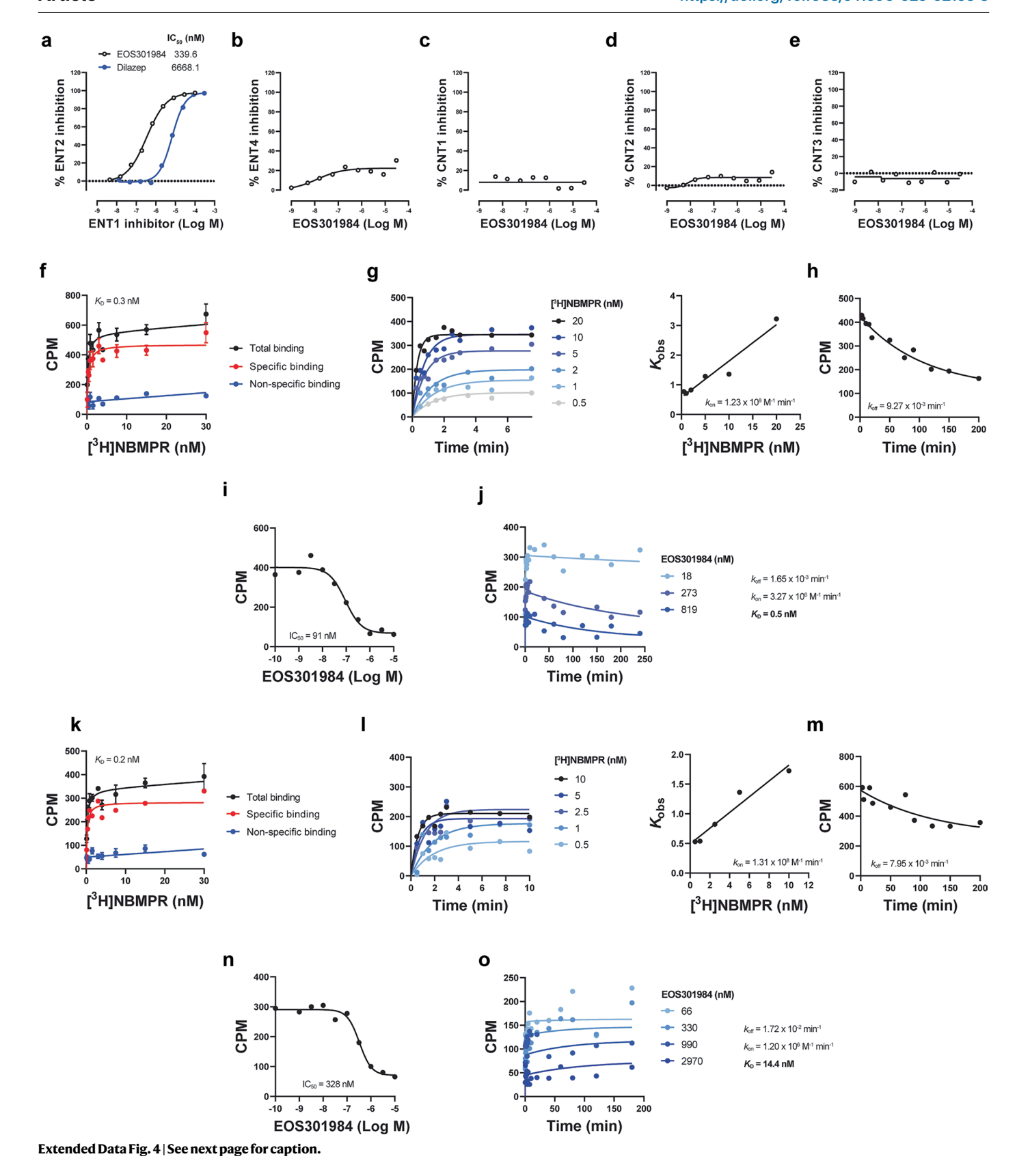
Extended Data Fig. 2 | **ENT1 expression is upregulated by T cells upon activation. a**, Western blot of ENT1 on WT and ENT1-KO JAR cells, representative of n = 2 experiments. **b**, FACS analysis of ENT1 on WT and ENT1-KO JAR cells with SAHENTA-DY647 following pre-incubation with DMSO or NBMPR. **c**, Summary analysis of ENT1 MFI values from (**b**). Mean values \pm s.d. from technical triplicates shown. **d**, FACS analysis of CD8+T cells activated for 24 hours and then cultured in the presence of NBMPR or DMSO prior to staining with SAHENTA-DY647. Representative of 3 donors. **e**, Summary analysis from Fig. 1d. Mean values \pm s.d. from 3 donors shown. **f**, FACS analysis of ENT1 expression on CD8+T cells activated for 72 hours in relation to CD25 expression. Representative of 3 donors.

g, FACS analysis of ENT1 and Ki-67 on CD8* T cell subsets in peripheral blood from healthy donors. Representative of 5 donors. An example gating strategy may be found in Supplementary Fig. 1. **h-i**, Summary data of percent ENT1* and ENT1* Ki-67* cells, respectively, from each CD8* T cell subset as shown in (**g**). Symbols represent each of n = 5 donors (biological replicates). Bars are group mean \pm s.d. **j**, Integrated Genome Viewer (IGV) browser display of the human *SLC29A1* gene and promoter region (chr6:44,218,675-44,235,202; GRCh38/hg38) with ChIP-data tracks showing NFAT1 binding in human naive CD4* T cells either in a resting state or after 5 h anti-CD3/28 activation¹³. Analysis by two-way ANOVA with Tukey's multiple comparisons test (**c**, **h-i**).



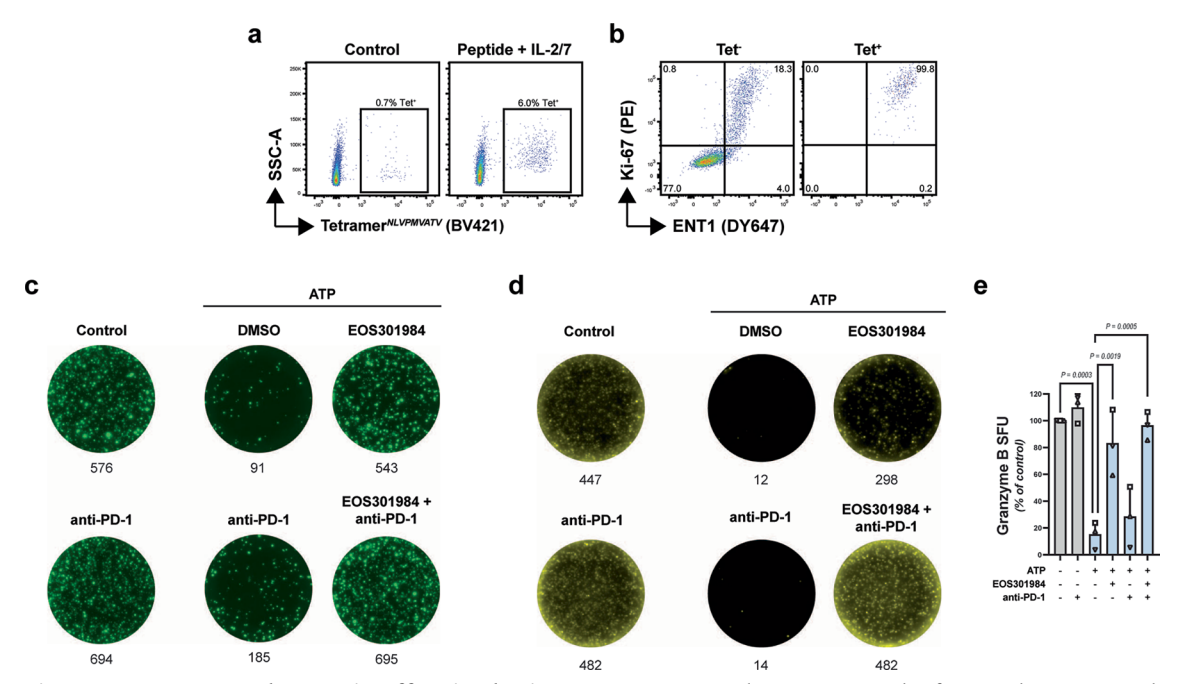
Extended Data Fig. 3 | Adenosine exerts immunosuppressive effects on T cells following uptake via ENT1. a-d, Dose-dependent effects of adenosine on production of TNF, IFN γ , CD8 $^+$ T cell proliferation and viability, respectively. Mean values \pm s.d. from 3 donors shown. Two-way ANOVA with Šídák's multiple comparisons test (d). e, Intracellular staining of IFN γ in peripheral blood T cells following 48 h activation with anti-CD3/CD28 microbeads in the presence of adenosine (100 μ M), inupadenant and dilazep (both 300 nM), as indicated.

Symbols in summary data represent each of n = 2 donors (biological replicates) and bars are the group mean. **f**, Expression of CD73 and CD39 in CD4 $^{\circ}$ T cells from peripheral blood. Representative of 5 donors. **g-i**, Effect of ATP (100 μ M) on CD8 $^{\circ}$ T cell proliferation, viability and production of TNF, respectively, in the presence or absence of dilazep and/or inupadenant. Symbols represent each of n = 3 donors (biological replicates), bars are group mean \pm s.d., analysis by two-way ANOVA with Tukey's multiple comparisons test.

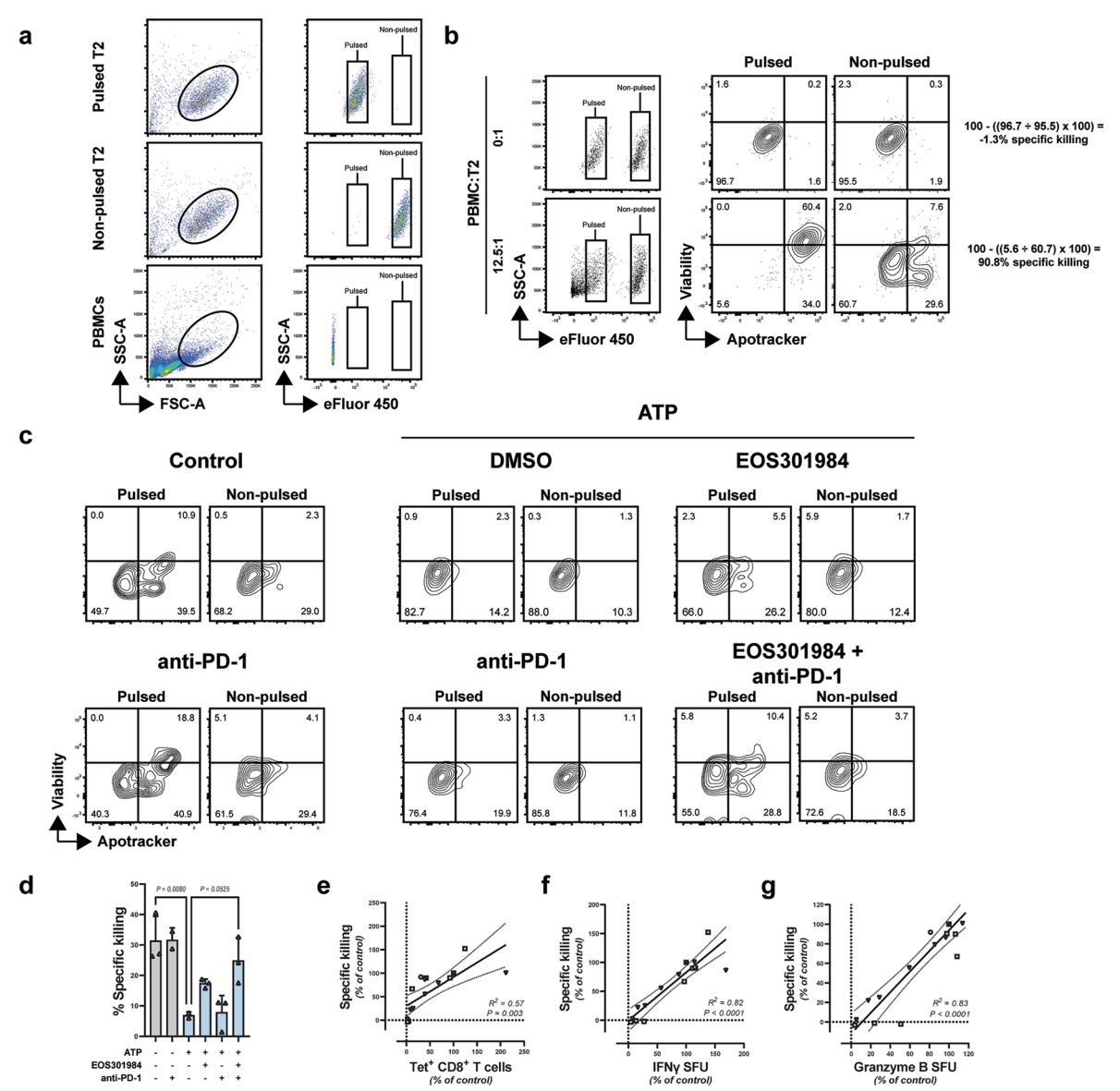


Extended Data Fig. 4 | **EOS301984 is a potent and selective human ENT1 antagonist. a**, Percent inhibition of ENT2 in a transporter assay by dose ranges of EOS301984 or dilazep. **b-e**, Inhibition profile of EOS301984 against ENT4, CNT1, CNT2 and CNT3, respectively. **f**, Saturation binding of [3 H]NBMPR against JAR cell membrane preparations in the presence (non-specific binding) and absence (total binding) of an excess (10 μ M) of unlabeled NBMPR. **g**, Derivation of k_{on} for [3 H]NBMPR against JAR cell membrane preparations. **h**, Derivation of k_{off} for [3 H]NBMPR against JAR cell membrane preparations. **i**, Competition binding experiments between [3 H]NBMPR and EOS301984 to generate the IC $_{50}$ of EOS301984. **j**, Derivation of K_D value for EOS301984 on human ENT1 from kinetic binding experiments in competition with [3 H]NBMPR. **k**, Saturation

binding of [3 H]NBMPR against MCA205-ENT2KO cell membrane preparations in the presence (non-specific binding) and absence (total binding) of a 200-fold excess of unlabeled NBMPR. **I**, Derivation of $k_{\rm on}$ for [3 H]NBMPR against MCA205-ENT2KO cell membrane preparations. **m**, Derivation of $k_{\rm off}$ for [3 H] NBMPR against MCA205-ENT2KO cell membrane preparations. **n**, Competition binding experiments between [3 H]NBMPR and EOS301984 to generate the IC $_{50}$ of EOS301984. **o**, Derivation of $K_{\rm D}$ value for EOS301984 on mouse ENT1 from kinetic binding experiments in competition with [3 H]NBMPR. Mean values displayed from technical duplicates (${\bf a}$ - ${\bf e}$, ${\bf g}$ - ${\bf j}$, ${\bf l}$ - ${\bf o}$) and mean values \pm s.d. displayed from technical triplicates (${\bf f}$, ${\bf k}$).

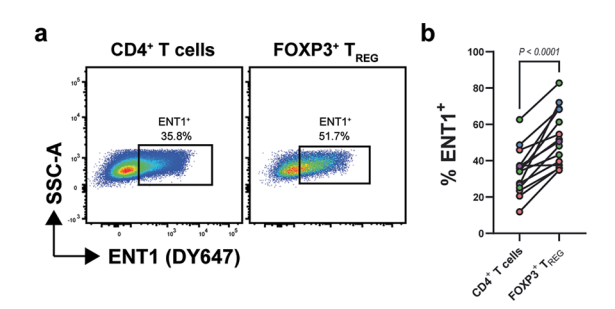


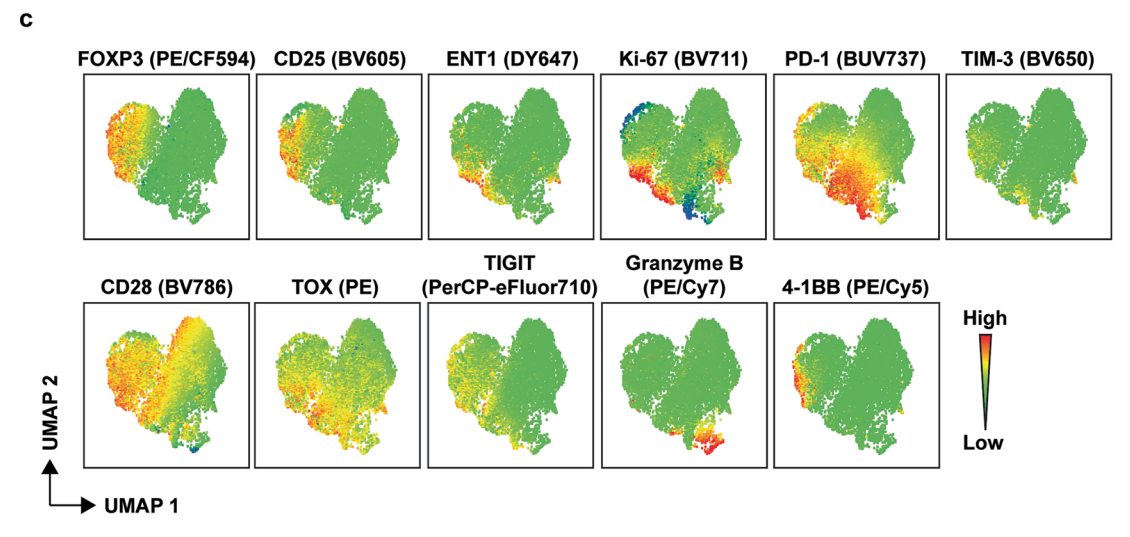
granzyme B production, respectively, of PBMC cultures generated as in Fig. 4i. Representative of 3 donors. e, Summary analysis of granzyme B FluoroSpot data from cultures generated as in Fig. 4i. Symbols represent each donor (biological replicates), bars are group mean \pm s.d. Two-way ANOVA with Tukey's multiple comparisons test.

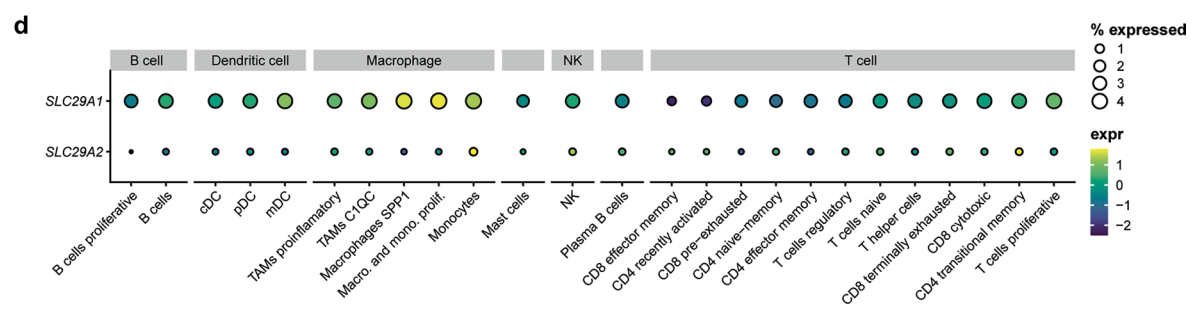


Extended Data Fig. 6 | Antigen-specific CD8* T cells expanded in the presence of high concentrations of adenosine by EOS301984 retain the capacity to kill antigen-bearing target cells. a, T2 cells were stained either with a low concentration of eFluor450 and then pulsed with NLVPMVATV peptide, or stained with a high concentration and left non-pulsed. Gating based on FSC-A vs SSC-A and eFluor450 distinguishes T2 cells from unstained PBMCs. b, T2 cells pulsed with NLVPMVATV peptide are selectively killed by PBMC populations enriched for NLVPMVATV-specific CD8* T cells whilst non-pulsed T2 cells are spared. Representative of 3 donors. c, PBMC populations generated as

in Fig. 4i were used in NLVPMVATV peptide-specific T2 killing assays. Representative of 3 donors. ${\bf d}$, Summary data from (${\bf c}$). Bars represent the mean value \pm s.d. from technical triplicates. Two-way ANOVA with Tukey's multiple comparisons test. Representative of 3 donors. ${\bf e}$ - ${\bf g}$, Pearson correlation of normalized specific killing activity and frequency of pp65-specific CD8' T cells, IFN γ SFU, or granzyme B SFU, respectively. 95% confidence bands of the best-fit line from simple linear regression indicated. Data pooled from 3 donors, p-values are two-tailed.

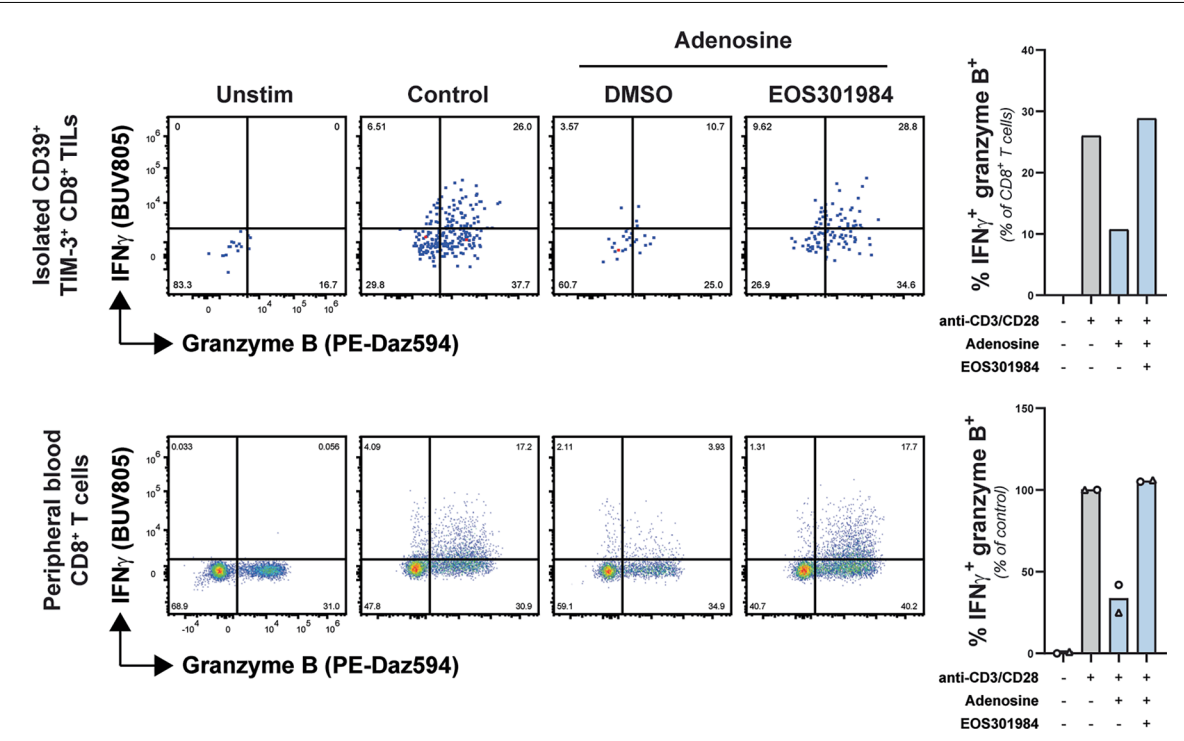






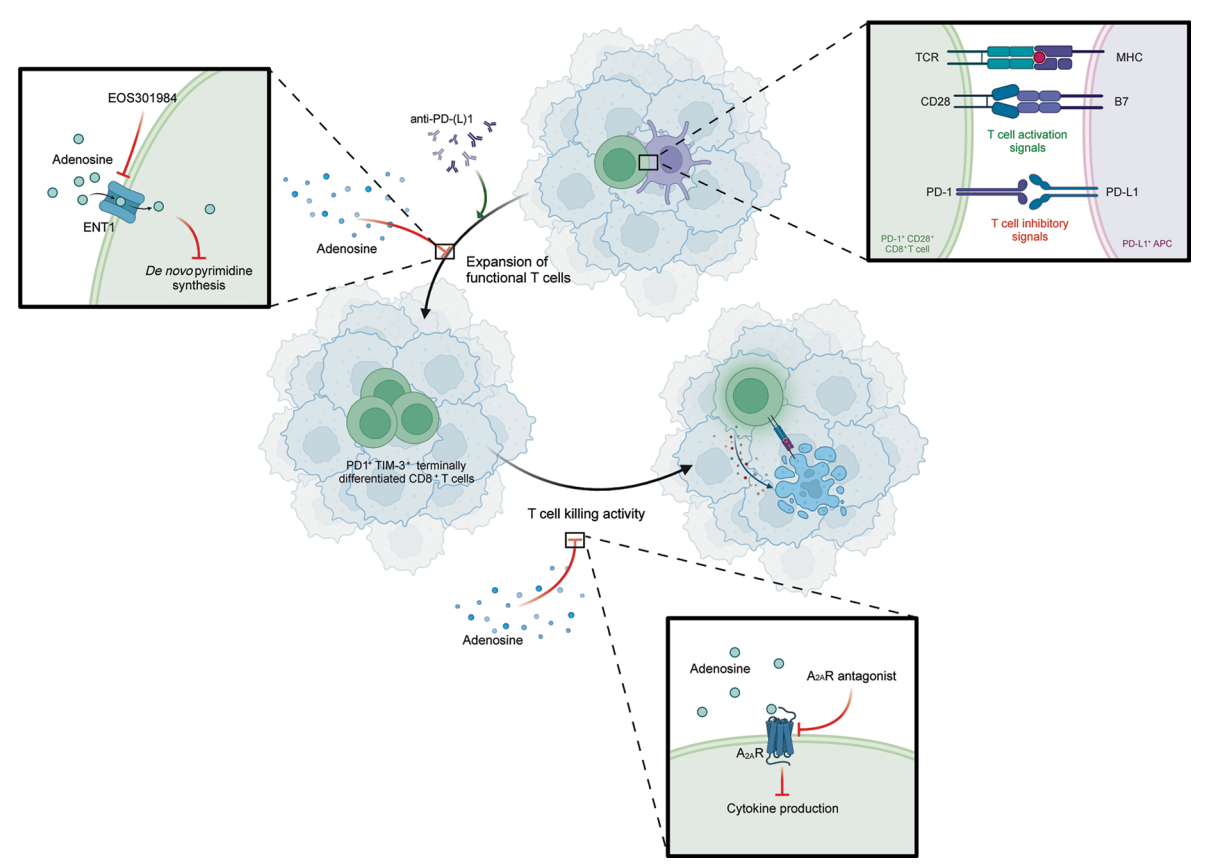
Extended Data Fig. 7 | **CD4*** **TILs including FOXP3*** **T**_{REG} **cells express ENT1. a**, Representative example of ENT1 staining on CD4* T cells and FOXP3* T_{REG} cells from a dissociated NSCLC tumor. Example gating strategy may be found in Supplementary Fig. 4. **b**, Analysis of percent ENT1* CD4* T cells and FOXP3* T_{REG}

cells within (n = 15) tumor samples (biological replicates) by two-tailed paired t-test. \mathbf{c} , UMAP analysis of CD4 $^{\circ}$ TILs. Pooled data from 9 donors. \mathbf{d} , Expression of SLC29A1 and SLC29A2 in immune cells of tumor samples from the TICA scRNA-seq dataset 52 .



Extended Data Fig. 8 | EOS301984 rescued cytokine production by isolated 'exhausted' CD8* TILs in high adenosine concentrations. FACS analysis of cytokine production by TIM-3* CD39* CD8* TILs isolated from a NSCLC sample (n = 1) and T cells from peripheral blood of healthy volunteers (n = 2),

as indicated, stimulated with anti-CD3/CD28 microbeads for 72 or 48 h, respectively, in the presence of adenosine (100 μ M) and/or EOS301984 (300 nM). Symbols in lower panel represent each donor (biological replicates), bars are mean value.



Extended Data Fig. 9 | EOS301984 overcomes the suppressive intracellular effects of adenosine on TIL functional expansion within the TME to enhance the anti-cancer immune response. The T cell boosting effect of ICB such as anti-PD-(L)1 agents may be limited by the presence of highly elevated concentrations of adenosine in certain TMEs. EOS301984 can act with $A_{2\Delta}R$ antagonists to prevent

suppressive effects of both intra- and extracellular adenosine, respectively, to enhance TIL expansion and function in such sites and may promote more effective overall immune responses during cancer immunotherapy. This schema was created in BioRender.

nature portfolio

Corresponding author(s):	Erica Houthuys
Last updated by author(s):	Mar 25, 2025

Reporting Summary

Nature Portfolio wishes to improve the reproducibility of the work that we publish. This form provides structure for consistency and transparency in reporting. For further information on Nature Portfolio policies, see our Editorial Policies and the Editorial Policy Checklist.

For all statistical analyses, confirm that the following items are present in the figure legend, table legend, main text, or Methods section.

\sim .					
C t	$\overline{}$	+1	ıci	ы	CC
่วเ	а	ш	וכו	ш	CS

n/a	Confirmed
	$oxed{\boxtimes}$ The exact sample size (n) for each experimental group/condition, given as a discrete number and unit of measurement
	🔀 A statement on whether measurements were taken from distinct samples or whether the same sample was measured repeatedly
	The statistical test(s) used AND whether they are one- or two-sided Only common tests should be described solely by name; describe more complex techniques in the Methods section.
	A description of all covariates tested
	🔀 A description of any assumptions or corrections, such as tests of normality and adjustment for multiple comparisons
	A full description of the statistical parameters including central tendency (e.g. means) or other basic estimates (e.g. regression coefficient) AND variation (e.g. standard deviation) or associated estimates of uncertainty (e.g. confidence intervals)
	For null hypothesis testing, the test statistic (e.g. <i>F</i> , <i>t</i> , <i>r</i>) with confidence intervals, effect sizes, degrees of freedom and <i>P</i> value noted <i>Give P values as exact values whenever suitable.</i>
\boxtimes	For Bayesian analysis, information on the choice of priors and Markov chain Monte Carlo settings
\boxtimes	For hierarchical and complex designs, identification of the appropriate level for tests and full reporting of outcomes
	\boxtimes Estimates of effect sizes (e.g. Cohen's d , Pearson's r), indicating how they were calculated

Our web collection on statistics for biologists contains articles on many of the points above.

Software and code

Policy information about availability of computer code

Data collection

Flow cytometry data was acquired on a BD LSRFortessa™ Cell Analyzer using BD FACS DIVA software (version 9.0.1) or a Cytek Aurora using SpectroFlo software (version 3.0.1).

QMSI data were acquired and analyzed with FlexImaging, Data Analysis and proprietary software MultImagingTM (version 1.2.6.2).

Pannoramic viewer (3D Histech) and ImageScope (Aperio) were used for the histology. Real-time PCR data were acquired using LightCycler96 software (version 1.1.0.1320).

 $FluoroSpot\ data\ were\ acquired\ and\ analyzed\ using\ a\ FluoroSpot\ MABTECH\ IRIS\ reader\ and\ associated\ software\ (version\ 1.1.45).$

AlphaLISA data was acquired using SoftMax Pro 7 software (version 7.0.3) on a SpectraMax i3x (Molecular Devices).

Data analysis

Flow cytometry analysis including generating of Uniform Manifold Approximation and Projection (UMAP) plots was performed using FlowJo (version 10.8.1).

Statistical analysis was performed using GraphPad Prism (version 10.0.2). Some data analysis was also performed using Microsoft Excel (version 2307).

Stability of reference gene expression across samples in real-time PCR was determined using the geNorm application of qbase+ software (version 3.3). Normalization of expression values against the reference genes was performed on LightCycler96 software (version 1.1.0.1320). Cytokine data generated using LEGENDplex™ was analyzed using the online software tool at https://legendplex.qognit.com/. Publicly available ChIP-seq, ATAC-seq and scRNAseq were processed and analysed using R (version 4.3.0). scRNA-seq TICA data were visualized with the R package Seurat (version 5.1.0).

Raw fastq were aligned on human genome hg38 (genbank accession: GCA_000001405.29) using bwa mem (v0.7.18) and bigwig files were generated using bamCoverage from deepTools (v3.5.4).

For manuscripts utilizing custom algorithms or software that are central to the research but not yet described in published literature, software must be made available to editors and reviewers. We strongly encourage code deposition in a community repository (e.g. GitHub). See the Nature Portfolio guidelines for submitting code & software for further information.

Data

Policy information about availability of data

All manuscripts must include a data availability statement. This statement should provide the following information, where applicable:

- Accession codes, unique identifiers, or web links for publicly available datasets
- A description of any restrictions on data availability
- For clinical datasets or third party data, please ensure that the statement adheres to our policy

ChIP-seq data for SLC29A1 expression in activated T cells and ATAC-seq data for SLC29A1 expression in TILs was obtained from the NCBI Geo Set Omnibus (accession numbers GSE116695 and GSE89309, respectively). Source data are provided with this paper.

Research involving human participants, their data, or biological material

Policy information about studies with <u>human participants or human data</u>. See also policy information about <u>sex, gender (identity/presentation)</u>, and sexual orientation and race, ethnicity and racism.

Reporting on sex and gender

Reporting on race, ethnicity, or other socially relevant groupings

Limited sample characteristics are provided in Supplementary Table 1.

Not included in the analysis.

Population characteristics

Tumor tissue was commercially sourced from BioPartners or Fidelis from cancer patients undergoing tumor resection surgery. Patient characteristics, including covariates, and sample uses are provided in Supplementary Table 1. Samples were used for QMSI analysis of adenosine levels (19 samples, median age 68, range 38 to 81), or assessment of ENT1 expression and function on TILs (20 samples, median age 66, range 47 to 75). Data were not analyzed or stratified on the basis of covariates with the exception of comparison of adenosine levels across cancer indications.

Venous blood from healthy volunteers, all of whom signed an informed consent approved by the Ethics Committee (FOR-UIC-BV-050-01-01 ICF_HBS_HD Version 5.0), was obtained by Centre Hospitalier Universitaire Tivoli, La Louviere, Belgium. Data were not analyzed or stratified on the basis of covariates.

No recruitment process was undertaken - patients were scheduled to undergo surgery and additional tumor material was distributed to iTeos Therapeutics for subsequent analysis.

Ethics oversight

Recruitment

Resected tumour samples were collected from subjects affected by cancer, all of whom voluntarily gave their informed consent according to the protocol approved by the local ethics commission at CNE KRD "Kyiv Regional Oncology Dispensary" (Ukraine, Kiev). Sample procurement and shipment were managed by BioPartners (California, United States; https://biopartners.science/). NSCLC samples for isolated TIL experiments were sourced by Fidelis Research (https://fidelisresearch.com/) according to the protocol approved by the National Commission for Bioethics of Medicines and Medical Supplies (Romania, Bucarest, Academia De Ştiinţe Medical).

Venous blood from healthy volunteers, all of whom signed an informed consent approved by the Ethics Committee (FOR-UIC-BV-050-01-01 ICF_HBS_HD Version 5.0), was obtained by Centre Hospitalier Universitaire Tivoli, La Louviere, Belgium.

Note that full information on the approval of the study protocol must also be provided in the manuscript. $\frac{1}{2} \int_{\mathbb{R}^{n}} \left(\frac{1}{2} \int_{\mathbb{R}^{$

Field-specific reporting

Please select the one below that is the best fit for your research. If you are not sure, read the appropriate sections before making your selection.					
∑ Life sciences	Behavioural & social sciences	Ecological, evolutionary & environmental sciences			

For a reference copy of the document with all sections, see nature.com/documents/nr-reporting-summary-flat.pdf

Life sciences study design

All studies must disclose on these points even when the disclosure is negative.

Sample size

No statistical methods were used to determine sample size. Sample size was chosen based on preliminary experiments or previously published results (Preillon et al., Restoration of T-cell Effector Function, Depletion of Tregs, and Direct Killing of Tumor Cells: The Multiple Mechanisms of Action of a-TIGIT Antagonist Antibodies. Mol Cancer Ther 20, 121-131 (2021)).

Data exclusions

No data were excluded from the study.

Replication

The number experimental repeats are noted in the relevant figure legends. Where experiments were repeated the findings were reliably reproduced.

Randomization

For in vivo assessment of EOS301984 in humanized mice bearing MDA-MB-231 tumors, randomization of mice into treatment groups was performed after engraftment confirmation (hCD45/total CD45>25%) on the basis of humanization rate, tumor volume and the cord blood donor ID. For in vivo assessment of tumor growth in wild type and ENT1-KO mice, no randomization was performed as the mice did not

For in vitro experiments, in all cases cells from a single donor were divided across treatment groups to receive all treatments. Covariates for each sample are therefore distributed across all treatment groups randomization of the samples was not required.

Blinding

Materials Q averagemental systems

Investigators were not blinded to group allocation during data collection or analysis as no data were excluded and only objective measurable criteria were used for this study.

Reporting for specific materials, systems and methods

Mathada

We require information from authors about some types of materials, experimental systems and methods used in many studies. Here, indicate whether each material, system or method listed is relevant to your study. If you are not sure if a list item applies to your research, read the appropriate section before selecting a response.

Materials & experimental systems		METHORS		
n/a	Involved in the study	n/a	Involved in the study	
	Antibodies	\boxtimes	ChIP-seq	
	Eukaryotic cell lines		Flow cytometry	
\boxtimes	Palaeontology and archaeology	\boxtimes	MRI-based neuroimaging	
	Animals and other organisms			
\boxtimes	Clinical data			
\boxtimes	Dual use research of concern			
∇	Plants			

Antibodies

Antibodies used

The following antibodies or specific reagents were used for cell culture:

CFSA,SE (CFSE) (Thermo Fisher Scientific, C1157, 1 µM)

Cell Proliferation Dye eFluor 450 (Thermo Fisher Scientific, 65-0842-90, 10 - 3 - 0.3 μΜ)

CMV pp65 peptide NLVPMVATV (Thermo Fisher scientific, 15312156, 10 µg/mL)

Anti-PD-1 (OPDIVO® (nivolumab)), (Bristol Meyers Squibb)

Anti-B-Gal IgG4 (S228P) (InvivoGen, Bgal-mab114, 10µg/mL)

GolgiPlug Protein Transport inhibitor (Containing Blefeldin A) (BD Biosciences, 555029)

The following antibodies were used for flow cytometry:

Alexa Fluor 488 anti-human CD8 (HIT8a, BioLegend, 300916, 1:50)

Alexa Fluor 700 anti-human CD4 (RPA-T4, BioLegend, 300526, 1:100)

Alexa Fluor 700 anti-human CD8 (SK1, BioLegend, 344724, 1:100)

APC-Fire810 anti-human CD27 (QA17A18, BioLegend, 393214, 1:100)

APC-R700 anti-human CD4 (RPA-T4, BD, 564975, 1:50)

BB515 anti-human CD3 (UCHT1, BD, 564465, Dil. 1:50)

BB515 anti-human CD45 (HI30, BD, 564585, 1:200) BB515 anti-human TIM-3 (CD366) (7D3, 565568, 1:50)

BUV395 anti-human CD8 (RPA-T8, BD, 563795, 1:50)

BUV395 anti-human CD45 (HI30, BD, 563791, 1:100)

BUV737 anti-human CD19 (SJ25C1, BD, 612756, 1:100)

BUV737 anti-human CD279 (PD-1) (EH12.1, BD, 612791, 1:50)

BUV805 anti-human IFNgamma (4S.B3, BD, 569652, 1:100)

BV421 anti-human CD4 (L200, BD, 562842, 1:50)

BV421 anti-human CD73 (AD2, BD, 562430, 1:200)

BV510 anti-human CD8 (SK1, BD, 563919, 1:200)

```
BV510 anti-human CD3 (OT3, BioLegend, 317332, 1:50)
BV605 anti-human CD3 (SK7, BD, 563219, 1:50)
BV605 anti-human CD25 (2A3, Mouse, BD, 562660, 1:100)
BV650 anti-human TIM-3 (F38-2E2, BioLegend, 345028, 1:25)
BV711 anti-human CD39 (A1, BioLegend, 328228, 1:100)
BV711 anti-human Ki-67 (Ki-67, BioLegend, 350515, 1:50)
BV786 anti-human CD4 (SK3, BD, 563877, 1:100)
BV786 anti-human CD28 (CD28.2, BioLegend, 302950, 1:50)
cFluor B515 anti-human CD8 (SK1, Cytek, R7-20036, 1:20)
cFluor B690 anti-human CD45RA (HI100, Cytek, R7-20086, 1:20)
cFluor BYG575 anti-human CCR7 (G043H7, Cytek, R7-20076, 1:20)
cFluor BYG710 anti-human CD19 (HIB19, Cytek, R7-20010, 1:20)
cFluor R780 anti-human CD4 (SK3, Cytek, R7-20084, 1:20)
cFluor V420 anti-human CD3 (SK7, Cytek, R7-20054, 1:20)
cFluor V547 anti-human CD45 (HI30, Cytek, R7-20012, 1:20)
Fixable Viability dye eFluor 506 (Thermo Fisher Scientific, 65-0866-14, 1:500)
Fixable Viability dye eFluor 660 (Thermo Fisher Scientific, 65-0864-14, 1:500)
Fixable Viability dye eFluor 780 (Thermo Fisher Scientific, 65-0865-14, 1:1000)
Fixable Viability ViaDye red (Cytek, R7-60008, 1:5000)
PE anti-human Ki-67 (SolA15, Thermo Fisher Scientific, 12-5698-82, 1:200)
PE anti-human CD56 (5.1H11, BioLegend, 362507, 1:100)
PE anti-human TOX (REA473, Miltenyi Biotec, 130-120-716, 1:25)
PE anti-human TOX (TXRX10, eBioscience, 12-6502-80, 1:100)
PE-Cy5 anti-human CD137 (4-1BB) (4B4-1, BD, 551137, 1:50)
PE-Cy7 anti-human Granzyme B (QA16A02, Mouse, BioLegend, 372214, 1:50)
PE-Cy7 anti-human CD3 (SK7, BD, 557851, 1:100)
PE-Cy7 anti-human CD25 (BC96, BioLegend, 302612, 1:100)
PE-Cy7 anti-human PD-1 (EH12.2H7, BioLegend, 329918, 1:100)
PE-Dazzle594 anti-human/mouse granzyme B (QA16A02, BioLegend, 372216, 1:200)
PE-CF594 anti-human FoxP3 (259D/C7, BD, 562421, 1:100)
PerCP-Cy5.5 anti-human CD39 (A1, Biolegend, 328218, 1:50)
PerCP/eF710 anti-human TIGIT (MBSA43, Thermo Fisher Scientific, 46-9500-42, 1:25)
Apotracker Green (BioLegend 427402 400M)
BV421 MHC Tetramer (peptide NLVPMVATV, Tetramer Shop, HA02-010, 1:25)
Human FcBlock (BD, 564220, 1:100)
BUV395 anti-mouse CD45 (30-F11, BD, 564279, 1:100)
FITC anti-mouse CD4 (RM4-5, Thermo Fisher Scientific, 11-0042-82, 1:100)
BV711 anti-mouse CD8α (53-6.7, BD, 563046, 1:100)
BV605 anti-mouse TCRβ (H57-597, BioLegend, 109241, 1:100)
```

BUV395 anti-mouse CD45 (30-F11, BD, 564279, 1:100) FITC anti-mouse CD4 (RM4-5, Thermo Fisher Scientific, 11-0042-82, 1:100) BV711 anti-mouse CD8 α (53-6.7, BD, 563046, 1:100) BV605 anti-mouse TCR β (H57-597, BioLegend, 109241, 1:100) BV421 anti-mouse IFN γ (XMG1.2, BD, 563376, 1:100) PE/Dazzle594 anti-mouse Ki-67 (11F6 BioLegend, 151220, 1:400) Anti-mouse Fc block (Thermo Fisher Scientific, 14-0161-81C, 1:100) Live/dead Fixable Violet Dead Cell Stain Kit (Life technologies, L34955, 1:500)

SAHENTA-DY647 was synthesized at the Faculté de Pharmacie de Strasbourg from 5'-S-[2-[(6-Amino-1-oxohexyl)amino]ethyl]-N-[(4-nitrophenyl)methyl]-5'-thioadenosine (ACI) (1191264-90-0) and DY-647P1-NHS-ester (purchased from Dyomics GmbH) in adapted conditions described in J. Med. Chem. 2010, 53, 6040.

The following antibodies were used for Western blot: Anti-human ENT1 (SP120, Abcam, Ab182023, 1:1000) HRP anti-rabbit IgG (7074S, Cell signaling Technology, 7074S, 1:1000) Anti-B-actin (D6A8, Cell signaling Technology, 8457S, 1:1000)

The following antibodies were used for in vivo experiments: InVivoPlus anti-mouse CD8α (53-6.7, BioXcell, BP004-1) Anti-PD-1 (OPDIVO® (nivolumab)), (Bristol Meyers Squibb)

Validation

SAHENTA was validated for the binding to human ENT1 in this publication: Robins, M. J., Peng, Y., Damaraju, V. L., Mowles, D., Barron, G., Tackaberry, T., Young, J. D. & Cass, C. E. Improved Syntheses of 5'-S-(2-Aminoethyl)-6-N-(4-nitrobenzyl)-5'-thioadenosine (SAENTA), Analogues, and Fluorescent Probe Conjugates: Analysis of Cell-Surface Human Equilibrative Nucleoside Transporter 1 (hENT1) Levels for Prediction of the Antitumor Efficacy of Gemcitabine. J Med Chem 53, 6040–6053 (2010). The DY-647-conjugated version of SAHENTA was validated for staining of human ENT1 in this study in Extended Data Fig. 2. Alexa Fluor 488 anti-human CD8 (HIT8a, BioLegend, 300916, 1:50)

https://www.biolegend.com/en-gb/products/alexa-fluor-488-anti-human-cd8a-antibody-3432

Validated by manufacturer through staining of Human peripheral blood lymphocytes (flow cytometry)

Alexa Fluor 700 anti-human CD4 (RPA-T4, BioLegend, 300526, 1:100) https://www.biolegend.com/en-gb/products/alexa-fluor-700-anti-human-cd4-antibody-3395 Validated by manufacturer through staining of human peripheral blood lymphocytes (flow cytometry)

Alexa Fluor 700 anti-human CD8 (SK1, BioLegend, 344724, 1:100)

https://www.biolegend.com/en-gb/products/alexa-fluor-700-anti-human-cd8-antibody-9062

Validated by manufacturer through staining of human peripheral blood lymphocytes (flow cytometry)

APC-Fire810 anti-human CD27 (QA17A18, BioLegend, 393214, 1:100)

https://www.biolegend.com/en-gb/products/apc-fire-810-anti-human-cd27-recombinant-antibody-19572

Validated by manufacturer through staining of human peripheral blood lymphocytes (flow cytometry)

APC-R700 anti-human CD4 (RPA-T4, BD, 564975, 1:50)

https://www.bdbiosciences.com/en-be/products/reagents/flow-cytometry-reagents/research-reagents/single-color-antibodies-ruo/apc-r700-mouse-anti-human-cd4.564975?tab=product_details

Validated by manufacturer through staining of human peripheral blood lymphocytes (flow cytometry)

BB515 anti-human CD3 (UCHT1, BD, 564465, Dil. 1:50)

https://www.bdbiosciences.com/en-au/products/reagents/flow-cytometry-reagents/research-reagents/single-color-antibodies-ruo/bb515-mouse-anti-human-cd3.564465?tab=product_details.

Validated by manufacturer through staining of human peripheral blood lymphocytes (flow cytometry)

BB515 anti-human CD45 (HI30, BD, 564585, 1:200)

https://www.bdbiosciences.com/en-be/products/reagents/flow-cytometry-reagents/research-reagents/single-color-antibodies-ruo/bb515-mouse-anti-human-cd45.564585?tab=product_details

Validated by manufacturer through staining of human peripheral blood leucocytes (flow cytometry)

BB515 anti-human TIM-3 (CD366) (7D3, 565568, 1:50)

 $https://www.bdbiosciences.com/en-au/products/reagents/flow-cytometry-reagents/research-reagents/single-color-antibodies-ruo/bb515-mouse-anti-human-tim-3-cd366.565568?tab=product_details$

Validated by manufacturer through staining of human peripheral blood leucocytes (flow cytometry)

BUV395 anti-human CD8 (RPA-T8, BD, 563795, 1:50)

https://www.bdbiosciences.com/en-au/products/reagents/flow-cytometry-reagents/research-reagents/single-color-antibodies-ruo/buv395-mouse-anti-human-cd8.563795?tab=product_details

Validated by manufacturer through staining of human peripheral blood lymphocytes (flow cytometry)

BUV395 anti-human CD45 (HI30, BD, 563791, 1:100)

https://www.bdbiosciences.com/en-au/products/reagents/flow-cytometry-reagents/research-reagents/single-color-antibodies-ruo/buv395-mouse-anti-human-cd45.563791?tab=product_details

Validated by manufacturer through staining of human peripheral blood leucocytes (flow cytometry)

BUV737 anti-human CD19 (SJ25C1, BD, 612756, 1:100)

https://www.bdbiosciences.com/en-au/products/reagents/flow-cytometry-reagents/research-reagents/single-color-antibodies-ruo/buv737-mouse-anti-human-cd19.612756?tab=product_details

Validated by manufacturer through staining of human peripheral blood lymphocytes (flow cytometry)

BUV737 anti-human CD279 (PD-1) (EH12.1, BD, 612791, 1:50)

 $https://www.bdbiosciences.com/en-au/products/reagents/flow-cytometry-reagents/research-reagents/single-color-antibodies-ruo/buv737-mouse-anti-human-cd279-pd-1.612791?tab=product_details$

Validated by manufacturer through staining of human peripheral blood lymphocytes (flow cytometry)

BUV805 anti-human IFNgamma (4S.B3, BD, 569652, 1:100)

 $https://www.bdbiosciences.com/en-au/products/reagents/flow-cytometry-reagents/research-reagents/single-color-antibodies-ruo/buv805-mouse-anti-human-ifn.569652?tab=product_details$

Validated by manufacturer through staining of stimulated (PMA-ionomycin, 6 hours) human peripheral blood lymphocytes (flow cytometry)

BV421 anti-human CD4 (L200, BD, 562842, 1:50)

 $https://www.bdbiosciences.com/en-au/products/reagents/flow-cytometry-reagents/research-reagents/single-color-antibodies-ruo/bv421-mouse-anti-human-cd4.562842?tab=product_details$

Validated by manufacturer through staining of Rhesus macaque peripheral blood lymphocytes (flow cytometry)

BV421 anti-human CD73 (AD2, BD, 562430, 1:200)

 $https://www.bdbiosciences.com/en-au/products/reagents/flow-cytometry-reagents/research-reagents/single-color-antibodies-ruo/bv421-mouse-anti-human-cd73.562430?tab=product_details$

Validated by manufacturer through staining of human peripheral blood lymphocytes (flow cytometry)

BV510 anti-human CD8 (SK1, BD, 563919, 1:200)

 $https://www.bdbiosciences.com/en-au/products/reagents/flow-cytometry-reagents/research-reagents/single-color-antibodies-ruo/bv510-mouse-anti-human-cd8.563919?tab=product_details$

Validated by manufacturer through staining of human peripheral blood lymphocytes (flow cytometry)

BV510 anti-human CD3 (OT3, BioLegend, 317332, 1:50)

https://www.biolegend.com/en-gb/products/brilliant-violet-510-anti-human-cd3-antibody-8009?GroupID=BLG4203

Validated by manufacturer through staining of human peripheral blood lymphocytes (flow cytometry)

BV605 anti-human CD3 (SK7, BD, 563219, 1:50)

https://www.bdbiosciences.com/en-au/products/reagents/flow-cytometry-reagents/research-reagents/single-color-antibodies-ruo/bv605-mouse-anti-human-cd3.563219

Validated by manufacturer through staining of human peripheral blood lymphocytes (flow cytometry)

BV605 anti-human CD25 (2A3, Mouse, BD, 562660, 1:100)

 $https://www.bdbiosciences.com/en-au/products/reagents/flow-cytometry-reagents/research-reagents/single-color-antibodies-ruo/bv605-mouse-anti-human-cd25.562660?tab=product_details$

Validated by manufacturer through staining of stimulated (PHA, 3 days) human peripheral blood lymphocytes (flow cytometry)

BV650 anti-human TIM-3 (F38-2E2, BioLegend, 345028, 1:25)

https://www.biolegend.com/en-gb/products/brilliant-violet-650-anti-human-cd366-tim-3-antibody-12008 Validated by manufacturer through staining of stimulated (PHA, 3 days) human peripheral blood lymphocytes

BV711 anti-human CD39 (A1, BioLegend, 328228, 1:100)

https://www.biolegend.com/en-gb/products/brilliant-violet-711-anti-human-cd39-antibody-13900 Validated by manufacturer through staining of human peripheral blood lymphocytes (flow cytometry)

BV711 anti-human Ki-67 (Ki-67, BioLegend, 350515, 1:50)

https://www.biolegend.com/en-gb/products/brilliant-violet-711-anti-human-ki-67-antibody-7946

Validated by manufacturer through staining of stimulated (PHA, 3 days) human peripheral blood lymphocytes (flow cytometry)

BV786 anti-human CD4 (SK3, BD, 563877, 1:100)

 $https://www.bdbiosciences.com/en-au/products/reagents/flow-cytometry-reagents/research-reagents/single-color-antibodies-ruo/bv786-mouse-anti-human-cd4.563877? tab=product_details$

Validated by manufacturer through staining of human peripheral blood lymphocytes (flow cytometry)

BV786 anti-human CD28 (CD28.2, BioLegend, 302950, 1:50)

https://www.biolegend.com/en-us/products/brilliant-violet-785-anti-human-cd28-antibody-13510 Validated by manufacturer through staining of human peripheral blood lymphocytes (flow cytometry)

cFluor B515 anti-human CD8 (SK1, Cytek, R7-20036, 1:20)

https://cytekbio.com/products/cfluor-b515-anti-human-cd8-sk1?variant=32613864669220

Validated by manufacturer through staining of human peripheral blood (flow cytometry)

cFluor B690 anti-human CD45RA (HI100, Cytek, R7-20086, 1:20)

https://cytekbio.com/products/cfluor-immunoprofiling-kit-14-colors?variant=32509237231652

Validated by manufacturer through staining of human peripheral blood or whole blood (flow cytometry)

cFluor BYG575 anti-human CCR7 (G043H7, Cytek, R7-20076, 1:20)

https://cytekbio.com/products/cfluor-immunoprofiling-kit-14-colors?variant=32509237231652

Validated by manufacturer through staining of human peripheral blood or whole blood (flow cytometry)

cFluor BYG710 anti-human CD19 (HIB19, Cytek, R7-20010, 1:20)

https://cytekbio.com/products/cfluor-byg710-anti-human-cd19-hib19?variant=39324642476068

Validated by manufacturer through staining of human peripheral blood (flow cytometry)

cFluor R780 anti-human CD4 (SK3, Cytek, R7-20084, 1:20)

https://cytekbio.com/products/cfluor-r780-anti-human-cd4-sk3?variant=40060795027492

Validated by manufacturer through staining of human peripheral blood (flow cytometry)

cFluor V420 anti-human CD3 (SK7, Cytek, R7-20054, 1:20)

https://cytekbio.com/products/cfluor-v420-anti-human-cd3-sk7? variant=32613908906020

Validated by manufacturer through staining of human peripheral blood (flow cytometry)

cFluor V547 anti-human CD45 (HI30, Cytek, R7-20012, 1:20)

https://cytekbio.com/products/cfluor-v547-anti-human-cd45-hi30?variant=32613926010916

Validated by manufacturer through staining of human peripheral blood (flow cytometry)

Fixable Viability dye eFluor 506 (Thermo Fisher Scientific, 65-0866-14, 1:500)

https://www.thermofisher.com/order/catalog/product/65-0866-14

Validated by manufacturer through staining of C57BI/6 thymocytes (flow cytometry)

Fixable Viability dye eFluor 660 (Thermo Fisher Scientific, 65-0864-14, 1:500)

https://www.thermofisher.com/order/catalog/product/65-0864-14

Validated by manufacturer through staining of BALB/c thymocytes (flow cytometry)

Fixable Viability dye eFluor 780 (Thermo Fisher Scientific, 65-0865-14, 1:1000)

https://www.thermofisher.com/order/catalog/product/65-0865-14?SID=srch-srp-65-0865-14

Validated by manufacturer through staining of BALB/c thymocytes (flow cytometry)

Fixable Viability ViaDye red (Cytek, R7-60008, 1:5000)

https://cytekbio.com/products/viadye-red-fixable-viability-dye-kit?variant=39443962036260

Validated by manufacturer through staining of mouse splenocytes (flow cytometry)

PE anti-human Ki-67 (SolA15, Thermo Fisher Scientific, 12-5698-82, 1:200)

https://www.thermofisher.com/antibody/product/Ki-67-Antibody-clone-SolA15-Monoclonal/12-5698-82

Validated by manufacturer through staining of stimulated (aCD3, 2 days) C57BI/6 splenocytes (flow cytometry)

PE anti-human CD56 (5.1H11, BioLegend, 362507, 1:100)

https://www.biolegend.com/en-us/products/pe-anti-human-cd56-ncam-antibody-9958

Validated by manufacturer through staining of human peripheral blood lymphocytes (flow cytometry)

PE anti-human TOX (REA473, Miltenyi Biotec, 130-120-716, 1:25)

https://static.miltenyibiotec.com/asset/150655405641/document_gn18op180p335eseq2poduff46?content-disposition=inline Validated by manufacturer through staining of thymocytes from C57BL/6 mice (flow cytometry)

PE anti-human TOX (TXRX10, eBioscience, 12-6502-80, 1:100)

https://www.thermofisher.com/antibody/product/TOX-Antibody-clone-TXRX10-Monoclonal/12-6502-82

Validated by manufacturer through staining of C57Bl/6 thymocytes (flow cytometry)

PE-Cy5 anti-human CD137 (4-1BB) (4B4-1, BD, 551137, 1:50)

 $https://www.bdbiosciences.com/en-au/products/reagents/flow-cytometry-reagents/research-reagents/single-color-antibodies-ruo/pe-cy-5-mouse-anti-human-cd137.551137?tab=product_details$

Validated by manufacturer through staining of stimulated (ConA, 3 days) human peripheral blood lymphocytes (flow cytometry)

PE-Cy7 anti-human Granzyme B (QA16A02, Mouse, BioLegend, 372214, 1:50)

https://www.biolegend.com/en-us/products/pe-cyanine7-anti-humanmouse-granzyme-b-recombinant-antibody-15582

Validated by manufacturer through staining of human peripheral blood mononuclear cells (flow cytometry)

PE-Cy7 anti-human CD3 (SK7, BD, 557851, 1:100)

https://www.bdbiosciences.com/en-au/products/reagents/flow-cytometry-reagents/research-reagents/single-color-antibodies-ruo/pe-cy-7-mouse-anti-human-cd3.557851?tab=product_details

Validated by manufacturer through staining of human peripheral blood lymphocytes (flow cytometry)

PE-Cv7 anti-human CD25 (BC96, BioLegend, 302612, 1:100)

https://www.biolegend.com/en-us/products/pe-cyanine7-anti-human-cd25-antibody-1909

Validated by manufacturer through staining of stimulated (PHA, 3 days) human peripheral blood lymphocytes (flow cytometry)

PE-Cy7 anti-human PD-1 (EH12.2H7, BioLegend, 329918, 1:100)

https://www.biolegend.com/en-us/products/pe-cyanine7-anti-human-cd279-pd-1-antibody-6154

Validated by manufacturer through staining of stimulated (PHA, 3 days) human peripheral blood lymphocytes (flow cytometry)

PE-Dazzle594 anti-human/mouse granzyme B (QA16A02, BioLegend, 372216, 1:200)

https://www.biolegend.com/en-us/products/pedazzle-594-anti-humanmouse-granzyme-b-recombinant-antibody-15598 Validated by manufacturer through staining of human peripheral blood mononuclear cells (flow cytometry)

PE-CF594 anti-human FoxP3 (259D/C7, BD, 562421, 1:100)

https://www.bdbiosciences.com/en-au/products/reagents/flow-cytometry-reagents/research-reagents/single-color-antibodies-ruo/pe-cf594-mouse-anti-human-foxp3.562421?tab=product_details

Validated by manufacturer through staining of human peripheral blood mononuclear cells (flow cytometry)

PerCP-Cy5.5 anti-human CD39 (A1, Biolegend, 328218, 1:50)

https://www.biolegend.com/en-us/products/percp-cyanine5-5-anti-human-cd39-antibody-9112

Validated by manufacturer through staining of human peripheral blood lymphocytes (flow cytometry)

PerCP/eF710 anti-human TIGIT (MBSA43, Thermo Fisher Scientific, 46-9500-42, 1:25)

https://www.thermofisher.com/antibody/product/TIGIT-Antibody-clone-MBSA43-Monoclonal/46-9500-42

Validated by manufacturer through staining of normal human peripheral blood cells (flow cytometry)

Apotracker Green (BioLegend, 427402, 400M)

https://www.biolegend.com/en-us/products/apotracker-green-18527

Validated by manufacturer through staining of one day old splenocytes, extracellular vesicles isolated from human plasma (flow cytometry)

BV421 MHC Tetramer (peptide NLVPMVATV, Tetramer Shop, HA02-010, 1:25)

https://tetramerstore.com

Validated by manufacturer through staining of lymphoid cells (PBMCs, TILs, or splenocytes) (flow cytometry).

Human FcBlock (BD, 564220, 1:100)

 $https://www.bdbiosciences.com/en-au/products/reagents/flow-cytometry-reagents/research-reagents/single-color-antibodies-ruo/human-bd-fc-block.564220?tab=product_details$

Validated by manufacturer through staining of human peripheral blood mononuclear cells (flow cytometry)

BUV395 anti-mouse CD45 (30-F11, BD, 564279, 1:100)

 $https://www.bdbiosciences.com/en-ca/products/reagents/flow-cytometry-reagents/research-reagents/single-color-antibodies-ruo/buv395-rat-anti-mouse-cd45.564279?tab=product_details$

Validated by manufacturer through staining of mouse splenic leucocytes (flow cytometry)

FITC anti-mouse CD4 (RM4-5, Thermo Fisher Scientific, 11-0042-82, 1:100)

https://www.thermofisher.com/antibody/product/CD4-Antibody-clone-RM4-5-Monoclonal/11-0042-82

Validated by manufacturer through staining of C57BL/6 splenocytes (flow cytometry)

BV711 anti-mouse CD8α (53-6.7, BD, 563046, 1:100)

https://www.bdbiosciences.com/en-us/products/reagents/flow-cytometry-reagents/research-reagents/single-color-antibodies-ruo/

bv711-rat-anti-mouse-cd8a.563046?tab=product_details

Validated by manufacturer through staining of splenic leucocytes from α BALB/c mouse (flow cytometry)

BV605 anti-mouse TCRβ (H57-597, BioLegend, 109241, 1:100)

https://www.biolegend.com/fr-lu/products/brilliant-violet-605-anti-mouse-tcr-beta-chain-antibody-13533

Validated by manufacturer through staining of C57BL/6 mouse splenocytes (flow cytometry)

BV421 anti-mouse IFNv (XMG1.2, BD, 563376, 1:100)

https://www.bdbiosciences.com/en-us/products/reagents/flow-cytometry-reagents/research-reagents/single-color-antibodies-ruo/bv421-rat-anti-mouse-ifn.563376?tab=product_details

Validated by manufacturer through staining of stimulated (PMA-ionomycin, 5 hours) mouse splenic leucocytes (flow cytometry)

PE/Dazzle594 anti-mouse Ki-67 (11F6 BioLegend, 151220, 1:400)

https://www.biolegend.com/fr-lu/products/pe-dazzle-594-anti-mouse-human-ki-67-antibody-21653

Validated by manufacturer through staining of stimulated (ConA and IL-2, 3 days) C57BL/6J splenocytes (flow cytometry)

Anti-mouse Fc block (Thermo Fisher Scientific, 14-0161-81C, 1:100)

https://www.thermofisher.com/antibody/product/CD16-CD32-Antibody-clone-93-Monoclonal/14-0161-82

Validated by manufacturer through staining of BALB/c splenocytes (flow cytometry)

Live/dead Fixable Violet Dead Cell Stain Kit (Life technologies, L34955, 1:500)

https://www.thermofisher.com/order/catalog/product/L34955

Validated by manufacturer through staining of Jurkat cells (flow cytometry)

Anti-ENT1 antibody [SP120] (Abcam, Ab182023)

https://www.abcam.com/en-us/products/primary-antibodies/ent1-antibody-sp120-ab182023?

srsltid=AfmBOoqf6ejJqd3Q3rv98bzKeABY81DqNwmwxSuG9F8PWUZeUgub-BPQ

Validated by manufacturer through labelling different human cell lines: HAP1 (WT and SLC29A1 knockout) by western blot and immunocytochemistry; HEK-293T (WT and SLC29A1 knockout), HeLa, and U-87 by western blot; HepG2 by flow cytometry; and through labelling human tissue sections (colon carcinoma and pancreas) by immunohistochemistry.

β-Actin (D6A8) Rabbit mAb #8457 (Cell Signaling Technology, 8457S)

https://www.cellsignal.com/products/primary-antibodies/b-actin-d6a8-rabbit-mab/8457

Validated by manufacturer through labelling recombinant actin isoforms and different cell lines by western blot: HeLa (human), C6 (rat), MCF7 (human), NIH/3T3 (mouse), COS-7 (monkey); through labelling HeLa by immunofluorescence and flow cytometry.

InVivoPlus anti-mouse CD8α (BioXcell BP0004-1)

https://bioxcell.com/invivoplus-anti-mouse-cd8-alpha-bp0004-1

Validated by manufacturer through staining of normal murine splenocytes (flow cytometry) and purified mouse CD8α (western blot)

Eukaryotic cell lines

Policy information about cell lines and Sex and Gender in Research

Cell line source(s)

MDA-MB-231 (ATCC, HTB-26) CT26 (ATCC, CT26.WT) HT29 (ATCC, HTB-38)

A375 (ATCC, CRL-1619) JAR (ATCC, HTB-144)

T2 (ATCC, CRL-1992)

MCA205 (Sigma-Aldrich, SCC173) MC38 (Sigma-Aldrich, SCC172)

KPC (Kerafast, EUP005-FP)

Pan02 (National Cancer Institute DCTD Tumor Repository (NCI), 0507406)

MDCKII (German Cancer Research Center, Heidelberg, Germany)

HEK293 (Invitrogen)

Authentication

Cell line authentication was performed by the supplier, no additional cell line authentication was performed.

Mycoplasma contamination

All tumour cell lines were tested regularly for mycoplasma contamination by PCR and were verified to be negative before using for different assays and studies.

Commonly misidentified lines (See ICLAC register)

None of the cell lines used in this study appear in the ICLAC register of commonly misidentified lines.

Animals and other research organisms

Policy information about <u>studies involving animals</u>; <u>ARRIVE guidelines</u> recommended for reporting animal research, and <u>Sex and Gender in Research</u>

Laboratory animals

Mice were purchased from Taconic and were housed under pathogen-free conditions at ULB facilities, following all animal the guidelines set by FELASA (Federation of European Laboratory Animal Science Associations). Furthermore, the animal protocols underwent thorough review and received approval from the Institute of Animal Care and Use Committee at ULB, agreement LA-150055-18, project code BUC 2020-03. Mice were on 12-hour light/dark cycles that coincide with daylight in Gosselies, Belgium. The housing facility was maintained at 20-25 °C and 30-70% humidity.

ENT1-KO mice were generated upon request from Cyagen, utilizing a C57BL/6J mice background. A colony of ENT1-KO mice was established and maintained at Taconic Facilities in Denmark. Once established, the mice were transported to the animal facility at Université libre de Bruxelles (ULB) for experimentation. For comparative purposes, wild-type C57BL/6J female mice, aged between seven-to-eight weeks, were obtained from Taconic Inc. (Denmark). Mice were inoculated at 8 weeks of age.

Human cell line xenograft experiments were performed at Transcure (France) and all associated animal procedures were reviewed and approved by the local ethics committee (CELEAG—TCS agreement number A7418324, 09DEC2021:

APAFIS##30873-202112011817784 V2; 17MAR2021: APAFIS#38383-2022082413416895 V7). The experiment was carried out with the NOD-Prkdcem26Cd52ll2rgem26Cd22/NjuCrl immunodeficient mouse strain (NCG from Charles River Laboratories, Wilmington, MA, USA). Mice were engrafted at 4 weeks of age with human cord-blood derived CD34+ hematopoietic stem and progenitor cells. Mice were inoculated with MDA-MB-231 cells 14 weeks after engraftment.

Wild animals

The study did not involve wild animals.

Reporting on sex

Only female mice were included in relevant analyses reported in this manuscript.

Field-collected samples

The study did not involve samples collected from the field.

Ethics oversight

Animal protocols performed at iTeos Therapeutics underwent thorough review and received approval from the Institute of Animal Care and Use Committee at ULB, agreement LA-150055-18, project code BUC 2020-03.

Humanized mice experiments were reviewed and approved by the local ethics committee (CELEAG-TCS agreement number A7418324. 09DEC2021: APAFIS##30873-202112011817784 V2; 17MAR2021: APAFIS#38383-2022082413416895 V7).

Note that full information on the approval of the study protocol must also be provided in the manuscript.

Flow Cytometry

Plots

Confirm that:

- \square The axis labels state the marker and fluorochrome used (e.g. CD4-FITC).
- 💢 The axis scales are clearly visible. Include numbers along axes only for bottom left plot of group (a 'group' is an analysis of identical markers).
- All plots are contour plots with outliers or pseudocolor plots.
- A numerical value for number of cells or percentage (with statistics) is provided.

Methodology

Sample preparation

Cells were centrifuged at 450 x g for 5 minutes (used for all subsequent centrifugation steps) and the supernatant was discarded. For proliferation experiments (without ENT1 staining), cells were resuspended in PBS containing fixable viability dye and human Fc block (BD) and incubated for 15 minutes at 4°C. For ENT1 staining, cells were resuspended in 50 µL NBMPR solution (20µM − 0.02% DMSO; used as negative control for ENT1 expression) or DMSO (0.02% DMSO − for the ENT1 staining), as well as Fc block, incubated 15 min at 4°C, and then, 50 µL of PBS containing SAHENTA-DY647 (0.2 µM for final concentration 0.1 µM) and fixable viability dye was added, followed by an incubation step of 30 min at 4°C. Cells were then washed in FACS buffer (PBS with 2 mM EDTA and 0.1% BSA), and resuspended in a solution of FACS buffer and relevant antibodies. After an additional 15 minutes of incubation at 4°C cells were centrifuged and resuspended in FACS buffer. In some experiments cells were subsequently prepared for intracellular staining using the eBioscience™ Foxp3/Transcription Factor Staining Buffer Set (human cells) or alternatively IC fixation buffer and permeabilization buffers (mouse cells, eBioscience) were used according to the manufacturer's instructions. Samples were analyzed on a BD LSRFortessa™ Cell Analyzer using BD FACS DIVA software (version 9.0.1, Becton, Dickinson and Company) or a Cytek Aurora (SpectroFlo software 3.0.1).

Instrument

Flow cytometry data was acquired on a BD LSRFortessa™ Cell Analyzer or a Cytek Aurora.

Software

Flow cytometry data was acquired using BD FACS DIVA software (version 9.0.1) or SpectroFlo software (version 3.0.1).

Cell population abundance

Sorted cell populations were immediately assessed post-sort and were typically >75% of total viable cells.

Gating strategy

Debris was first excluded on the basis of FSC v SSC plots, then single cells were selected based on FSC-A vs FSC-H or SSC-A vs

Tick this box to confirm that a figure exemplifying the gating strategy is provided in the Supplementary Information.